The influence of soil moisture, oxygen, and temperature on naphthalene biodegradation and CO_2 and CH_4 effluxes

by

Jane Ye

A thesis

presented to the University of Waterloo

in fulfilment of the

thesis requirement for the degree of

Master of Science

in

Earth Sciences

Waterloo, Ontario, Canada, 2023

© Jane Ye 2023

Author’s declaration

This thesis consists of material all of which I authored or co-authored: see Statement of Contributions included in the thesis. This is a true copy of the thesis, including any required final revisions, as accepted by my examiners. I understand that my thesis may be made electronically available to the public.

Statement of contributions

Chapter 2 of this thesis consists of a co-authored, manuscript-format paper. Chapter 3 of this thesis will be modified for submission. As the first author of both chapters, I was primarily responsible for the study design, execution, data collection and analysis, and writing. The contributions of the listed co-authors are as follows: I designed the experiment with the guidance of Fereidoun Rezanezhad, Philippe Van Cappellen, Marianne Vandergriendt, and Stephanie Slowinski. I performed the laboratory work with the assistance of Marianne Vandergriendt. Mehdi Ramezanzadeh contributed to laboratory work in Chapter 2. Stephanie Slowinski provided guidance on data interpretation. Fereidoun Rezanezhad and Philippe Van Cappellen supervised the project and provided guidance on data interpretation. I performed the data analysis, visualization, and curation, and wrote the chapters. Chapter 2 was reviewed and approved by all co-authors, while Chapter 3 will be modified for journal submission and reviewed and approved by all co-authors.

Abstract

Petroleum hydrocarbons (PHCs) are essential to the functioning of the industrialized world yet serve a potential threat to human and ecosystem health when they inadvertently enter the environment. In recent decades, recognition of natural attenuation as a viable approach to PHC remediation is increasing. Natural attenuation includes the biodegradation of PHCs through respiration, fermentation, and methanogenesis, processes which are also central to the biodegradation of natural background soil organic matter. Biodegradation of both PHCs and natural soil organic matter are a major component of the global carbon cycle and an important source of atmospheric greenhouse gases (GHGs). As a biologically mediated set of reactions, environmental factors like temperature and moisture are important controls on the rates and pathways of biodegradation. It is therefore important to understand the influence of these environmental factors on PHC biodegradation and associated carbon dioxide (CO_2) and methane (CH_4) effluxes to improve predictions of PHC remediation efficiency and soil GHG emissions under ongoing and future climate change.

In Chapter 2, I investigated the effect of soil moisture on PHC biodegradation kinetics, using naphthalene as a representative PHC compound. I performed microcosm incubations with naphthalene-spiked soil at 60, 80, and 100% water-filled pore space (WFPS) under oxic headspace, and at 100% WFPS under anoxic headspace. Incubations lasted 44 days. The results showed that the total naphthalene in soil decreased to below detection after Day 9, 17, and 44 in incubations at 60, 80, and 100% WFPS under oxic headspace, respectively. At 100% WFPS under anoxic headspace, total soil naphthalene concentrations decreased over time but were still detectable past Day 44. Fitting of the naphthalene data to first order decay equations revealed two distinct kinetic

regimes of degradation in the oxic incubations: an initial fast regime characterized by an apparent first order rate constant on the order of 10^{-1} day^{-1} followed by dominance of a slower degradation regime. In the anoxic incubations, only the slow end-member regime was observed with a corresponding rate constant of 10^{-2} day^{-1}. Porewater electron acceptor and organic acid data indicated that in the fast regime, naphthalene degradation was dominated by microbial respiration pathways, while in the slow regime fermentative pathways dominated. Results from Chapter 2 imply that spatial and temporal fluctuations in soil moisture – and the associated oxygen (O_2) availability – can cause order-of-magnitude variability in the degradation kinetics of PHCs in the vadose zone.

In Chapter 3, I investigated the effect of temperature and O_2 availability on CO_2 and CH_4 accumulations in the presence of naphthalene. I performed naphthalene-spiked microcosm incubations under oxic or anoxic headspace at temperatures of 10, 20, and 30°C. Time series data of net accumulated CH_4, accumulated CO_2, consumed O_2, accumulated dissolved inorganic carbon (DIC), and consumed organic acids (OAs) were analyzed using Arrhenius temperature sensitivity curve-fitting. Q_{10} temperature sensitivity quotients were estimated from this analysis, indicating a greater temperature sensitivity of anaerobic CO_2 and CH_4 production processes than their aerobic equivalents. I observed that methanogenesis under anoxic conditions had a particularly high Q_{10} of 9.

Overall, findings from this research confirm our understanding of field biodegradation rates. PHC biodegradation in oxic, drier zones is expected to be 10 times faster than in anoxic, saturated zones. The two distinct regimes of biodegradation activity identified in Chapter 2 could also be used as simplified representations of PHC biodegradation when modelling variable moisture and oxygen

conditions. Chapter 3 additionally suggests that the CH_4:CO_2 ratio of soil carbon emissions from anoxic soils may potentially increase with warming temperature. Thus, PHC contaminated sites may see increasing GHG emissions potential, but also increasing contaminant biodegradation rates, in a warming climate, especially those located in saturated soils and cold regions. These expected alterations in soil carbon fluxes are important for the consideration of site managers concerned with site-scale carbon cycling and GHG emissions.

Acknowledgements

Thank you to my supervisors, Dr. Fereidoun Rezanezhad and Dr. Philippe Van Cappellen, for being the first to open the door for me as wide-eyed second year undergrad, and your unwavering belief in me since then. You both taught me to trust myself, to think critically, and to communicate with purpose. I am where I am today thanks to your mentorship. Thank you also to my committee members, Dr. Neil Thomson and Dr. David Rudolph, for your thoughtful questions that improved the way I approached my work, and for reviewing my thesis.

Thank you to Steph Slowinski and Marianne Vandergriendt, who can seemingly solve every problem and make anything possible in the lab. I and everyone in the lab appreciate endlessly everything you both do. Thank you also to Dr. Shuhuan Li and Shirley Chatten for your generosity and patience in helping me with sample analyses. Linden Fairbairn also deserves recognition for designing the experiments that I took inspiration from, and for documenting her work so clearly. Thank you to co-op students Anthony Dang, Richard Dinh Pham, Tara Ferguson, Maitri Lad, and Sam Smith for your invaluable assistance running experiments and analyses.

This research would not have been possible without the support of our funding sources: a National Science and Engineering Research Council of Canada (NSERC) Strategic Partnership Grant with Imperial Oil Resources Ltd. (Collaborative Research and Development Grant to Philippe Van Cappellen: CRDPJ 533227–18), and the Global Water Futures (GWF) program funded by the Canada First Research Excellence Fund (CFREF). I am also very grateful for support from the Alexander Graham Bell Canada Graduate Scholarship (NSERC), the Queen Elizabeth II Graduate Scholarship in Science and Technology (Government of Ontario), and the President's Graduate Scholarship (University of Waterloo).

Thank you to all the past and present members of the lab who have brought so much joy to my grad school experience: Bowen Zhou, Jovana Radosavljevic, Ari Ligorsky, Riley Mills, and Mehdi Ramezanzadeh. Bowen, your enthusiasm for travel taught me to see the world around me with new eyes. Jovana, your dedication to your work and your relationships inspires me to be a better scientist and friend. Ari, I can only hope to pay forward a tenth of the kindness you show to everyone you meet. Riley, your commitment to everything you do has shown me that even the biggest mountains are conquered one step at a time. Mehdi, you were the best officemate on this journey. Our conversations on topics both trivial and passionate have been a bright light during long days in the lab and office.

Finally, thank you to my parents, the dreamers, for encouraging me to also follow my dreams, and to Sam Phillips, for being my best friend, teammate, and partner in all things in life.

Table of contents

List of figures

List of tables

List of abbreviations

PHC	Petroleum hydrocarbon
CO_2	Carbon dioxide
CH_4	Methane
NSZD	Natural source-zone depletion
EA	Electron acceptor
O_2	Oxygen
NO_3^-	Nitrate
Fe^{3+}	Iron (III)
Mn^{4+}	Manganese (IV)
SO_4^{2-}	Sulphate
ED	Electron donor
H_2	Hydrogen gas
ABM	Acetate-based (aceticlastic) methanogenesis
HBM	Hydrogen-based (hydrogenotrophic) methanogenesis
GHG	Greenhouse gas
WFPS	Water-filled pore space
TSR	Total soil respiration
CSR	Contaminant-related soil respiration
NSR	Natural soil respiration
OC	Organic carbon
TC	Total carbon
ON	Organic nitrogen
TN	Total nitrogen
MDL	Method detection limit
TPH	Total petroleum hydrocarbons
N_2	Nitrogen gas
APW	Artificial porewater
$HgCl_2$	Mercuric (II) chloride
F^-	Fluoride

Cl^-	Chloride
NO_2^-	Nitrite
Br^-	Bromide
PO_4^{3-}	Phosphate
DIC	Dissolved inorganic carbon
GC	Gas chromatography
PAH	Polyaromatic hydrocarbon
SD	Standard deviation
OA	Organic acids
TEA	Terminal electron acceptor

List of symbols

K_H	Henry's law constant
K_d	Sorption distribution coefficient
K_{ow}	Octanol-water partitioning coefficient
Q_{10}	Temperature sensitivity ratio
C_0	Concentration of reactant at time = 0
C_{0max}	Maximum C_0 value from all treatments
$C_{0actual}$	Actual C_0 value for treatment of interest
t	Time
C	Concentration of reactant at time = t
k	Apparent rate constant (0^{th} or 1^{st} order)
k_{fast}	k representing fast regime kinetics
k_{slow}	k representing slow regime kinetics
E_a	Activation energy of reaction
R	Universal gas constant
T	Temperature

1 Introduction

1.1 Petroleum hydrocarbons (PHCs) and natural attenuation

Petroleum hydrocarbons (PHCs) are essential to the functioning of the industrialized world yet serve a potential threat to human and ecosystem health when they inadvertently enter the environment (Canadian Council of Ministers of the Environment, 2001). In addition to human toxicity risks through ingestion and exposure, soil and (ground)water ecosystems affected by PHCs are altered or reduced in their ability to support vital functions such as nutrient and carbon cycling, plant growth, and water retention (Canadian Council of Ministers of the Environment, 2001; Haider *et al*., 2021). Despite over half a century of remediation efforts to date (Mayer & Hassanizadeh, 2005), over 5000 federally recognized and currently active PHC contaminated soil sites persist in Canada (Treasury Board of Canada Secretariat, 2022). In more recent decades, recognition of natural attenuation as a viable approach to PHC remediation is increasing (Garg *et al*., 2017).

Broadly, natural attenuation encompasses abiotic and biotic PHC mass-loss, stabilization, or dilution processes which take place in the absence of engineering interventions. Abiotic processes include volatilization, sorption, and dissolution. Biotic processes include biodegradation through respiration, fermentation, and methanogenesis. For the remediation of PHC-contaminated soil, it is desirable to maximize biodegradation with the complete mineralization of PHCs into carbon dioxide (CO_2) and methane (CH_4) gases (Mozo *et al*., 2012), or incorporated into biomass. When describing remediation of the free phase, PHC natural attenuation has been referred to as natural source-zone depletion (NSZD) (Garg *et al*., 2017). Of note, the term *enhanced* natural attenuation has been recently used in the literature to refer to several different lightly engineered remediation

strategies, including manipulation of soil moisture, oxygen, and nutrient conditions to increase biodegradation rates (Kolhatkar & Schnobrich, 2017; Lv *et al*., 2018; Wegwu *et al*., 2010), and is not within the scope of this thesis.

1.1.1 Abiotic PHC natural attenuation processes

Volatilization refers to mass transfer from an aqueous or liquid (free phase) PHC into the vapour phase. The intrinsic gas-liquid partitioning (*i.e.*, volatility) of a compound is described by the temperature-dependant Henry's law constant, K_H (Illman & Alvarez, 2006). In the field, fluxes of volatile-phase PHCs from contaminated soils have been shown to be most strongly controlled by groundwater level, soil moisture, and atmospheric pressure (Marr *et al*., 2006).

Aqueous adsorption refers to mass transfer from an aqueous phase compound into the solid phase, via attraction to or a chemical bond with a solid surface. Experimental aqueous-solid adsorption partitioning can often be empirically described by the Freundlich isotherm which, in its linear form, relates concentration in aqueous and solid phases by a distribution coefficient K_d (Illman & Alvarez, 2006). K_d is an extrinsic value and is dependant on factors external to the compound's own properties. For PHCs, the value of K_d is controlled by K_{ow} (octanol-water partitioning coefficient, a physical property of the compound describing its hydrophobicity) (Kozerski *et al*., 2014) as well as properties including soil organic content and temperature (Hur *et al*., 2013; Illman & Alvarez, 2006; Shi *et al*., 2020). Although sorbed PHCs are considered immobilized, the process is usually reversible, and even slight changes in geochemistry may cause "immobilized" PHCs to desorb and re-enter the mobile phase (Illman & Alvarez, 2006). Since sorbed PHCs are considered biologically unavailable (Ehlers & Loibner, 2006), the degree of a compound's aqueous-solid partitioning can be a significant control on reaction rates involving PHC compounds.

1.1.2 Biotic PHC natural attenuation processes

Biodegradation of both natural soil organic matter, and organic contaminants such as PHCs, proceeds through a similar set of processes. Complex PHCs are first hydrolyzed into simpler intermediate metabolites (Conrad, 2020; Moscoso *et al*., 2012; Umar *et al*., 2017) which are then converted to CH_4 or CO_2 via fermentation and methanogenesis or respiration. Aerobic and anaerobic respiration (Figure 1-1A) involves the reduction of electron acceptors (EAs) such as oxygen (O_2), nitrate (NO_3^-), iron (III) (Fe^{3+}), manganese (IV) (Mn^{4+}), and sulphate (SO_4^{2-}) paired with the oxidation of an electron donor (ED) such as a PHC or another organic compound. This process of respiration produces CO_2. Where EAs are depleted, a PHC or other organic compound can act as both the EA and ED of an electron exchange through the process of fermentation, producing hydrogen (H_2) and/or acetate (Conrad, 2020; Dolfing *et al*., 2009; Gieg *et al*., 2014). These fermentation products are then consumed via methanogenesis into CO_2 and/or CH_4 (Conrad, 2020; Dolfing *et al*., 2009; Gieg *et al*., 2014).

Methanogenesis can proceed via one of two pathways (Figure 1-1B) (Conrad, 2020; Dolfing *et al*., 2009; Gieg *et al*., 2014; S. G. T. Vincent *et al*., 2021). One pathway is acetate-based methanogenesis (ABM) or aceticlastic methanogenesis, wherein acetate is fermented, producing inorganic carbon and CH_4. The other is hydrogen-based methanogenesis (HBM) or hydrogenotrophic methanogenesis, where H_2 is the electron donor and inorganic carbon is the electron acceptor, producing CH_4. The ratio of CO_2 to CH_4 in soil emissions therefore depends on the relative contributions of soil respiration, ABM, and HBM to the biodegradation of PHC and other organic compounds. Figure 1-2 illustrates this theoretical reaction network in the PHC-contaminated subsurface. At a global scale, these soil carbon fluxes in the form of CO_2 and CH_4

emissions comprise a significant contribution to atmospheric greenhouse gas (GHG) emissions (Oertel *et al*., 2016; Peters *et al*., 2011; Raich & Potter, 1995; Raich & Schlesinger, 1992).

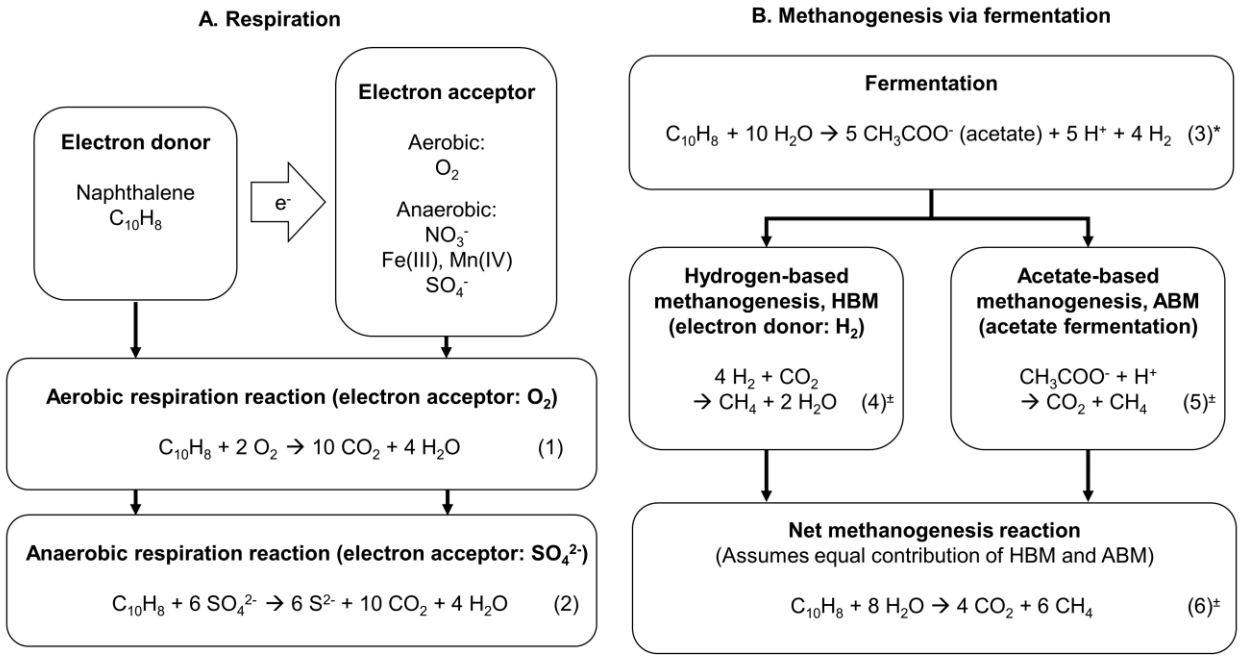

Figure 1-1. Petroleum hydrocarbon degradation via respiration (A) and methanogenesis/fermentation (B) pathways. Compiled from *Gieg *et al*. (2014) and ±Dolfing *et al*. (2009).

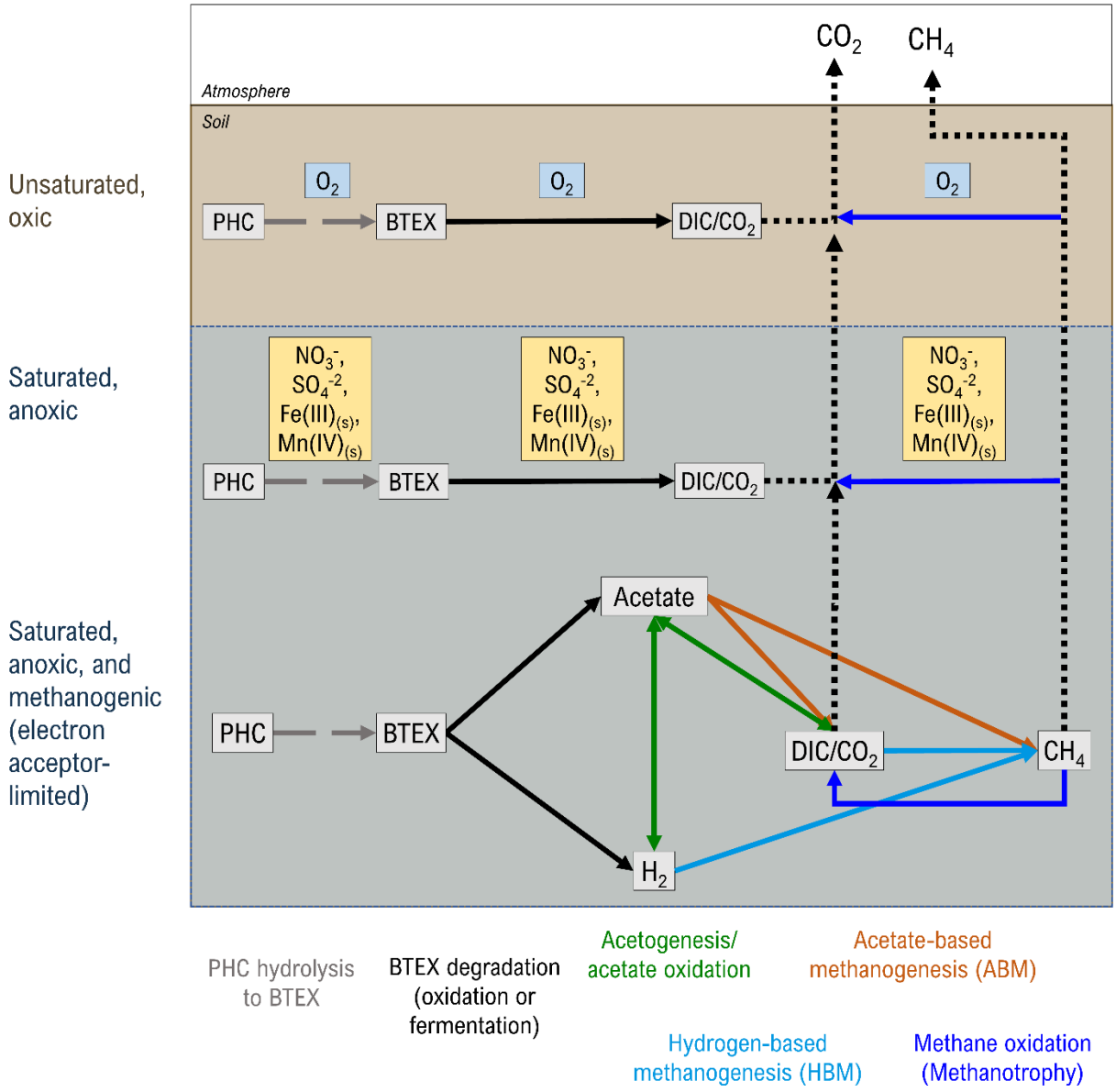

Figure 1-2. Theoretical reaction network of PHC biodegradation processes in the subsurface (Ramezanzadeh *et al*., 2023).

1.2 Environmental controls on soil biodegradation

The biodegradation of soil organic matter and petroleum hydrocarbons (PHCs) are biologically mediated processes and are therefore influenced by environmental factors such as temperature,

soil moisture, availability of O_2, availability of substrates, and pH (Illman & Alvarez, 2006; Martínez Álvarez *et al*., 2020; Yadav & Hassanizadeh, 2011). Out of these factors, temperature and soil moisture are investigated in this thesis.

1.2.1 Soil moisture control on biodegradation

The presence of water in soil is required for biological reactions to occur, being the medium for the dissolution and transport of substrates. However, the limited solubility of O_2 in water compared to air means that an excess of water-filled soil pores reduces the availability of O_2 for aerobic reactions. Thus, the trade-off between substrate and O_2 availability, and resulting microbial reaction rates, are mediated by soil moisture content (Atagana *et al*., 2003; Byun *et al*., 2021; Fairbairn *et al*., 2023; Moyano *et al*., 2012, 2013; Schjønning *et al*., 2011; Sierra *et al*., 2017; Skopp *et al*., 1990; Yadav & Hassanizadeh, 2011). In general, the optimal range of soil moisture where aerobic soil respiration is maximized is between 50 to 80% water-filled pore space (WFPS) (Byun *et al*., 2021; Fairbairn *et al*., 2023; Moyano *et al*., 2012; Schjønning *et al*., 2011; Sierra *et al*., 2017; Skopp *et al*., 1990). Similar optimal ranges have been identified for PHC biodegradation rates (Atagana *et al*., 2003; Calvo *et al*., 2009; Dibble & Bartha, 1979; Holman & Tsang, 1995; Silva-Castro *et al*., 2016; Tibbett *et al*., 2011).

Soil moisture content in the subsurface is highly spatially and temporally heterogeneous. From the upper vadose zone to the water table, there is a gradient in soil moisture from drained (~30% WFPS) or dry (<10% WFPS) to fully saturated (100% WFPS). Daily, seasonal, and longer-term variations in water table level and precipitation serve to constantly alter the distribution of this vertical gradient (Carretero & Kruse, 2012; Lautz, 2008; Tanco & Kruse, 2001; G. Vincent *et al*., 2006).

1.2.2 Soil temperature control on biodegradation

The temperature sensitivity of biological reactions, including contaminant biodegradation and associated soil respiration and methanogenesis, is described by the Q_{10} rate quotient (Barcelo Culleres *et al*., 2007; Byun *et al*., 2021). The value of Q_{10} is the ratio of two reaction rates at two temperatures 10°C or K apart (Barcelo Culleres *et al*., 2007; Davidson & Janssens, 2006) and is traditionally assumed to fall within the range of 2 to 3 for temperatures 20 to 30°C (Davidson & Janssens, 2006), representing a doubling or tripling of reaction rates for a temperature increase from 20 to 30°C. On a global scale, soil temperatures tend to follow the general latitudinal and seasonal trends of air temperatures, with higher mean annual temperatures near the equator and lower towards the poles (Lembrechts *et al*., 2022). However, soil temperatures have significantly less temporal and spatial variability than air temperatures, with the soil-air temperature differential ranging globally from a few to 20°C in certain biomes (Lembrechts *et al*., 2022; Zheng *et al*., 1993).

1.2.3 Climate change impacts on soil temperature and moisture

Soil temperature and moisture, two dominant controls on PHC biodegradation and soil respiration rates (Aislabie *et al*., 2006; Chang *et al*., 2011), are themselves dictated by local climate conditions. Therefore, climate and its trajectory are overarching considerations in any discussion about long term controls on PHC biodegradation and associated soil respiration.

The effects of climate change on soil moisture are difficult to generalize, as soil moisture is predicted to increase in some regions and decrease in others (Bradford *et al*., 2019; Lal *et al*., 2023). However, on average, more drying trends are expected than wetting trends, which is

globally correlated to regions with decreasing precipitation and/or increasing evapotranspiration and temperature (Lal *et al*., 2023).

The average global surface air temperature has increased by 1.1°C since the pre-industrial period, and the increase is expected to reach 1.5°C by 2040 (IPCC, 2023). However, in Canada the observed and projected increase in temperature is double that the global average, and four times the global average in northern regions (X. Zhang *et al*., 2019). This air temperature increase is expected to be reflected in global soil temperatures as well (Bradford *et al*., 2019). As described above, warmer soil temperatures have implications on the rates of biological soil processes such as respiration and methanogenesis. Warming cold region soils are also experiencing an increased incidence of freeze thaw cycles as soils experience decreasing snow cover and soil temperatures fluctuating above and below freezing in the winter (Henry, 2008; Y. Zhang *et al*., 2005). Freeze thaw cycles lead to an increase in net carbon dioxide CO_2 and CH_4 emissions compared to more stable soil temperature conditions (Priemé & Christensen, 2001; Ramezanzadeh *et al*., 2023; Yang *et al*., 2023; Zhu *et al*., 2009) and increased bioavailability of soil organic carbon (Ramezanzadeh *et al*., 2023).

1.3 Greenhouse gas fluxes from PHC contaminated sites

GHG fluxes from PHC contaminated soils have been shown to be higher than in unaffected soils (Martin *et al*., 2016; Sihota *et al*., 2011; Wozney *et al*., 2021). The increase in this total soil-respired (TSR) carbon flux (Sihota *et al*., 2011; Wozney *et al*., 2021) is mostly attributable to an increase in the contaminant-related soil respiration (CSR) component of total flux. Wozney *et al.* (2021) and Sihota *et al.* (2011) define TSR flux as the sum of CSR and background natural soil respiration (NSR) (*i.e.*, TSR = CSR + NSR). The common approach to distinguishing NSR from

CSR is to measure NSR at comparable uncontaminated site and subtract this reference NSR from TSR measured at contaminated locations to obtain CSR, but other methods like isotopic tagging have recently been explored (Sihota *et al*., 2011; Sihota & Mayer, 2012; Wozney *et al*., 2021).

At the global scale, the contributions of CSR-derived soil GHG emissions are likely very small compared to total soil GHG emissions – from values in the literature, it is roughly estimated that GHG emissions from CSR are 6 orders of magnitude less than total GHG emissions from all soil respiration in Canada (based on figures cited for average global soil GHG flux (Oertel *et al*., 2016), fractions of CSR contributions to TSR measured at one PHC contaminated field site (Wozney *et al*., 2021), and total size of PHC contaminated soil sites in Canada (Treasury Board of Canada Secretariat, 2022)). However, an understanding of CSR and NSR contributions may be important for contaminated-sites project managers or researchers interested in soil carbon fluxes at the site-scale, including the over-5000 PHC-contaminated soil sites in Canada (Treasury Board of Canada Secretariat, 2022).

1.4 Thesis objectives

The objective of this thesis was to investigate the influence of soil moisture, O_2, and temperature on the rates and pathways of PHC biodegradation and associated soil respiration and methanogenesis processes. I pursued these investigations through laboratory soil microcosm incubation experiments and curve fitting analyses using common reaction kinetics and temperature sensitivity models.

The specific objective of Chapter 2 was to address how the kinetics of naphthalene biodegradation are influenced by soil moisture and oxygen availability. The specific objective of Chapter 3 was

to investigate how aerobic and anaerobic soil respiration and methanogenesis rates are affected by temperature in the presence of naphthalene.

1.5 Thesis outline

This thesis is composed of four chapters, including the current Chapter 1. Chapter 2 is a manuscript on which I am the first author. A modified version of Chapter 2 has been submitted as a standalone document for publication to the Journal *Frontiers in Environmental Chemistry*. The chapter describes a soil microcosm experiment where soil was spiked with naphthalene and incubated under different soil moisture and headspace O_2 conditions to investigate naphthalene biodegradation kinetics under these different conditions. Chapter 3 describes another soil microcosm experiment incubated under different temperature and headspace O_2 conditions to investigate the temperature sensitivity of aerobic and anaerobic soil respiration and methanogenesis processes in the presence of naphthalene. Chapter 4 summarizes research findings from the previous chapters and proposes recommendations for future research. Following Chapter 4, Appendices I and II contain additional experimental results and discussion that were omitted from Chapters 2 and 3.

Naphthalene biodegradation kinetics under variable soil moisture and oxygen availability

Jane Ye[a*], Fereidoun Rezanezhad[a], Stephanie Slowinski[a], Mehdi Ramezanzadeh[a], Marianne Vandergriendt[a], Philippe Van Cappellen[a]

[a] Ecohydrology Research Group, Department of Earth and Environmental Sciences and Water Institute, University of Waterloo,
200 University Avenue West, Waterloo, Ontario, Canada, N2L 3G1

[*]Corresponding author: Jane Ye
Ecohydrology Research Group, Department of Earth and Environmental Sciences and Water Institute, University of Waterloo
200 University Avenue West, Waterloo, Ontario, Canada, N2L 3G1
jxjye@uwaterloo.ca

A modified version of this chapter has been submitted to *Frontiers in Environmental Chemistry*.

2 Naphthalene biodegradation kinetics under variable soil moisture and oxygen availability

2.1 Introduction

Natural attenuation processes of petroleum hydrocarbons (PHCs) in the subsurface include volatilization, sorption, and biodegradation (Illman and Alvarez, 2006). For the remediation of PHC-contaminated soils, the preferred outcome is complete mineralization of PHCs by the resident microorganisms (Mozo *et al.*, 2012). Where microbial communities with the capacity for PHC biodegradation are present, biodegradation rates of PHCs are primarily controlled by temperature, moisture content, pH, redox state, and substrate availability, accessibility, and potential toxicity (Illman and Alvarez, 2006; Martínez Álvarez *et al*., 2020; Yadav and Hassanizadeh, 2011).

The role of moisture content in mediating soil microbial activity has been extensively addressed and has usually been linked to a trade-off between O_2 and dissolved substrate availability to microbial cells (Atagana *et al*., 2003; Byun *et al*., 2021; Fairbairn *et al*., 2023; Moyano *et al*., 2013, 2012; Schjønning *et al*., 2011; Sierra *et al*., 2017; Skopp *et al*., 1990; Yadav and Hassanizadeh, 2011). Supply of O_2 to the pore water is enhanced at lower soil moistures, while solute transport is enhanced at higher soil moistures. Aerobic PHC biodegradation should therefore be maximized at some intermediate soil moisture level, where the trade-off between dissolved O_2 and substrate availability is optimized (Schjønning *et al*., 2011; Skopp *et al*., 1990). In general, the optimal soil moisture for aerobic activity is in the range ~50-80% saturation (Atagana *et al*., 2003; Byun *et al*., 2021; Calvo *et al*., 2009; Fairbairn *et al*., 2023; Moyano *et al*., 2012; Schjønning *et al*., 2011; Sierra *et al*., 2017; Skopp *et al*., 1990).

Previous laboratory studies have investigated the effect of soil moisture on PHC biodegradation in soils. Dibble and Bartha (1979) reported oil sludge biodegradation over a broad range of soil moisture, from 30 to 90% WFPS. Holman and Tsang (1995) found favorable soil moisture conditions for aromatic hydrocarbon biodegradation to be within 50-70% WFPS. These authors remarked that the optimal soil moisture was compound-specific and likely also dependent on soil composition. Atagana *et al.* (2003) similarly observed peak biodegradation of creosote at 60-70% WFPS. Tibbett *et al.* (2011) investigated the biodegradation of petrogenic oil; they identified an optimal soil moisture range of 40-70% WFPS, with maximal microbial activity around 60% WFPS. In their review paper, Calvo *et al.* (2009) proposed that soil hydrocarbon biodegradation generally requires soil moisture between 50 and 80% WFPS. Within this range of soil moisture, PHC biodegradation activity is further affected by the soil type, nutrient availability, microbial community structure, and the identity of the PHC compound (Holman and Tsang, 1995; Kebede *et al*., 2021; Silva-Castro *et al*., 2016; Wu *et al*., 2017). The range of chemical properties of PHC compounds spans across several orders of magnitude. Naphthalene, being semi-volatile and with a density slightly higher than water, is most representative of mid-weight PHC compounds.

In soils, the moisture content exhibits large spatial and temporal changes. Across the vadose zone, drier conditions in the topmost layer are progressively replaced by fully saturated conditions at the water table. Transpiration by vegetation, droughts, rain plus snowmelt events, and groundwater extraction further cause transient soil moisture patterns, including at PHC-contaminated sites. Given this variability, there is a need to better delineate the effects of soil moisture on PHC biodegradation, especially because changes in moisture content co-vary with the redox controls on microbial activity. In this study, we conducted a soil microcosm incubation experiment in which different soil moisture contents were imposed to modulate the relative contributions of oxic and

anoxic biodegradation of the model PHC compound naphthalene. Soil incubations with 60, 80, and 100% water-filled pore space (WFPS) were run under oxic headspace, and with 100% WFPS under anoxic headspace. Over the 44-day incubation, headspace gas concentrations, porewater geochemistry, and total soil naphthalene were monitored periodically. We hypothesized that the observed naphthalene biodegradation rates would reflect the variable combinations of oxic and anoxic regimes in the microcosms.

2.2 Materials and methods

2.2.1 Soil collection and characterization

Soil cores were collected from a former PHC-contaminated industrial site in London, Ontario, Canada. The site was used from the early 1950s to 2001 for storage and distribution of various petroleum products. The cores (~75 cm long) were obtained from 1.4 to 2.3 m below ground surface, straddling the water table. The soil cores were sealed after flushing with nitrogen and kept at 4°C until used in the laboratory experiments.

The soil from several cores and grab samples was homogenized and then dried at room temperature for 8 weeks either open to the air or under a dinitrogen-only atmosphere. The total porosity and bulk density of the homogenized and dried soil samples were determined gravimetrically from the saturated mass, the oven-dried mass (at 105°C for 48 hours), the original sample volume, and an assumed particle density of 2.65 g cm^{-3}, following the method of Hao *et al.* (2008). The average bulk density and porosity of the homogenized and dried soil were 1.53 g cm^{-3} and 0.39, respectively.

Particle size distributions were analyzed via laser diffraction by suspending samples in a 4%-w/w sodium metaphosphate solution for several hours on a stir plate, then pipetting suspended samples into a wet dispersion unit feeding into a Analysette 22 Microtec Plus particle size analyzer (Fritsch, Germany). Based on the Wentworth grain size scale (Wentworth, 1922), almost all particles were silt-sized or smaller, with the majority falling in the range of medium to coarse silt. There was also a significant portion (18%) of clay-sized particles and a very small presence of fine sand (a representative particle size distribution is shown in Figure AI-1).

Soil organic carbon (OC), total carbon (TC), organic nitrogen (ON), and total nitrogen (TN) were measured via combustion and thermal conductivity detection on a CHNS Elemental Analyzer (Carlo Erba Elementar vario EL cube NA-1500; method detection limit, MDL: 1% by mass for all). Measured TC was 1.86%. OC, ON, and TN were below detection. The soil is an inorganic clayey silt with moderate plasticity, classified as an MH silt within the USCS scheme (ASTM Standard D2488 − 09a, 2009). Additionally, X-ray diffraction spectroscopy analysis (Empyrean II diffractometer, Malvern PanAnalytical) revealed the mineralogy to be composed of approximately 33% carbonate minerals (dolomite, calcite, ankerite) with the remainder made up of silicate minerals.

The soil was analyzed for Total Petroleum Hydrocarbon (TPH) fractions present at the time of core collection (*i.e.*, background hydrocarbons) by ALS Environmental Laboratory in Waterloo, Canada. TPH analysis was conducted according to the Canadian Council of Ministers of the Environment Tier 1 methods (Canadian Council of Ministers of the Environment, 2016). F1 hydrocarbons were present at <5.0 μg g^{-1} (MDL: 5 μg g^{-1}), F2 hydrocarbons at 262 μg g^{-1} (MDL:

10 µg g^{-1}), F3 hydrocarbons at 351 µg g^{-1} (MDL: 50 µg g^{-1}), F4 hydrocarbons at <50 µg g^{-1} (MDL: 50 µg g^{-1}), and TPH at 613 µg g^{-1} (MDL: 72 µg g^{-1}).

2.2.2 Naphthalene sorption experiments

Naphthalene sorption isotherms to the soil were measured at 25±2°C in 125 mL amber jars each containing 80 g of undried soil and topped up to no headspace with Milli-Q water spiked with dissolved naphthalene at three concentrations: 1.25, 2.5, and 5 mg L^{-1}. The soils, jars and solutions were sterilized as described in section *2.2.3*. The aqueous naphthalene concentrations were determined before starting the incubations and after 48 hours of equilibration. The naphthalene concentrations were measured according to the methodology described in section *2.2.4.2*.

2.2.3 Soil incubation experiment

Incubations were prepared by adding 80 g of homogenized, dried soil to 250 mL wide-mouthed clear glass jars. The total headspace volume in each jar was 197 mL. The jars were kept open in a fume hood or anaerobic chamber to equilibrate for 4 days with either air (oxic) or N_2 gas (anoxic). Oxic jars were further flushed with excess O_2 prior to capping to prevent depletion of oxygen during the incubation. Next, the soil moisture content in the oxic jars was adjusted to 60%, 80%, and 100% WFPS using an artificial pore water (APW) solution containing 1 mmol L^{-1} $KHCO_3$, 0.15 mmol L^{-1} $MgCl_2$, 0.8 mmol L^{-1} $CaCl_2 \cdot 2H_2O$, and 1 mmol L^{-1} $NaHCO_3$ by dissolving high purity salts (Sigma Aldrich) into Milli-Q water while stirring at room temperature. The APW composition was designed to match the composition of the native soil porewater. The soil in the anoxic jars was fully saturated (100% WFPS) with APW that was sparged beforehand with N_2 gas to a dissolved O_2 concentration below 2.6 mg L^{-1}. The total APW volumes added to the jars were

13, 18, 22, and 28 mL for the 60% WFPS oxic, 80% WFPS oxic, 100% WFPS oxic, and 100% WFPS anoxic treatments, respectively.

The different soil moisture treatments and their controls are illustrated in Figure 2-1. The "Nap" treatments were spiked with aqueous naphthalene ($C_{10}H_8$), while the "No Nap" controls did not receive naphthalene. For the Nap experimental treatments, the APW was spiked with 5 mg L^{-1} (39 µmol L^{-1}) naphthalene, prepared by dissolving naphthalene crystals (Sigma Aldrich, >99%) in Milli-Q water for one week at room temperature under continuous mixing. The "Abiotic" controls were prepared by autoclaving soil three times over five days at 121°C and 15 psi for one hour. The controls further received aqueous mercuric chloride ($HgCl_2$) at a concentration of 2.21 mmol kg^{-1} at the same time APW with naphthalene was added. All jars, lab apparatus, and solutions that contacted the sterile soil were autoclaved before use, at 120°C and 15 psi for 30 minutes.

The jars were capped airtight with Teflon®-facing lids and incubated at 25°C. The experiment lasted for a minimum of 44 days, during which jars were sacrificially sampled at 5-6 time points. The oxic headspace treatments were sampled at 2, 9, 17, 30, 38, and 44 days, the anoxic headspace treatments at 2, 9, 17, 30, and 44 days. The 100% WFPS oxic and 100% WFPS anoxic incubations were sampled again at 58 and 100 days, respectively. Triplicate jars were prepared for each sacrificial sampling point, for a total of 156 jars incubated. The anoxic jars were incubated in N_2-flushed anaerobic glove bags to prevent O_2 contamination. The initial O_2 in oxic incubations was 49% v/v after flushing with excess O_2, and 2% v/v in anoxic incubations after equilibration with the N_2-flushed anaerobic chamber.

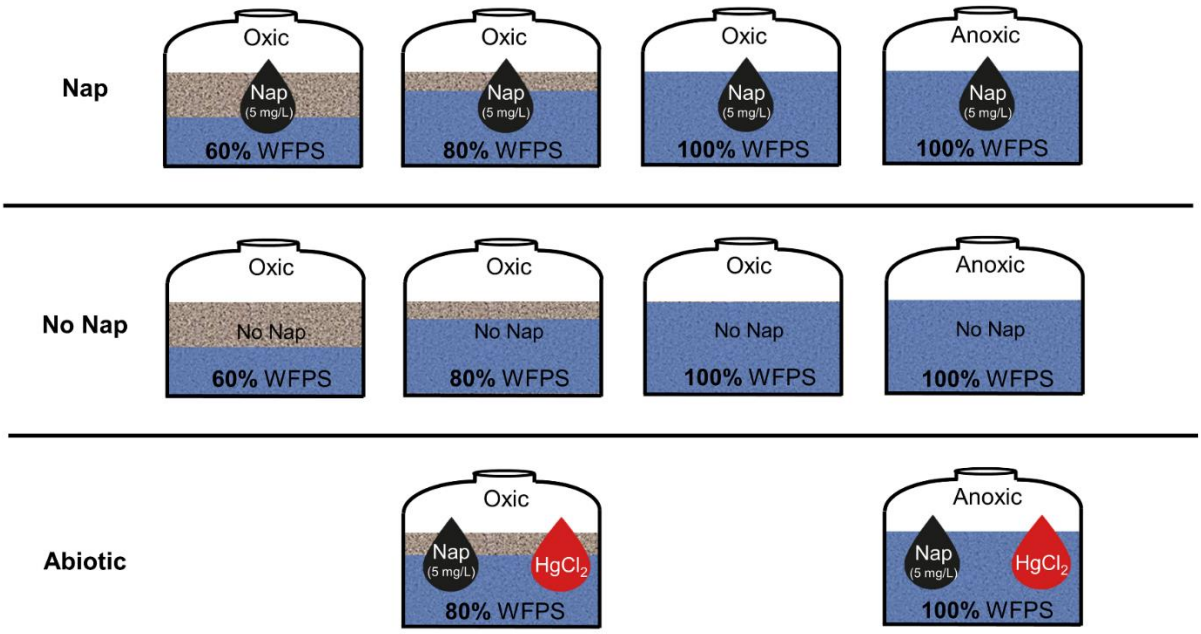

Figure 2-1. Experimental design: 60%, 80%, and 100% WFPS with oxic headspace, and 100% WFPS with anoxic headspace. "Nap" treatments were spiked with aqueous naphthalene, "No Nap" treatments were not spiked. "Abiotic" treatments were spiked with aqueous naphthalene and sterilized with a combination of autoclaving and mercuric chloride ($HgCl_2$) addition.

2.2.4 Sampling and analytical methods

2.2.4.1 Gas analyses

At each sampling time point, headspace gas samples were collected in 10-mL Luer-Lok™ syringes from the sacrificed jars by piercing the septum of the lid. Aliquots of a gas sample were then transferred into Luer-Lok™ syringes pre-filled with helium gas to dilute the sample into the calibration range. The diluted gas samples were injected into a gas chromatograph (Shimadzu, Model GC-2014) equipped with a flame ionization detector and methanizer (for CO_2 and CH_4) and thermal conductivity detector (for O_2).

2.2.4.2 Porewater extraction and geochemistry analyses

To extract porewater, soil was transferred from the jar into 50 mL Nalgene® Oak Ridge Teflon® FEP Centrifuge Tubes (Thermo Fisher Scientific) and centrifuged at 5000 rpm and 4°C for 30 minutes and then collecting the supernatant. However, this method only yielded about 0.5 mL pore water for the 60% WFPS treatment. Therefore, to increase the volume of water required for the analyses, jars were topped up with known volumes of ultrapure Milli-Q filtered water to reach 100% WFPS. Next, these jars were gently agitated upright on a shaker plate at 150 rpm for 1 hour before centrifugation of the soil suspension in the same way as the other treatments. Aliquots of the supernatant solutions were used for the analyses described below.

The pH was measured with a handheld pH probe (LAQUA Twin meter, model B-213, Horiba) on the unfiltered porewater samples. Approximately 0.5 mL of sample was filtered through a 0.2 µm pore size nylon membrane syringe filter (Choice^{TM}, Thermo Fisher Scientific) into a glass vial and preserved with 10 mg L^{-1} chromate and stored at -20°C for later analysis. Fluoride (F^-), chloride (Cl^-), nitrite (NO_2^-), nitrate (NO_3^-), sulfate (SO_4^{2-}), bromide (Br^-), phosphate (PO_4^{3-}), lactate, propionate, formate, butyrate, pyruvate, succinate, citrate, and acetate were measured using ion chromatography (IC, Dionex ICS-5000 with a capillary IonPac® AS18 column; ± 3.0% error and ± 1.6% precision; MDL: 0.59, 1.29, 1.13, 1.47, 6.66, 1.16, 0.81, 0.43, 0.84, 1.49, 0.37, 0.31, 0.57, 1.81, 0.65 µmol L^{-1}, respectively).

Naphthalene concentrations in the porewater were determined using a solvent micro-extraction technique: 2 mL of porewater sample were transferred to a 5 mL glass vial and 1 mL of dichloromethane solvent extractant spiked with metafluorotoluene tracer was added to the vial. The vial was capped with a Teflon®-facing septum and shaken for 20 min at 350 rpm, then left

inverted for 30 min. The dichloromethane extractant was removed from the vial using a 1 mL gas-tight glass syringe and transferred into a 1 mL glass vial. The extractant was analyzed on an Agilent 7890A Gas Chromatograph (Agilent Technologies) at 275°C after passage through a capillary column. The naphthalene concentration was measured using a flame ionization detector (MDL: 5 μg L^{-1}).

2.2.4.3 Total soil hydrocarbon analysis

After centrifuging and decanting the supernatant, the hydrocarbon concentration of the remaining soil material was analyzed by ALS Environmental Laboratory for quantification of polyaromatic hydrocarbon (PAH) compounds, including naphthalene, at each of the sampling time points. The PAH analysis was conducted using SW-846 Methods 3510 and 8270, which are comparable to the dichloromethane solvent extraction/GC analysis method described in section *2.2.4.2*. Triplicate sets of samples were composited into a single sample for analysis by ALS. Total soil naphthalene mass was then calculated by summing up the mass of naphthalene measured in the decanted porewater (section *2.2.4.2*) and that of the remaining soil material. Hereafter, the "total" soil naphthalene mass or concentration refers to the summed mass or concentration (per unit mass dry soil). The MDL for total soil naphthalene was 0.081 μmol-C or 0.013 μg g^{-1}. Further note that hereafter the difference between total soil naphthalene mass and aqueous naphthalene mass is referred to as the sorbed-phase naphthalene mass.

2.3 Results

2.3.1 Biogeochemistry

The gas and porewater chemistry results of the No Nap treatments closely followed those of the Nap treatments. In the biotic incubations (Nap and No Nap), headspace CO_2 accumulation over the course of the incubations was observed, as indicated by the positive (+) values in Table AI-1.

Accumulation of CO_2 was an order of magnitude lower in the abiotic controls (Table AI-1) confirming effective sterilization. Net CH_4 accumulation in the biotic oxic headspace treatments (i.e., 60, 80, and 100% WFPS) was negligible ($\leq 10^{-2}$ µmol L^{-1}). By contrast, in the biotic 100% WFPS anoxic treatment headspace CH_4 accumulation was order of magnitude higher (~1 µmol L^{-1}). This CH_4 accumulation, in combination with evidence from the isotopic evolution of CH_4 and CO_2 (Figure AI-2), confirms the development of methanic conditions in the 100% WFPS anoxic treatment despite minor contamination with O_2 during the course of the incubation (Table AI-1). In the oxic incubations, the headspace remained oxygenated (>16% v/v) throughout the incubations (Table AI-1).

The pore water NO_3^- concentration increased from Day 0 to Day 2 in the Nap and No Nap biotic and oxic jars followed by values decreasing to near-detection (Figure 2-2A). In the 100% WFPS anoxic treatment, the NO_3^- concentration remained near zero over the entire experimental duration. The 60% WFPS oxic treatment saw the highest initial NO_3^- peak concentration and the longest period of subsequent decline. While the abiotic controls also experienced an initial increase in the NO_3^- concentration, the subsequent drop in concentration was not observed. The NO_2^- concentrations followed similar trends as for NO_3^- in the different treatments and controls (data not shown). Thus, overall, the results indicate that NO_3^- and NO_2^- were released to the pore water

from the original soil and, in the biotic incubations, were subsequently used as a terminal electron acceptor (TEA) by the soil microbial community.

The pore water SO_4^{2-} concentrations increased in all treatments during the first 1-2 weeks and then plateaued at near-constant values (Figure 2-2A). The plateau SO_4^{2-} concentrations were highest in the 60% WFPS oxic treatment and decreased in the biotic treatments with increasing WFPS (60% > 80% > 100%). The lowest plateau SO_4^{2-} concentrations were found in the 100% WFPS anoxic treatment. Moreover, the SO_4^{2-} plateau concentrations in the abiotic controls were higher than in the corresponding biotic treatments (i.e., at 80 and 100% WFPS). Thus, as for NO_3^- and NO_2^-, the SO_4^{2-} originated from the soil itself, while the systematic difference between abiotic and biotic jars suggests that some of the released SO_4^{2-} may have been consumed in the biotic treatments.

Significant accumulation of pore water acetate and propionate occurred after Day 9 in all the oxic (60, 80, and 100% WFPS) treatments (Figure 2-2B). By contrast, the concentrations of these organic acids (OAs) increased right from the start of the 100% WFPS anoxic incubations (that is, peak values were reached by the first sampling point on Day 2). The OA concentrations were also 1-2 orders of magnitude higher than in the oxic treatments. Similar patterns to those of acetate and propionate were observed for the lactate, formate, butyrate, and succinate concentrations (data not shown). Pyruvate and citrate concentrations did not exhibit any discernable temporal trends (data not shown). Note that OA data were not available for the abiotic controls because of the interference of mercuric chloride with low molecular weight OAs in the chromatograms.

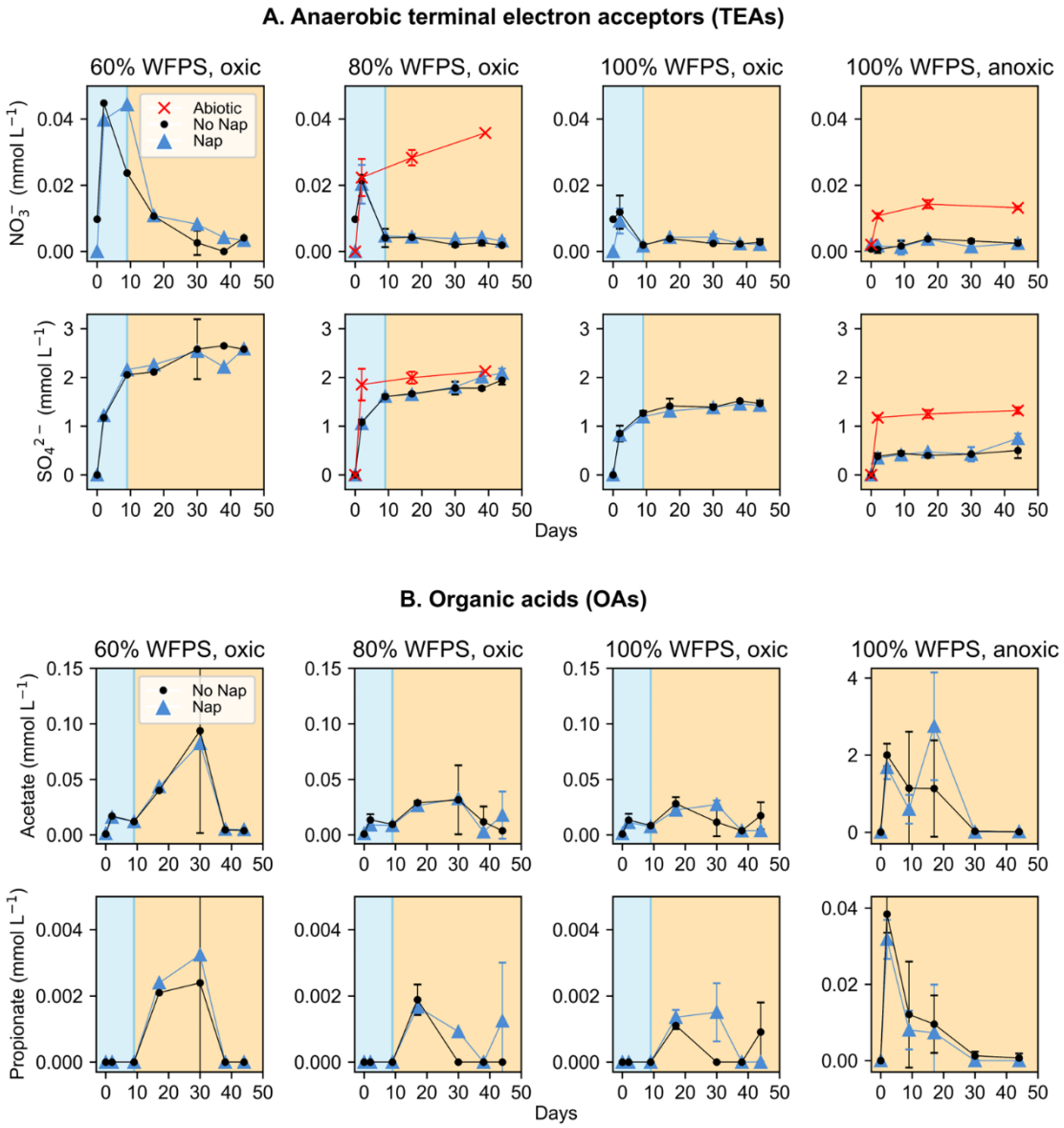

Figure 2-2. Time series of (A) nitrate (NO_3^-) and sulphate (SO_4^{2-}) alternative TEA and (B) acetate and propionate OA concentrations. Data shown are the average of triplicate samples at each sampling time point, with error bars representing one SD. Where no error bars are seen in the 60% oxic and 80% oxic conditions, triplicate jars did not yield enough sample volume to analyze, and SD could not be calculated. In some cases, SD of triplicate averages was quite high, and the full extent of the error bars is not shown to display the average trends more clearly. Day 0 data for all components shown were not measured but assumed to be zero, as the initial artificial porewater composition did not contain any NO_3^-, SO_4^{2-}, or organic acids. Blue and orange shaded zones approximately correspond to fast and slow kinetic phases, respectively.

2.3.2 Naphthalene sorption

After 48 hours of reaction time, the sorbed fraction of naphthalene in the sorption experiment was 80% at all concentrations tested (Figure AI-3). Shi *et al.* (2020) showed that naphthalene sorption reached near-equilibrium within 2 hours, thus it is reasonable to treat naphthalene sorption as an instantaneous process in our study. The Day 0 starting masses of aqueous naphthalene in Figure 3A were therefore assumed equal to 20% of the initial total naphthalene masses added.

2.3.3 Time series data: aqueous naphthalene

The mass of aqueous naphthalene decreased exponentially with time in all Nap incubations (Figure 2-3A). In the 60, 80, and 100% WFPS oxic treatments the aqueous naphthalene measurements were above the detection limit (MDL) for the first 2, 2, and 30 days of incubation, respectively. In the 100% WFPS anoxic Nap treatment, the aqueous naphthalene remained detectable for the full duration of the experiment. In the abiotic controls, the mass of aqueous naphthalene also decreased but with values remaining higher than in the corresponding biotic incubations.

In line with previous studies (see discussion in Mozo *et al.*, 2012), we assumed that volatilization occurred only from the aqueous phase. The fraction of the initial total naphthalene that was volatilized was then calculated from the difference between the initial mass of aqueous naphthalene mass and that after equilibration in the abiotic controls. Based on the visual inspection of the abiotic control data in Figure 2-3A, equilibrium between aqueous and gaseous naphthalene was assumed to have been reached by Day 2 in the 80% WFPS oxic treatment and Day 15 in the 100% WFPS anoxic treatment, resulting in volatilized fractions of 13 and 12%, respectively. Linear extrapolation of these estimates to the biotic treatments without corresponding abiotic

controls, then yielded volatilized fractions of 13.5 and 12.5% in the oxic 60% and 100% WFPS treatments, respectively.

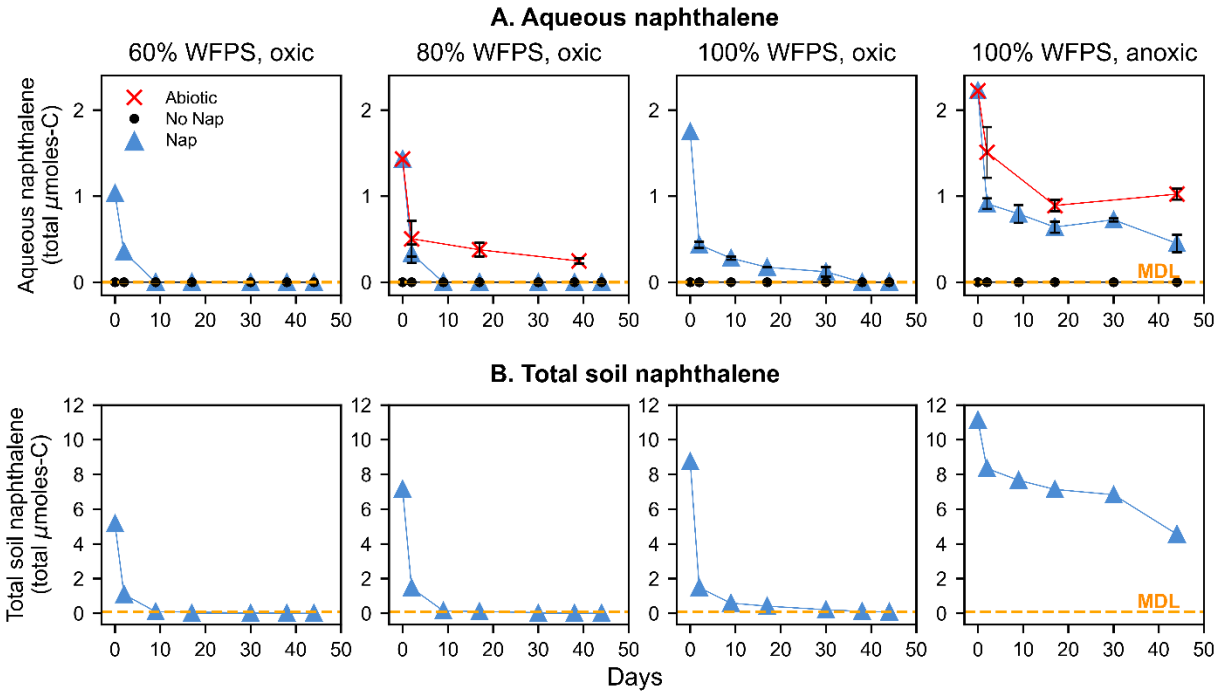

Figure 2-3. Time series of the masses of (A) aqueous phase naphthalene and (B) total soil naphthalene (representing the sum of aqueous and sorbed phases, see section *2.2.4.3*). Aqueous phase naphthalene data shown in panel A are the averages of the triplicate samples collected at each time point, with error bars representing one SD. Where no error bars are seen in the 60% oxic and 80% oxic conditions, triplicate jars did not yield enough sample volume for analysis, and a SD could not be calculated. For panel B, at each sampling time point, there is only one measurement of total soil naphthalene that was measured on the composite sample of all triplicate samples. Non-detect measurements are shown as zero values for visualization purposes. See sections *2.3.3* and *2.3.4* for further details.

Following the approach of Pathak *et al.* (2009), we calculated for each biotic treatment the "effective initial naphthalene mass" as the initial total naphthalene mass × (1 – volatilized fraction). The results are summarized in Table AI-2. The effective initial naphthalene masses were assumed to represent the actual masses of naphthalene that were potentially available to microorganisms

for biodegradation. The effective initial naphthalene masses were used in the analysis of degradation kinetics (section *2.4.3*). Note that the effective initial naphthalene mass corresponds to the sum of the total soil plus aqueous naphthalene mass. Assuming the volatilized fraction remained constant throughout the incubation, use of the effect initial naphthalene mass essentially accounts for naphthalene mass in the volatile phase in section *2.4.3*.

2.3.4 Time series data: total soil naphthalene

The total soil naphthalene masses in the Nap treatments followed temporal trends paralleling those observed for the aqueous naphthalene (Figure 2-3B). In the 60, 80, and 100% WFPS oxic incubations, total soil naphthalene was detectable (*i.e.*, above the MDL) until Day 9, 17, and 44, respectively. An additional measurement of total soil naphthalene on Day 58 of the 100% WFPS oxic incubation was below the MDL (data not shown). In the 100% WFPS anoxic incubation, the total soil naphthalene mass was still slightly above the MDL in an additional sample collected on Day 100 (data not shown).

2.4 Discussion

2.4.1 Biogeochemical regimes

The similarities in pore water and headspace chemistry in the Nap and No Nap treatments imply that the naphthalene additions did not significantly change the biogeochemical trajectories in the incubations. In what follows we therefore assume that the microbial degradation of the soil organic matter represents the main driver of the observed biogeochemical changes, and that added naphthalene was being biodegraded as a secondary substrate.

Across the biotic incubations, initial conditions ranged from most oxic in the 60% WFPS treatments to the most reducing in the 100% WFPS anoxic treatments. In the oxic treatments, the data imply that both dissolved O_2 supplied by the oxygenated headspace and NO_3^- leached from the soil were utilized as terminal electron acceptors (TEAs) in microbial respiration. While the microbial reduction of other TEAs, including SO_4^{2-}, in the oxic incubations cannot be excluded, subsequent re-oxidation of the reduced forms of the TEAs may have masked their utilization. Note that, for the oxic treatments, the differences in the maximum NO_3^- concentrations, as well as the variable values at which the SO_4^{2-} concentrations stabilize can be accounted for by the different moisture contents, that, is the different soil to pore water ratios.

By contrast to the oxic incubations, no initial pore water build-up of NO_3^- was observed in the 100% WFPS anoxic treatment, which we attribute to the rapid consumption of any NO_3^- released from the soil before the first sampling on Day 2. This interpretation is consistent with the accumulation of NO_3^- in the abiotic 100% WFPS anoxic control. Similarly, the differences in pore water SO_4^{2-} concentrations between the biotic and abiotic 100% WFPS anoxic incubations suggest microbial SO_4^{2-} reduction during the very early stage of the anoxic treatment (*i.e.*, before Day 2).

All the biotic treatments, oxic and anoxic, as well as Nap and No Nap, exhibited the production of small organic acids, including acetate and propionate, followed by their subsequent removal from the pore water (Figure 2-3B). These organic acids, which are known byproducts of soil organic matter degradation under anoxic conditions (*e.g.*, Cozzarelli *et al*., 1994), appear right from the start of the experiment in the 100% WFPS anoxic treatments. As expected, in the oxic treatments the presence of strong TEAs, including O_2 and NO_3^-, not only delays the first appearance of the organic acids but also limits their build-up to much lower concentrations than in the 100% WFPS

anoxic treatment. The observed CH_4 concentrations in the 100% WFPS anoxic treatment suggest that the progressive removal of organic acids with time may be due to their mineralization under methanogenic conditions. Much lower production rates plus reoxidation of any CH_4 produced explain the absence of measurable headspace CH_4 in the oxic treatments.

Overall, the evidence shows that microbially-mediated transformations ranging from aerobic respiration to methanogenesis occurred in the experimental incubations. In the variable moisture oxic treatments, the initial 1-2 weeks revealed a dominant role of O_2, followed by progressively more reducing conditions during which biogeochemical signatures indicative of anaerobic respiration and fermentation were observed. The pace at which conditions became more reducing in the oxic treatments accelerated with increasing moisture content, from 60 to 100% WFPS, because of decreasing porewater O_2 availability. In the 100% WFPS anoxic treatment, the conditions became methanic within days. In the next section, we assess how the different biogeochemical regimes affect the biodegradation of naphthalene.

2.4.2 Naphthalene biodegradation: time scales

The durations for the naphthalene measurements to fall below the method detection limit (MDL) in the biotic treatments are plotted in Figure 2-4 with the solid symbols and connecting solid line. The data seem to imply a systematic increase in the time scale of naphthalene degradation with increasing moisture content for the oxic treatments. This trend is somewhat misleading, however, because the added volume of naphthalene-spiked artificial pore water (APW) varied between the different moisture content conditions (section *2.2.3*). Note that the APW volumes were adjusted to obtain comparable aqueous naphthalene concentrations across the different % WFPS tested.

Hence, the starting total soil naphthalene concentration, C_0 expressed in µg g^{-1}, was lowest in the 60% WFPS incubations and highest in the 100% WFPS incubations.

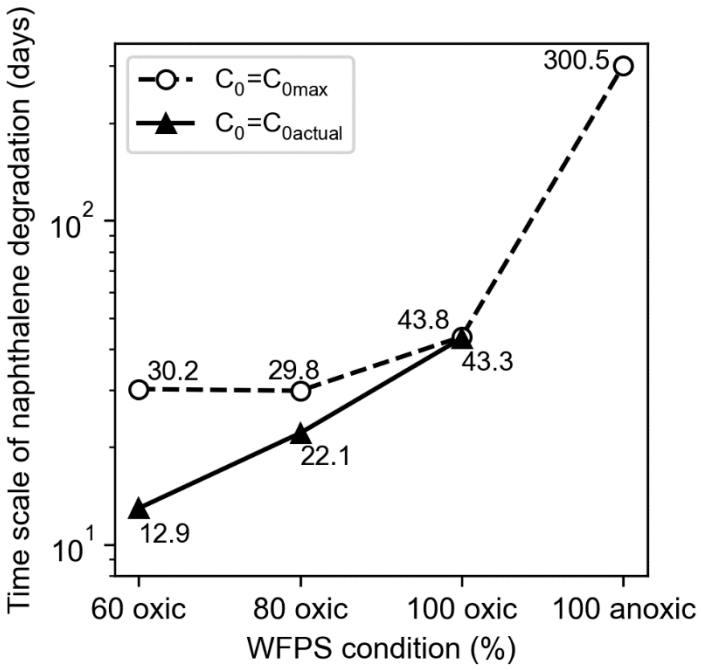

Figure 2-4. Time scales of naphthalene biodegradation (*i.e.,* the number of days of incubation until the total soil naphthalene reaches the method detection limit or MDL) in the different experimental treatments. The full black triangles represent time scales calculated with the actual initial total soil naphthalene concentrations (C_0) values in the incubations, the open black circles represent time scales calculated when imposing the same initial total soil naphthalene concentrations (C_{0max}) to all treatments as that in the 100% WFPS anoxic treatment. The time scales (values in days are indicated next to the data points) are calculated as the time required for the concentration to drop to the MDL (0.013 µg g^{-1}, section *2.2.4.3*) using the linear kinetics model presented in section *2.4.3*.

To account for the differences in initial total soil naphthalene masses added, the observed durations in Figure 2-4 are compared to the hypothetical values if all incubations would start with the same initial concentration (C_{0max} in Figure 2-4) as the 100% WFPS anoxic treatment (i.e., C_{0max} is the actual C_0 in the 100% WFPS anoxic treatment). The new durations, indicated by the open symbols and broken connecting line, are estimated using the linear rate model discussed below in section

2.4.3. When corrected to the same initial mass of total soil naphthalene, the results show only a relatively minor effect of soil moisture on the time scale of degradation in the oxic treatments. A much larger effect is seen between the oxic treatments on the one hand, and the anoxic treatment on the other. Thus, the presence or absence of O_2 appears to be the key determinant of the order of magnitude variations in the net rates of naphthalene degradation observed between the oxic and anoxic treatments.

2.4.3 Naphthalene biodegradation: rate model

Naphthalene biodegradation has frequently been modelled using simple first order kinetics (e.g., Agarry *et al*., 2013; Agarry & Oghenejoboh, 2015; Beolchini *et al*., 2010; Guerin & Boyd, 1992; Macintyre *et al*., 1993; Thierrin *et al*., 1993). To facilitate comparison with previous studies, we follow the same approach using:

$$\frac{dC}{dt} = -k \cdot C \qquad (1)$$

where k is the apparent first order degradation rate constant (in units of day^{-1}), C is the concentration (or mass) of naphthalene, t is time, and dC/dt is the rate of change in C. Integrating and rearranging Equation (1) gives the value of C as a function of t:

$$C = C_0 \cdot \exp(-kt) \qquad (2)$$

where C_0 is the concentration (or mass) of the reactant at time $t = 0$. Equation (2) was fitted to the total soil naphthalene concentrations exceeding the MDL (Figure 2-3B). To check whether time-dependent concentration data fit Equation (2), the normalized concentration C/C_0 is typically plotted on a log-linear scale.

On a log-linear plot, the total soil naphthalene concentrations of the 100% WFPS anoxic treatment define a straight line (Figure 2-5). That is, the degradation kinetics can be described by a single first-order rate constant *k*. The data for the 60% WFPS oxic treatment also follows a straight line but with a much steeper slope and, hence, a larger *k* value. The other two oxic treatments show an initial rapid decline in concentration similar to that of the 60% WFPS treatment, followed by a slower degradation. The 80 and 100% WFPS oxic treatments therefore require at least two *k* values to reproduce their data on a log-linear plot.

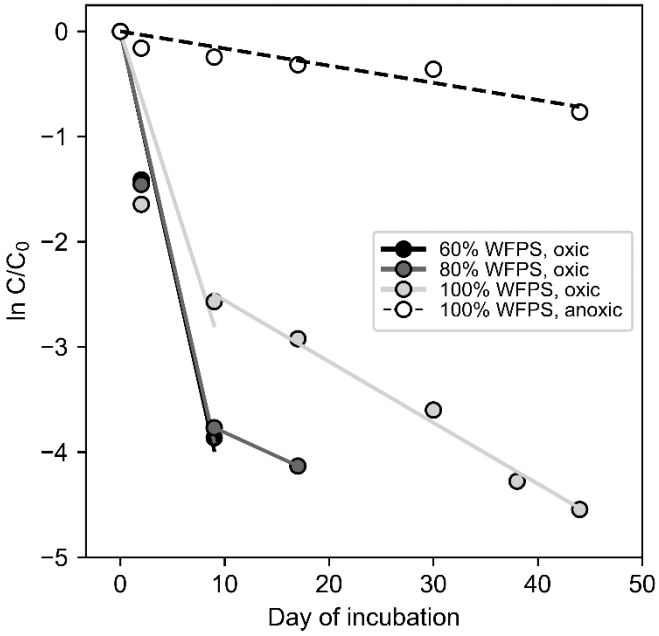

Figure 2-5. Fitting the first order kinetic rate model of naphthalene biodegradation to the total soil naphthalene data (*i.e.,* the data in Figure 2-3B) corrected for volatilization (as described in section *2.3.3*). The data shown only include naphthalene measurements above the MDL. The time series data for the 100% WFPS anoxic treatment and the 60% WFPS oxic treatment define two distinct linear trends on the log-linear plot with first order rate constant (*k*) values of 0.016 and 0.44 day^{-1}, respectively. In the 80 and 100% WFPS oxic treatments, the naphthalene degradation is characterized by an initial fast phase, followed by a slow phase. The *k* values derived from fitting the linear segments shown on the plot can be found in Table 2-1.

In the 80 and 100% WFPS oxic treatments, the transition between the initial fast phase and the following slow phase occurred around Day 9. This was also the time when the total soil naphthalene became undetectable in the 60% WFPS oxic treatment. For visual purposes, we therefore used two colors in Figure 2-2 to approximately indicate the fast and slow degradation regimes. For the 100% WFPS anoxic treatment, only one color appears because degradation falls entirely in the slow kinetics regime.

Table 2-1. Fast and slow apparent first order naphthalene biodegradation rate constants (*k*), Pearson's *r* correlation coefficients, and number of data points used in fitting the *k* value (*n*).

Treatment	Fast phase			Slow phase		
	k_{fast} (day^{-1})	Pearson's *r*	*n*	k_{slow} (day^{-1})	Pearson's *r*	*n*
60% WFPS, oxic	0.44	0.98	3	--	--	--
80% WFPS, oxic	0.43	0.97	3	0.045	1.00	2
100% WFPS, oxic	0.31	0.82	3	0.058	0.99	5
100% WFPS, anoxic	--	--	--	0.016	0.93	6

Apparent first order rate constants (*k*) and Pearson's *r* correlation coefficients for the different experimental treatments and the two kinetics regimes (fast and slow) are summarized in Table 2-1. The highest *k* value (0.44 day^{-1}) is that observed in the 60% WFPS oxic treatment, the lowest value (0.016 day^{-1}) in the 100% WFPS anoxic treatment. The rate constants for the fast regime in the 80 and 100% oxic incubations are relatively close to the maximum *k* value. The lower values of 0.31 day^{-1} in the 100% WFPS oxic treatment likely reflects the reduced diffusional O_2 supply into the soil under fully saturated moisture conditions (Fairbairn *et al.*, 2023). The apparent rate

constants for the slow regime are one order of magnitude lower than those for the fast regime. However, even in fully saturated soil conditions, the presence of an oxygenated headspace results in faster degradation kinetics of naphthalene than when the headspace is O_2-free (compare k_{slow} for the 100% WFPS oxic and anoxic treatments in Table 2-1).

2.4.4 Environmental implications

Apparent first-order rate constants in the literature include those reported by Agarry *et al.* (2013) and Agarry *et al.* (2015) for motor oil biodegradation in an arid-region soil (0.015-0.064 day^{-1}) and by Beolchini *et al.* (2010) for the biodegradation of aliphatic and PAH compounds in a marine sediment (0.18-0.24 day^{-1}). These studies, however, did not identify the dominant processes or redox conditions controlling the biodegradation rates. Ngueleu *et al.* (2019) reported lower degradation rate constants, in the 10^{-2} to 10^{-3} day^{-1} range, for benzene and naphthalene in a saline groundwater in a semi-arid region across redox conditions ranging from aerobic to sulfate reducing. Thus, overall, the available data show that petroleum hydrocarbons (PHCs) biodegradation kinetics under in-situ conditions are highly variable and depend on many different biogeochemical factors, including the environmental redox conditions.

Our results emphasize the importance of the presence or not of O_2. This is clearly seen by the much longer time scale of naphthalene degradation in the 100% WFPS anoxic treatment compared to its fully saturated but oxic counterpart (Figure 2-4 and Table 2-1). Increasing dissolved O_2 availability by manipulating soil moisture is a proven strategy to accelerate bioremediation of organic contaminants. For example, landfarming, involving the excavation, spread, and tilling of contaminated saturated soil onto the land surface while maintaining moderate soil moisture, is a conventional method to remediate petroleum hydrocarbons (PHCs) that has been practiced for over

100 years because of its effectiveness (Brown *et al*., 2017; Guarino *et al*., 2017; Khan *et al*., 2004; Ossai *et al*., 2020). Many other commonly used and cost-effective remediation techniques are similarly based on increasing the availability and accessibility of O_2 (Bass *et al*., 2000; Kao *et al*., 2008; Khan *et al*., 2004; Ossai *et al*., 2020; Philp and Atlas, 2014).

Nonetheless, even under fully anoxic conditions we observed naphthalene degradation, in agreement with previous studies (e.g., Liang *et al*., 2015; Liu *et al*., 2021; Weiner & Lovley, 1998). In these studies, low molecular-weight organic acids, including acetate and propionate, have been shown to be by-products of the fermentative degradation of naphthalene and other PAH compounds. The build-up of the organic acids is observed right from the start in the 100% WFPS anoxic treatment (*i.e*., at the first sampling time point, Figure 2-2B). The simultaneous drop in the total soil naphthalene mass (Figure 2-3B) suggests that the soil microbial consortium is able to degrade the added naphthalene immediately, that is, without a significant adaptation time. This is not entirely unexpected given that the soil was recovered from a PHC-contaminated site.

The degradation efficiency of naphthalene degradation under the fermenting-methanogenic conditions in the fully anoxic treatment is characterized by an apparent rate constant (0.016 day^{-1}) that is nearly 30 times lower than the maximum value in the 60% WFPS oxic treatment (0.44 day^{-1}). Together, our results thus imply that (1) the soil is inhabited by a functionally versatile microbial community that can rapidly switch between terminal accepting processes, and (2) this switching is accompanied by order-of-magnitude changes in the naphthalene degradation kinetics. Similar large differences between aerobic and anaerobic biodegradation kinetics have been reported for a wide variety of organic compounds, environments, and media (*e.g*., Rockne and Strand, 1998; Shibata *et al.*, 2006; Carballeira *et al.*, 2017; Krumina *et al.*, 2017). Recognizing the existence of

the fast and slow kinetic regimes is key to developing predictive models of PHC biodegradation in redox-dynamic subsurface environments (*e.g.*, Verginello and Baciocchi, 2011).

2.5 Conclusion

In this study, naphthalene degradation kinetics were measured in incubations of a soil collected at a former petroleum-contaminated site. The incubations were performed under either oxygenated or anoxic headspace and for variable soil moisture contents. In the presence of the O_2-containing headspace, two distinct kinetic regimes were observed: an initial fast phase dominated by aerobic biodegradation followed by a much slower degradation phase dominated by anaerobic processes, including fermentation reactions and methane production. In the fully anoxic incubations, only the slow phase was observed. The apparent rate constants of naphthalene degradation ranged from 0.016 day^{-1} for the slow (anoxic) regime to 0.44 day^{-1} for the fast (oxic) phase. Whether or not O_2 was present, total soil naphthalene mass declined without an apparent lag time, implying a functionally diverse microbial community capable of degrading naphthalene using a range of terminal electron-accepting processes, from aerobic respiration to methanogenesis.

Temperature sensitivity of soil respiration and methanogenesis processes in the presence of naphthalene

Jane Ye[a*], Fereidoun Rezanezhad[a], Stephanie Slowinski[a], Marianne Vandergriendt[a], Philippe Van Cappellen[a]

[a] Ecohydrology Research Group, Department of Earth and Environmental Sciences and Water Institute, University of Waterloo,
200 University Avenue West, Waterloo, Ontario, Canada, N2L 3G1

[*]Corresponding author: Jane Ye
Ecohydrology Research Group, Department of Earth and Environmental Sciences and Water Institute, University of Waterloo
200 University Avenue West, Waterloo, Ontario, Canada, N2L 3G1
jxjye@uwaterloo.ca

3 Temperature sensitivity of soil respiration and methanogenesis processes in the presence of naphthalene

3.1 Introduction

Decomposition of soil organic matter releases carbon stored in soils to the atmosphere. This soil carbon can be released in the form of CO_2 in the case of soil respiration as well as CH_4 in the case of methanogenesis. CO_2 and CH_4 are two key GHGs contributing to global climate change, with CH_4 contributing a 25 times stronger greenhouse effect than CO_2 (United States Environmental Protection Agency, 2023). The contribution of soil carbon to atmospheric GHGs is globally significant, with an estimated 8 times more carbon entering the atmosphere from soil emissions than from fossil fuel burning and cement manufacture combined in the 21st century (Oertel *et al*., 2016; Peters *et al*., 2011; Raich & Potter, 1995; Raich & Schlesinger, 1992). The study of soil carbon fluxes is then understandably a robust area of research, with almost 2 million results on the search engine Google Scholar for the search term "soil carbon flux" at the time of this writing.

Since soil organic matter decomposition is a biologically mediated set of processes, like other biologically mediated processes its rates are highly sensitive to temperature (Singh & Gupta, 1977). The temperature sensitivity of processes like contaminant biodegradation and soil respiration (Barcelo Culleres *et al*., 2007; Byun *et al*., 2021) is commonly described by its Q_{10} rate quotient, which represents the ratio of two reaction rates 10°C or K apart (Barcelo Culleres *et al*., 2007; Davidson & Janssens, 2006). The ratio Q_{10} is derived from the Arrhenius set of equations (see section *3.2.4*) relating reaction rate constants to activation energies (Barcelo Culleres *et al*., 2007; Byun *et al*., 2021; Fang & Moncrieff, 2001). The value of Q_{10} has historically been assumed to fall between 2-3 for biological reactions occurring at temperatures between 20 to 30°C

(Davidson & Janssens, 2006). Literature has reported a wider range of Q_{10} values of soil respiration measured for many soil types, including both above and below the 2-3 range (Table 3-1). Variations in Q_{10} values are often attributed to prevailing soil temperatures at different latitudes, with higher temperature sensitivities associated with colder climates (Byun *et al*., 2021; Chen & Tian, 2005; Zhou *et al*., 2009).

Table 3-1. Sample Q_{10} values reported in literature for soil respiration for different soil types from lab and in situ measurements.

Q_{10} of soil respiration	**Land cover/soil type**	**Region**	**Study type**	**Reference**
2.45 (SD = 0.41)	Boreal peat	Northern Ontario, Canada	Lab	(Byun *et al*., 2021)
1.91 (SD = 0.25)	Temperate peat	Southern Ontario, Canada	Lab	(Byun *et al*., 2021)
1.97 to 2.30	Spruce plantation	Scotland	Lab	(Fang *et al*., 2005)
1.2 to 2.8	Cropland, grassland, and forest soils	Germany, the Netherlands, and Belgium	Lab	(Meyer *et al*., 2018)
1.3 to 3.3 (mean = 2.4)	Various	Various	*In situ*	(Raich & Schlesinger, 1992)
4.2 (annual average) 3 (summer) 23 (winter)	Beech forest	Denmark	*In situ*	(Janssens & Pilegaard, 2003)

It is recognized that PHC contaminated soils contribute more GHG emissions than comparable clean soils (Martin *et al*., 2016; Sihota *et al*., 2011; Wozney *et al*., 2021). Most of this increase in total soil respiration (TSR) to the atmosphere is attributed to the contaminant-related soil

respiration (CSR) component, or soil respiration originating directly from the degradation of PHC compounds, (Sihota *et al*., 2011; Wozney *et al*., 2021). At the global scale, excess soil GHG emissions from contaminated sites are likely several orders of magnitude lower than overall GHG emissions from all soils (see section *1.3*). However, with over 5000 federally listed PHC-contaminated soil sites in Canada (Treasury Board of Canada Secretariat, 2022), an understanding of CSR and NSR contributions may be important for contaminated-sites project managers or researchers interested in soil carbon fluxes at the site-scale.

In this study, I performed a temperature- and O_2- variable soil microcosm incubation experiment to investigate how soil GHG fluxes and key processes relevant to PHC biodegradation respond to temperature in the presence of spiked naphthalene. Soil incubations were performed under oxic or anoxic headspace conditions for a total of 6 or 49 days, respectively, at 10, 20, and 30°C. Microcosms were sacrificially sampled approximately daily (for oxic incubations) or weekly (for anoxic incubations) with accumulated headspace CO_2 and CH_4 concentrations, porewater chemistry, and naphthalene measured at each sampling point. I hypothesized that the rates of key reactions identified in Chapter 2 (such as net CO_2 and CH_4 accumulation; OA production and oxidation) would increase at higher temperatures, with Q_{10} likely varying between reactions and under oxic or anoxic conditions.

3.2 Materials and methods

3.2.1 Soil collection and characterization

Soil cores were collected in September 2021 with a drill rig from a PHC-contaminated industrial site in London, Ontario, Canada, as described in Chapter 2 (see section *2.2.1*). After the homogenizing and drying of soil described in Chapter 2, it was stored at 4°C for a further one year

prior to the current study. The characterization of soil properties and background total petroleum hydrocarbons are also described in Chapter 2 (see sections *2.2.1* and *2.2.3.3*).

3.2.2 Soil incubation experiment

The temperature-variable soil incubation experiment was designed to investigate the effect of temperature on aerobic and anaerobic soil respiration and methanogenesis in the presence of PHC contamination. A total of 180 incubation vials were prepared by adding 40 g of dried soil to 41 mL amber VOA vials. Vials of soil were left uncapped for ten days of equilibration in incubators set to 10, 20, and 30°C under either oxic (air) or anoxic (N_2) atmospheric conditions.

After equilibration the soil was fully saturated with the addition of 14 mL of APW solution (composition described in section *2.2.2*). Figure 3-1 illustrates the different treatments applied in this experiment. In total, there were six incubation conditions of different combinations of headspace O_2 and temperature. Each incubation condition was further divided into Nap, No Nap, and Abiotic treatments. APW used in the "Nap" treatment was additionally spiked with naphthalene ($C_{10}H_8$), APW used in the "No Nap" control contained only the salts described below, and the "Abiotic" control was both spiked with aqueous naphthalene and sterilized. Sterilized controls were prepared by autoclaving soil three times over five days at 121°C and 15 psi for one hour, followed by addition of aqueous $HgCl_2$ at a concentration of 2.21 mmol kg^{-1} at the time of APW addition. All vials, lids, lab apparatus, and solutions that contacted the sterile soil were autoclaved before use, at 120°C and 15 psi for 30 minutes.

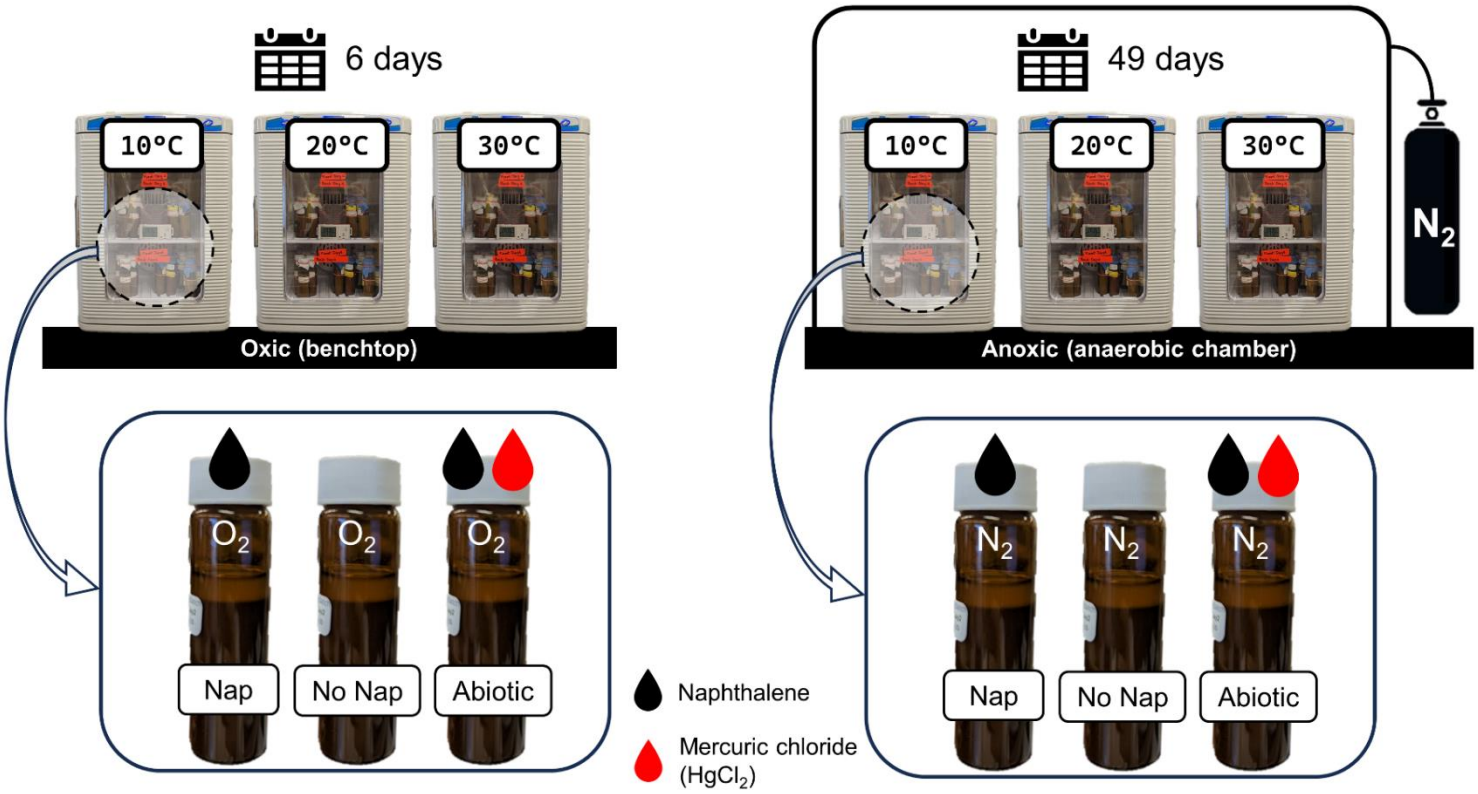

Figure 3-1. Schematic soil incubation experiment design with oxic/anoxic headspace treatments at different temperatures. "Nap" treatments were spiked with aqueous naphthalene. "No Nap" treatments were not spiked. "Abiotic" treatments were spiked with aqueous naphthalene and sterilized with a combination of autoclaving and $HgCl_2$ addition.

Anoxic APW solutions were additionally sparged with N_2 gas for 2 hours to deoxygenate the water to a dissolved O_2 concentration of <2.6 mg L^{-1}. After APW addition, the total headspace volume in each jar was 12 mL. For the Nap experimental treatments, the APW was additionally spiked with 5 mg L^{-1} (39 µmol L^{-1}) naphthalene, prepared by dissolving naphthalene crystals (Sigma Aldrich, >99%) in Milli-Q water for one week at room temperature while mixing.

Vials were capped with lids lined with Teflon®-facing septa. Oxic incubations were performed within benchtop incubators (MyTemp™ mini digital incubator H2200-HC, Benchmark Scientific) in ambient air, for a total incubation time of six days, with sampling every one to two days. Anoxic incubations were performed within the same benchtop incubators held in an anaerobic chamber containing only N_2, for a total incubation time of 49 days, with sampling every one to two weeks. Oxic incubations were sampled at 0, 2, 3, 4, and 6 days while anoxic incubations were sampled at 0, 7, 14, 28, and 49 days. Triplicate vials were prepared for each sacrificial sampling point, for a total of 180 jars incubated.

3.2.3 Sampling and analytical methods

Porewater extraction and sampling and analyses of gaseous (CO_2, CH_4, O_2), aqueous (pH, acetate, propionate, DIC, aqueous naphthalene) and solid phase (total soil naphthalene) parameters were conducted as described in Chapter 2 (section *2.2.3*) with the following exception: The pH of centrifuged supernatant was measured using a benchtop pH probe (Orion™ Versa Star Pro™, Thermo Scientific).

3.2.4 Fitting of reaction rates and Q_{10}

For each Nap incubation under different oxygen/temperature conditions (oxic or anoxic; 10, 20, or 30°C), 0^{th} order rate constants (k) of CO_2, DIC, CH_4, acetate, propionate, and O_2 net accumulation or consumption were obtained by fitting a straight line to time series concentration data (0^{th} order rate constants were determined to fit the data better than 1^{st} order rate constants). Inverse temperature (in units of K) was then plotted against ln k and fitted with a straight line for oxic and anoxic incubations to obtain an estimate of the activation energy of a reaction (E_a) from the slope using Equation 3.1, the Arrhenius equation, relating k to E_a (Byun *et al*., 2021; Fang & Moncrieff, 2001).

$$k = A \exp(-\frac{E_a}{RT}) \quad (3.1)$$

where k is the rate constant, A is a fitting parameter, E_a is the activation energy, R is the universal gas constant, and T is the temperature. Similarly, temperature (in units of K) was plotted against ln k and fitted with a straight line for oxic and anoxic incubations to obtain an estimate of Q_{10} from the slope using Equation 3.2, derived from the Arrhenius equation, relating k to the temperature of a reaction through the Q_{10} temperature sensitivity parameter.

$$k = \alpha \exp(\frac{ln(Q_{10})}{10} \times T) \quad (3.2)$$

where k is the 0^{th} order rate constant, α is a fitting parameter, T is the temperature in units of K, and Q_{10} is the unitless temperature sensitivity. Practically, the Q_{10} value represents the ratio of two reaction rates which are 10°C or K apart and is commonly derived from the first-order exponential function in Equation 3.2. Q_{10} of biological reactions are generally understood to fall between 2 to 3 (representing a doubling or tripling of reaction rates with a 10°C temperature increase), with

values of 2 to 2.2 commonly assumed for temperatures between 20 to 30°C for biologically mediation reactions such as the biodegradation of chemicals (Barcelo Culleres *et al*., 2007). All line-fittings and calculations of statistics were performed using the linear regression function "linregress" from the "stats" module of the SciPy library (v1.7.2) for Python (v3.9).

3.3 Results

3.3.1 Accumulated headspace gases

The headspace conditions on Day 0 for oxic incubations were in equilibrium with indoor laboratory atmosphere. For anoxic incubations, Day 0 headspace conditions were in equilibrium with the interior of an anaerobic chamber which had been flushed with pure N_2 gas. CO_2 and CH_4 accumulation in Nap incubations was observed to experience a lag period of between 4 to 28 days, which is discussed further in Appendix II (Figure AII-1).

CH_4 increased over time in Nap and No Nap anoxic incubations (Figure 3-2A). The effect of temperature was clear, with total anoxic CH_4 accumulation (*i.e.*, on Day 49) at 30°C being about double that at 20°C, and two orders of magnitude higher than at 10°C. Total anoxic CH_4 accumulation in No Nap treatments was similar to that in Nap treatments. CH_4 accumulation in oxic incubations was small but also increased with temperature. CH_4 data for No Nap and abiotic treatments were not available for the full duration of the oxic incubations. CO_2 also increased over time in all Nap and No Nap incubations (Figure 3-2B). The effect of temperature on total CO_2 accumulation was clear in all six temperature-oxygen treatments. Total CO_2 accumulation in both oxic and anoxic No Nap treatments was similar to that in Nap treatments. O_2 levels remained about ≤1% throughout all anoxic treatments at all temperatures. In oxic incubations, O_2 in Nap treatments

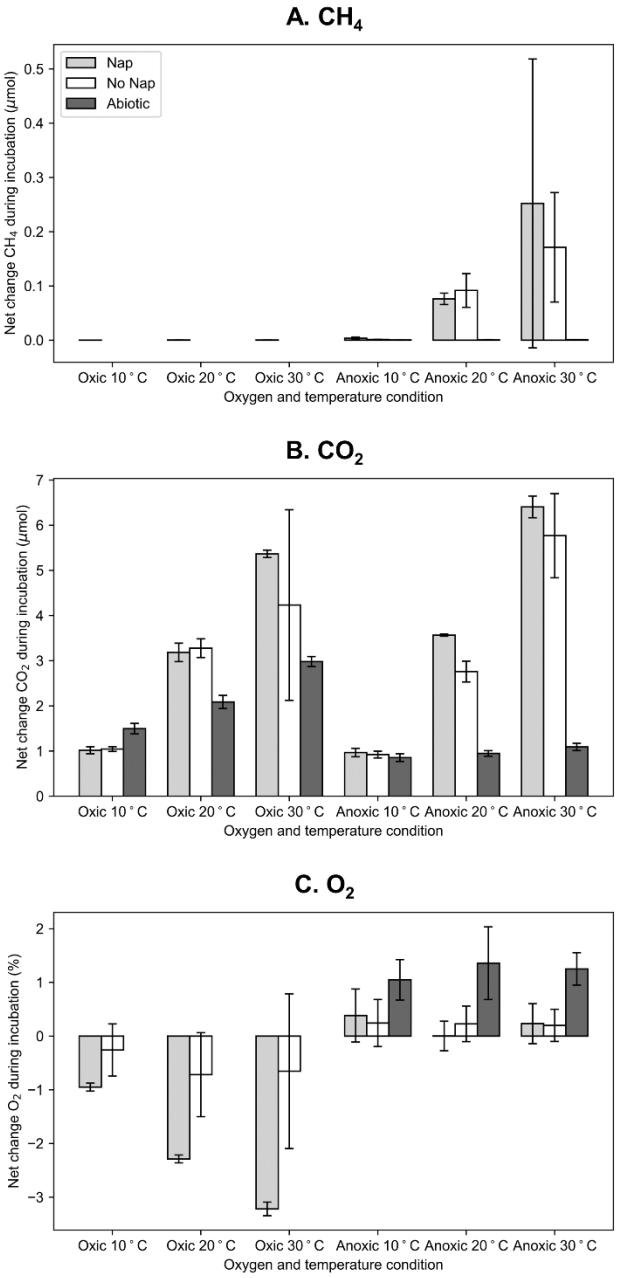

Figure 3-2. Net change in (A) CH_4, (B) CO_2, and (C) O_2 headspace gases, over the course of the entire incubations (6 days for oxic incubations, 49 days for anoxic incubations). Error bars represent one SD. Note that for abiotic No Nap and abiotic incubations, net change in CH_4 was not able to be calculated since CH_4 data was not collected for the entire length of the incubation for those incubations. For oxic abiotic controls, net change in O_2 was also not able to be calculated for the same reason. See Figures AII-1 and AII-2 for full time series data of CH_4, CO_2, and O_2.

decreased more at warmer temperatures. Time series data for accumulated O_2, CO_2, and CH_4 can be found in Figures AII-1 and AII-2.

3.3.2 Porewater chemistry

Time series of accumulated acetate and propionate are shown in Figure 3-3 as representative examples of accumulated OAs. OA time series data for abiotic controls are not available due to interference of $HgCl_2$ with chromatographic interpretation of low molecular weight OA compounds. In oxic incubations, accumulated OAs decreased steadily over time at all temperatures. In anoxic incubations, accumulated OAs fluctuated more over time than in oxic incubations. The net effect at 20 and 30°C was the decrease of OAs to near-undetectable levels by the end of the incubations at Day 49. At 10°C, the net effect of fluctuations throughout the incubations resulted in a net increase in OAs. The net change in OAs in No Nap treatments was similar to Nap treatments in all incubations.

pH decreased over time in all Nap and No Nap treatments (Figure 3-4). pH decreases were greater at lower temperatures. Changes over time in pH in abiotic controls were negligible. DIC increased over time in all Nap and No Nap incubations and had no change in abiotic controls (Figure 3-5). Total accumulated DIC in both oxic and anoxic incubations at 10°C was lower than at 20 and 30°C, with the difference being greater in anoxic incubations. Time series data for accumulated DIC can be found in Figure AII-3.

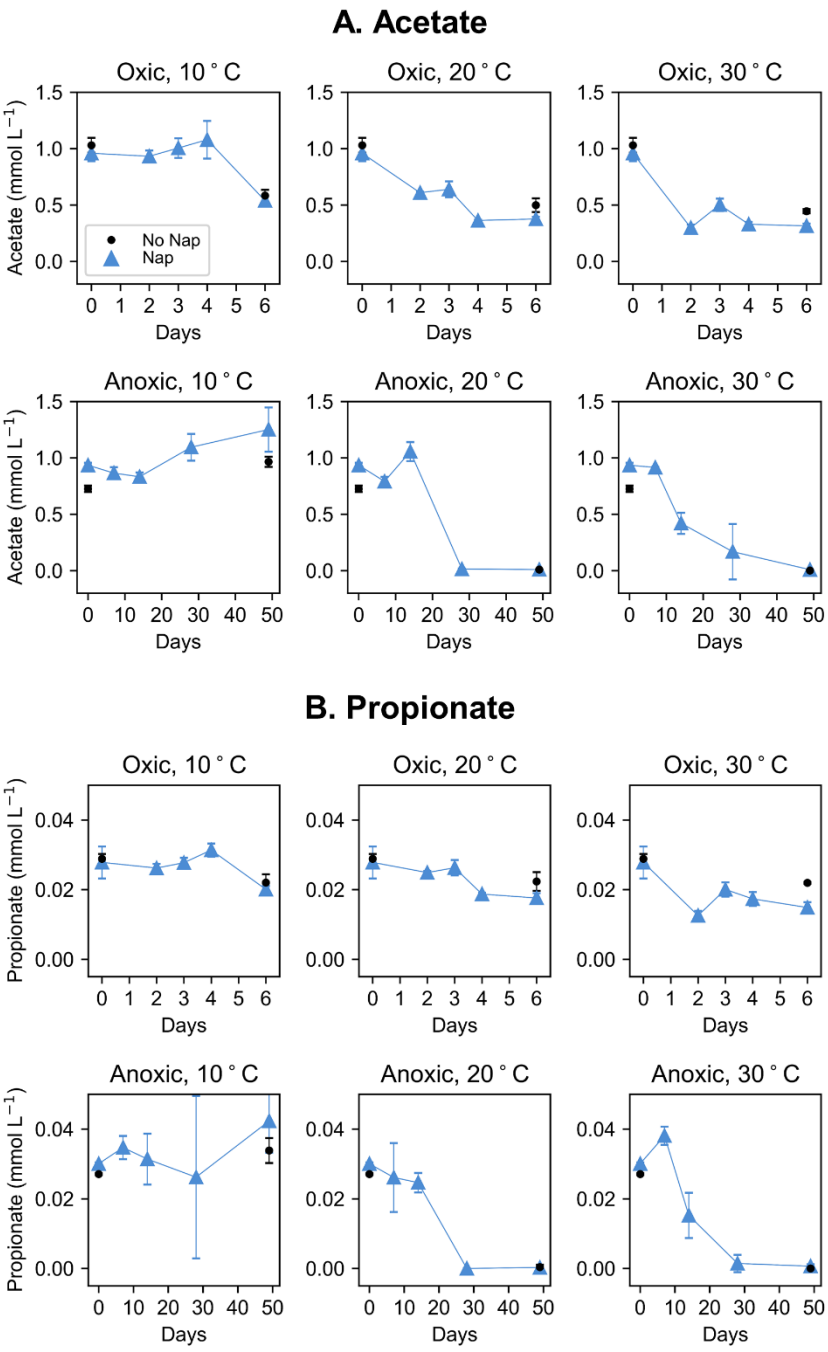

Figure 3-3. Time series of (A) acetate and (B) propionate organic acid concentrations in porewater. Data shown are the average of triplicate samples at each sampling time point, with error bars representing one SD. Note that abiotic control data are not available due to interference of $HgCl_2$ with chromatographic interpretation of low molecular weight OA compounds.

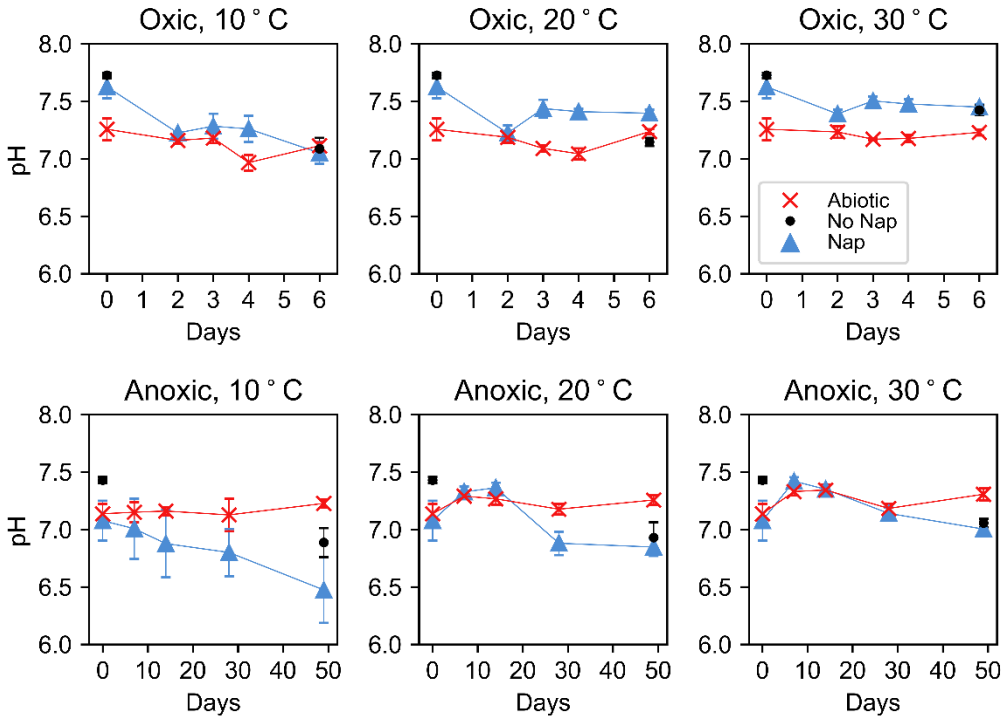

Figure 3-4. Time series of pH in porewater. Data shown are the average of triplicate samples at each sampling time point, with error bars representing one SD.

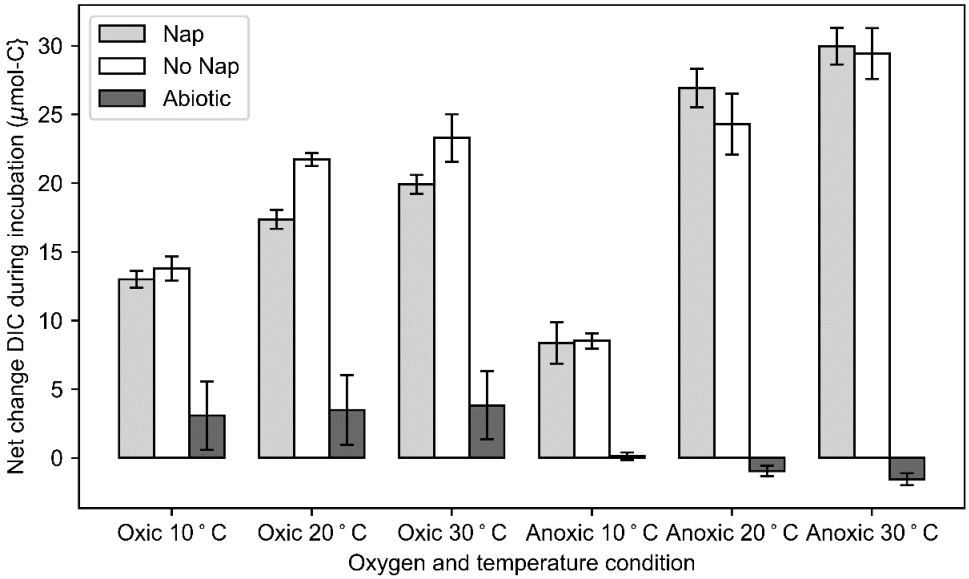

Figure 3-5. Net change in porewater DIC over the course of the entire incubations (6 days for oxic incubations, 49 days for anoxic incubations). Error bars represent one SD.

3.3.3 Naphthalene mass loss

Similar net decreases in aqueous naphthalene were observed in all abiotic and Nap incubations (Figure 3-6). Additionally, total soil naphthalene (Figure AII-4), which is a measure of the total naphthalene in both sorbed and aqueous phases, did not significantly decrease over time in Nap incubations (total soil naphthalene data for abiotic controls is not available). There was no apparent effect of temperature on the percent of total naphthalene mass lost in either Nap or abiotic incubations (Figure AII-5).

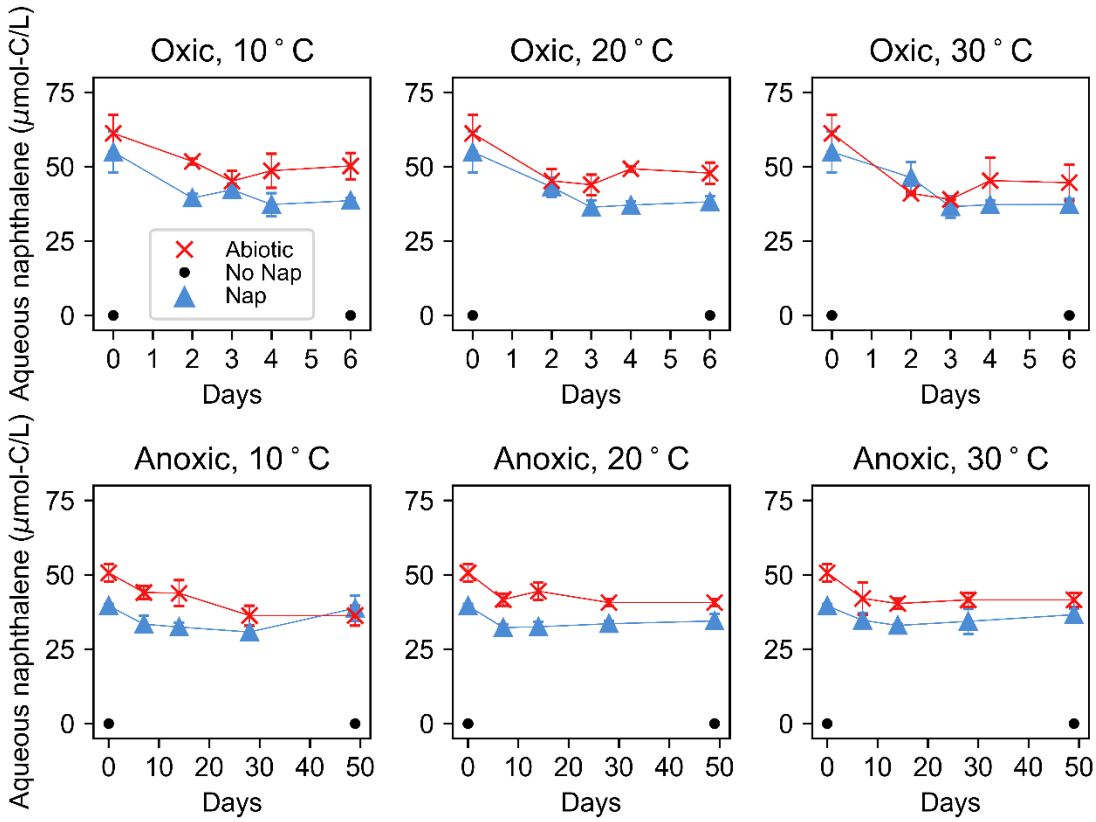

Figure 3-6. Time series of aqueous naphthalene in porewater. Data shown are the average of triplicate samples at each sampling time point, with error bars representing one SD.

3.3.4 Temperature sensitivity analysis

E_a and Q_{10} were estimated as described in section *3.2.4* using full time series data from both oxic and anoxic incubations, representing the net processes of CO_2 accumulation, DIC accumulation, CH_4 accumulation, and accumulation of the sum of inorganic carbon species (CO_2 + DIC + CH_4). Additionally, E_a and Q_{10} were estimated using time series data from only the oxic incubations, representing the net result of OA (acetate and propionate) consumption and O_2 consumption. E_a and Q_{10} estimates of O_2 consumption in anoxic incubations were not made due to a lack of change over time in accumulated O_2. E_a and Q_{10} estimates of OA consumption in anoxic incubations were also omitted due to the combination of production and consumption processes complicating the trend (see discussion in section *3.4.2*).

Table 3-2 summarizes measurements of E_a and Q_{10} in oxic and anoxic incubations, and these values are visually compared in Figure 3-7 (panels A-G). Curve fitting plots can be found in Figure AII-6, and further fitting statistical parameters in Table AII-1. Measurements of E_a and Q_{10}, curve fitting plots, and fitting statistical parameters for the same analysis excluding time series data from the initial lag period (as defined by the lag period in CO_2 accumulation time series, Figure AII-1B) can be found in Table AII-2, Figure AII-7, and Table AII-3, respectively.

Table 3-2. Summary of E_a and Q_{10} values in this experiment, along with associated errors, measured for various processes under oxic and anoxic Nap incubations. E_a and Q_{10} measurements of O_2 consumption in anoxic incubations are not included due to a lack of change over time in accumulated O_2. E_a and Q_{10} measurements of acetate and propionate consumption in anoxic incubations were also omitted due to the combination of production and consumption processes complicating the analysis (see discussion in section *3.4.2*).

Net reaction	Oxic				Anoxic			
	E_a (kJ mol^{-1})	E_a std. error (+/-)	Q_{10}	Q_{10} std. error (+/-)	E_a (kJ mol^{-1})	E_a std. error (+/-)	Q_{10}	Q_{10} std. error (+/-)
CO_2 accumulation	60	14.6	2.3	1.25	72	16.4	2.7	1.28
CH_4 accumulation	36	17.3	1.7	1.29	160	34.1	9.3	1.69
DIC accumulation	15	3.8	1.2	1.06	46	27.5	1.9	1.49
CO_2+DIC+CH_4 accumulation	21	4.5	1.3	1.07	50	24.5	2.0	1.43
O_2 consumption	47	14.9	1.9	1.25	--	--	--	--
Acetate consumption	10	11.3	1.2	1.18	--	--	--	--
Propionate consumption	23	15.8	1.4	1.26	--	--	--	--

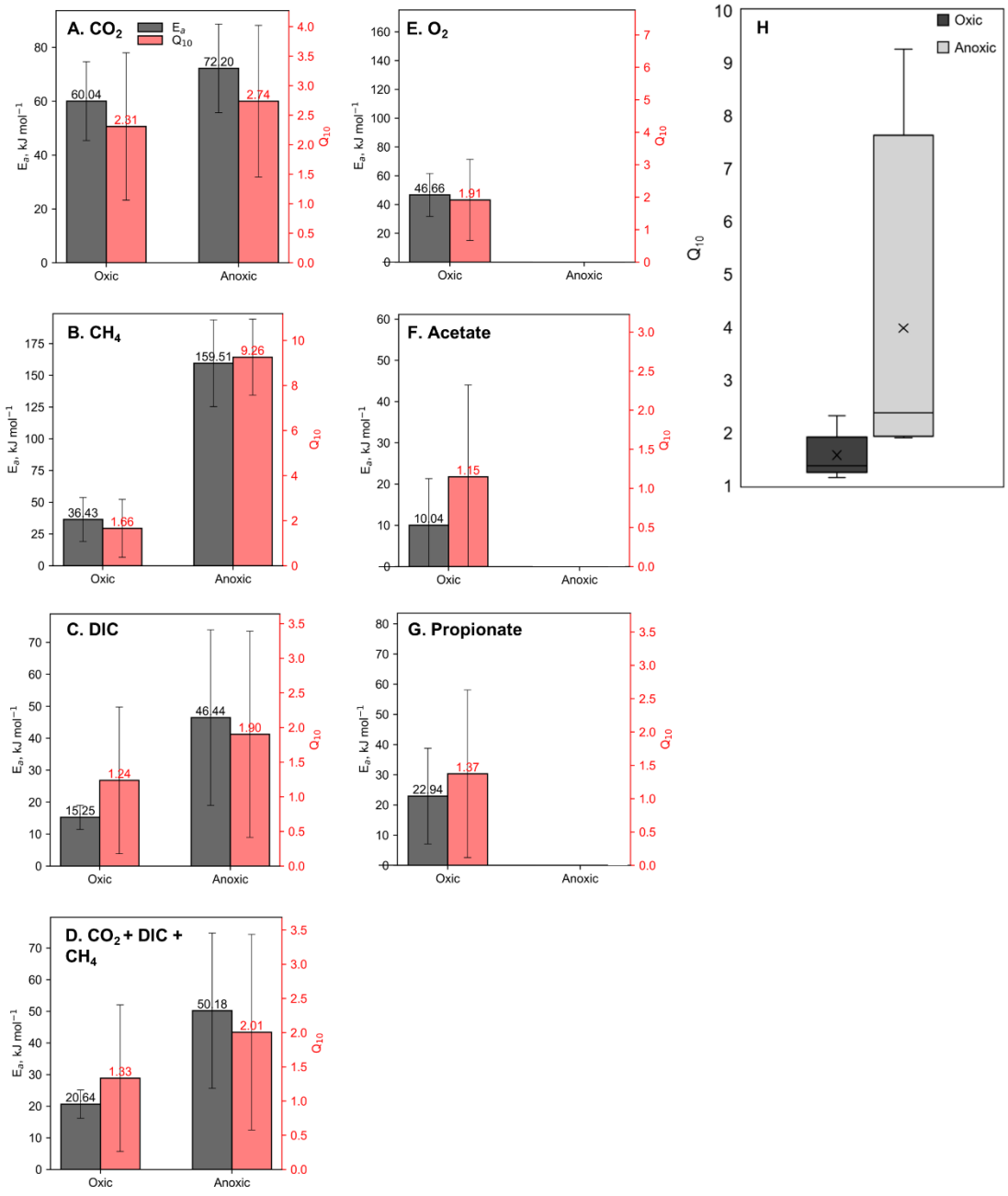

Figure 3-7. Comparison of E_a and Q_{10} for (A) CO_2 accumulation, (B) CH_4 accumulation, (C) DIC accumulation, (D) accumulation of CO_2 + DIC + CH_4 in oxic and anoxic Nap incubations, and (E) O_2 consumption, (F) acetate consumption, and (G) propionate consumption in oxic Nap incubations. Error bars represent the standard error resulting from curve fitting to obtain E_a and Q_{10} parameters (see Figure AII-6). Panel H shows a box plot summary of all Q_{10} values obtained for processes in oxic and anoxic incubations. The bottom whisker, bottom of the box, middle line in the box, top of the box, and top whisker represent the minimum value, 25th percentile, 50th percentile, 75th percentile, and maximum value, respectively. The "x" represents the mean value.

Q_{10} values from oxic incubations (Table 3-2, Figure 3-7) range from 1.15 (for net acetate consumption) to 2.31 (for net CO_2 accumulation), while those from anoxic incubations range from 1.90 (for net DIC accumulation) to 9.26 (for net CH_4 accumulation). It would not be appropriate to accept measured average Q_{10} and E_a values from this analysis quantitatively, due to the large uncertainties (summarized in Table 3-2) introduced through the curve fitting process (Figure AII-6) that are often of similar magnitude to the measured average values themselves. Despite these uncertainties, trends exist in the measured average values which can be assessed qualitatively. Where both anoxic and oxic Q_{10} values were measurable, Q_{10} for the anoxic processes were always higher than for oxic processes.

3.4 Discussion

3.4.1 Accumulated headspace gases

CH_4 and CO_2 total accumulations (Figure 3-2A and 3-2B) clearly show a dependence of gas accumulation rates on temperature. The temperature sensitivities of CH_4 and CO_2 accumulation are further quantified and discussed in sections *3.3.4* and *3.4.4*.

CH_4 accumulation was far greater in anoxic incubations, especially at higher temperatures. Small amounts of accumulated CH_4 in oxic incubations could result from methanogenesis in isolated anoxic pore spaces. However, the small volume of anoxic zones combined with the high rates of CH_4 oxidation at near-atmospheric O_2 levels likely greatly limited the accumulation of CH_4 in the oxic incubations. O_2 levels in all anoxic incubations (Figure 3-2C) changed little throughout the incubation time, confirming that minimal aerobic respiration activity was present in the anoxic incubations.

3.4.2 Porewater chemistry

The production of OAs (including acetate and propionate, see Figure 3-3) can be attributed to anaerobic organic matter fermentation. Processes contributing to the consumption of OAs, on the other hand, include both aerobic and anaerobic oxidation of OAs, as well as ABM (which converts acetate into CH_4 and CO_2). The observed net decrease, increase, or fluctuations in OAs would then be a result of simultaneous production and consumption processes.

Since both OA production and consumption processes may be promoted by higher temperatures, the effect of temperature on the net accumulated OAs over time in Nap and No Nap incubations (Figure 3-3) were not obvious. However, it can be observed that in both anoxic and oxic incubations, lower temperatures were related to slower decreases in OAs, or in the case of anoxic incubations at 10°C, reverse the trend to a net increase. This may indicate a greater inhibition of the decreasing process(es), such as OA oxidation, at lower temperatures. It may also have been the case in the anoxic incubations that at lower temperatures, there was less ABM methanogenic activity or increased acetate production, contributing to the positive accumulation of OAs in the anoxic incubations at 10°C. There is support for this hypothesis in the literature: Some studies have observed increasing contributions of ABM (relative to HBM) with higher temperatures from moderate temperature ranges (5-20°C) (Gill *et al*., 2017) up to 40°C (Metje & Frenzel, 2005). Saha *et al*. (2015) suggest the explanation of better adaptation of hydrogenotrophic methanogens, than aceticlastic methanogens, to low temperatures (<15°C). Conversely, Nozhevnikova *et al.* (2007) observed the stimulation of acetate production and domination of aceticlastic contributions to methanogenesis at low temperatures (5-15°C). Conrad (2020) and Kotsyurbenko (2005) also observe from literature reviews the strong dependence of temperature on ABM:HBM ratio and the dominance of ABM at low temperatures. Overall, the relationship between ABM:HBM ratio and

temperature is not straightforward in situations of incomplete organic matter degradation, such as in soil organic matter degradation settings (Conrad, 2020).

In this experiment, the decrease of OAs in oxic incubations also occurred earlier than in anoxic incubations. In oxic incubations, it was expected that very little if any fermentation activity would have taken place to replenish OAs as they were consumed. There was also abundant O_2 available in oxic incubations as an effective EA for aerobic OA oxidation. Therefore, faster OA decrease in oxic incubations can be explained by large contributions of OA consuming processes with little activity from OA producing processes. The additional contribution of OA production via fermentation in anoxic incubations is a possible explanation for why accumulated OAs fluctuate more over time in anoxic incubations, compared to more consistent decreasing patterns observed in oxic incubations (Figure 3-3).

The decreasing trends observed in pH during Nap and No Nap incubations are likely mostly controlled by the accumulation of OAs. Net decrease in pH was greater at lower temperatures in both oxic and anoxic incubations, in keeping with the greater accumulation of OAs at lower temperatures discussed above. This interpretation aligns with findings from Chapter 2 where OA and CO_2 accumulation were related to a drop in pH particularly in anoxic conditions.

3.4.3 Naphthalene mass loss

As described in section *3.3.3*, naphthalene mass loss from the aqueous phase in both Nap and abiotic incubations were similar (Figure 3-6), with no significant additional mass loss observed in total soil naphthalene (Figure AII-4) and no apparent affect of temperature on mass loss (Figure AII-5). If mass loss came from a biological process (*i.e.*, biodegradation of naphthalene), reaction

rates would be expected to vary noticeably by 2 to 3 times with every 10°C of temperature change. Together, these data indicate that most or all of the naphthalene mass loss observed was attributable to abiotic processes such as volatilization, and not biodegradation. Due to the temperature dependence of the Henry's law constant of gas-liquid partitioning, naphthalene volatilization is expected to also be affected by temperature, but to a much lesser extent than biological processes.

The explanation for the lack of naphthalene biodegradation observed is that naphthalene-degrading microbes were absent or slow to recover upon soil rehydration. Although the soil microbial community was demonstrated to contain naphthalene-degrading capabilities during the experiment conducted in Chapter 2, the subsequent one-year period of cold storage under dried conditions likely rendered much of the microbial community dormant or unable to reproduce. Upon rehydration with APW at the start of the experiment, the microbial community was able to recover after a lag period, but with an altered community composition compared to the original conditions of the soil. Soil from both this experiment and the experiment in Chapter 2 has been flash-frozen and preserved for future microbial community composition analysis to potentially verify this explanation.

3.4.4 Temperature sensitivity analysis

The measured average Q_{10} values listed in Table 3-2 range from 1.15 to 9.26 (or 2.74, if excluding CH_4 accumulation). Recently, Q_{10} values have been reported in the literature for many different climates and reactions (examples listed in Table 3-1). In this study, I found that all measured average Q_{10} values for oxic incubations, except for Q_{10} of CO_2 accumulation, were less than 2. For anoxic incubations, the measured average Q_{10} of CO_2 accumulation was close to 3, and much higher (9.26) for CH_4 accumulation. This study agrees with recent literature (Table 3-1) in

establishing a wider range of possible Q_{10} values for soil respiration and methanogenesis processes than commonly assumed, especially higher temperature sensitivities of CH_4 production compared to CO_2 (Gill *et al*., 2017; Leroy *et al*., 2017; Lupascu *et al*., 2018; Van Hulzen *et al*., 1999; Wang *et al*., 2015; Wei *et al*., 2021). Temperature sensitivities of CH_4 production or accumulation have not been measured as frequently as CO_2 production in temperature sensitivity studies. Van Hulzen *et al.* (1999) proposed that the higher average temperature sensitivities of soil methanogenesis relative to respiration could be a result of longer lag times at lower temperatures while alternate electron acceptors are preferentially utilized, combined with the slower growth of methanogenic communities at lower temperatures. This explanation is consistent with the results of the current experiment, given the observed temperature-sensitivity of CH_4 accumulation lag times (Figure AII-1A). Overall, the poor fit of the Arrhenius model for accumulated CH_4 (Table AII-1 and Figure AII-6, row B) suggests that temperature-variable mechanisms may be contributing to CH_4 accumulation rates at different temperatures, and that the temperature-independent Q_{10} assumption of the Arrhenius model may be inappropriate.

In addition, in this study I observed that the measured average Q_{10} values from anoxic incubations were consistently higher than those from oxic incubations for the same reaction (where both oxic and anoxic datasets were analyzed). Despite high error in measured Q_{10} values, this relationship holds for Q_{10} of CO_2 accumulation, DIC accumulation, and CH_4 accumulation, for which the anoxic Q_{10} is greater than the corresponding oxic Q_{10} by 1.2, 1.5, and 5.6 times, respectively. This result challenges past studies which have compared aerobic and anaerobic soil respiration Q_{10} values and observed higher Q_{10} values for aerobic soil respiration than anaerobic soil respiration (Blagodatskaya *et al*., 2014; Chen *et al*., 2018; Szafranek-Nakonieczna & Stêpniewska, 2014). In this experiment, the measured average Q_{10} for CH_4 accumulation in particular was much greater

in the anoxic incubation than in the oxic incubation. One possible explanation could be that, under oxic conditions, the rate of aerobic CH_4 oxidation also increases at higher temperatures, counteracting increased CH_4 production.

Despite being a small portion of total GHG accumulations in this study, CH_4 is 25 times more potent as a GHG than CO_2 (United States Environmental Protection Agency, 2023). Here, I estimated that the observed Q_{10} of CH_4 accumulation was about 3.4 times greater than the Q_{10} of CO_2 accumulation under anoxic conditions. Our findings suggest that increasing soil temperatures could potentially increase CH_4 emissions from anoxic or sub-oxic soils (such as wetlands and other seasonally or permanently saturated soils) on the scale of 3.4 times faster than increases in CO_2 emissions, increasing the CH_4:CO_2 ratio.

The increased potential for GHG emissions from PHC-contaminated sites compared to clean sites is of importance for project managers or researchers at these sites around the world, including the over 5000 federally listed active PHC-contaminated soil sites in Canada (Treasury Board of Canada Secretariat, 2022). In this study I found evidence that with increasing soil temperatures, the CH_4:CO_2 ratio of anoxic or sub-oxic soils may also increase. However, increasing soil temperatures will likewise increase the rates of potential PHC biodegradation. This may be of particular interest to the PHC-contaminated sites in Canada and worldwide that are located in cold regions, which are warming at a rate 4 times the global average (X. Zhang *et al*., 2019).

Recent studies have indicated that freeze-thaw cycles in cold regions, which are becoming more common with climate change, can increase net CO_2 and CH_4 emissions compared to more stable soil temperature conditions (Priemé & Christensen, 2001; Ramezanzadeh *et al*., 2023; Yang *et al*.,

2023; Zhu *et al*., 2009). Additionally, the Q_{10} of CO_2 production has been found to be higher in regions with colder climates (Byun *et al*., 2021; Chen & Tian, 2005; Zhou *et al*., 2009), suggesting that measured average Q_{10} of CO_2 accumulation in temperature-region soils in this study are the lower bounds of temperature sensitivity for soils in colder regions. Overall, the higher GHG emissions potential of PHC-contaminated sites combined with the possibility of increasing CH_4:CO_2 ratio of soil emissions, rapid climate warming, increasing incidence of freeze-thaw cycles, and higher temperature sensitivity of soil respiration in cold regions are all indicators that PHC-contaminated sites in cold regions in particular may see increasing GHG emissions, but faster PHC biodegradation, with progressing climate change. Although the contributions of CSR-derived soil GHG emissions are likely very small compared to total soil GHG emissions (TSR) at the global scale, this possibility is of relevance to contaminated site project managers or researchers interested in soil carbon fluxes at the site-scale.

3.5 Conclusion

This study agrees with recent literature in establishing a wider range of possible Q_{10} values than commonly assumed, especially for methanogenesis. A trend was identified, inconsistent with other published research, where anaerobic soil respiration and methanogenesis processes (including CO_2 accumulation, DIC accumulation, and CH_4 accumulation) were apparently more temperature-sensitive than their aerobic counterparts. The temperature sensitivity of anaerobic methane accumulation was found to be especially high with a Q_{10} of ~9, suggesting that the CH_4:CO_2 ratio of soil GHG emissions may potentially increase with warming soil temperatures. At PHC contaminated sites, GHG emissions, but also biodegradation rates, have the potential to increase in a warming climate.

4 Summary of findings and future research

4.1 Summary of key findings

The objective of this thesis was to advance understanding on the effects of soil moisture, O_2, and temperature on PHC biodegradation and associated soil respiration and methanogenesis processes. In Chapter 2, I designed and conducted a moisture-variable soil microcosm incubation experiment and identified two distinct kinetic regimes contributing to naphthalene biodegradation under different soil moisture and O_2 conditions. In Chapter 3, I further developed the experimental design from the previous chapter to conduct a temperature- and O_2- variable soil microcosm incubation experiment, observing novel trends in the temperature sensitivity of anaerobic and aerobic biodegradation reactions in the presence of PHC contamination.

In Chapter 2, the degradation of naphthalene was monitored in a naphthalene-spiked soil microcosm incubation experiment under 60%, 80%, and 100% WFPS moisture conditions with oxic headspace, and 100% WFPS moisture conditions with anoxic headspace. Microcosms were sacrificed weekly to biweekly and sampled for headspace accumulated gases, porewater chemistry, and dissolved and total soil naphthalene. First-order kinetic rate fitting analysis was used to interpret the effects of different moisture and oxygen conditions on naphthalene biodegradation rates, while time series of porewater pH, organic acids, and anions provided insight into biodegradation pathways in each incubation condition.

From the first-order kinetic rate fitting analysis of naphthalene concentration time series, two distinct degradation end-member regimes were identified: an initial fast regime characterized by an apparent first order rate constant on the order of 10^{-1} day^{-1} followed by the dominance of a

slower regime. In the anoxic incubations, only the slow regime was observed with a corresponding rate constant on the order of 10^{-2} day^{-1}. Porewater chemistry data revealed that the fast regime end-member was dominated by aerobic and anaerobic respiratory biodegradation, while the slow regime end-member was dominated by fermentative biodegradation. The order-of-magnitude difference between the fast and slow regimes was therefore the result of different dominant naphthalene biodegradation regimes. The varied mixing of respiratory and fermentative regime end-members were attributed as the probable control on differing time scales of biodegradation under different soil moisture and O_2 conditions observed in the experiment.

Findings from Chapter 2 confirmed that at PHC contaminated field sites, biodegradation rates of PHCs can vary greatly depending on soil moisture and oxygen conditions, with a 10 times or greater difference in rates expected between oxic, drier zones and anoxic, saturated zones. Our results also implied that by maintaining both soil moisture and O_2 at optimal conditions in active PHC remediation approaches, PHC biodegradation rates and remediation efficiency can be enhanced further than through the optimization of only one of these two highly variable physical soil parameters. Additionally, with the identification of distinct respiratory and fermentative PHC biodegradation regime end-members and the relationship between their respective rates, the two distinct phases of biodegradation activity could be used as simplified representations of PHC biodegradation when modelling variable moisture and oxygen conditions.

In Chapter 3, the experimental design in Chapter 2 was adapted for a similar naphthalene-spiked soil microcosm incubation experiment under oxic and anoxic headspace conditions at 10, 20, and 30°C. Microcosms were sacrificed daily for oxic incubations and weekly for anoxic incubations and sampled for headspace accumulated gases, porewater chemistry, and dissolved and total soil

naphthalene. Arrhenius temperature sensitivity curve-fitting analysis was conducted on time series data of headspace gases, porewater organic acids and dissolved inorganic carbon.

Results of curve-fitting analysis in Chapter 3 confirmed that the Q_{10} temperature sensitivity quotients of CO_2 and CH_4 accumulation processes encompass values beyond the commonly assumed range of 2 to 3, and a larger range of Q_{10} values were observed for CH_4 accumulation than CO_2 accumulation. In particular, I observed that measured Q_{10} values consistently indicated a greater temperature sensitivity of respiration and methanogenesis processes under anoxic conditions than under oxic conditions, contradicting previous relationships observed in literature. I observed that methanogenesis under anoxic conditions had a particularly high Q_{10} of 9. These findings suggest the potential for an increasing CH_4:CO_2 ratio from soil GHG emissions in a warming climate, especially from anoxic or cold region soils.

Findings and literature from Chapter 3 together suggest that PHC contaminated sites have the potential for increasing GHG emissions as well as increasing contaminant biodegradation rates in a warming climate, especially those in cold regions or with anoxic soils. While the total soil GHG emissions from PHC contaminated sites is small compared to clean soils at the global scale, these expected shifts in soil carbon fluxes are important for the consideration of site managers concerned with site-scale carbon cycling and GHG emissions.

The findings from Chapters 2 and 3 presented in this thesis altogether contribute to the framework in which to consider PHC biodegradation and soil respiration and methanogenesis in the context of variable soil moisture, temperature, and O_2. In Chapter 2, naphthalene biodegradation was identified to proceed under distinct fast and slow respiratory and fermentative end-member

regimes, with biodegradation time scales under different soil moisture and O_2 conditions controlled by the relative contributions of each end-member. This representation of soil moisture and O_2 controls on aerobic and anaerobic PHC biodegradation serves as a potential simplification of such processes in dynamic PHC biodegradation models. In Chapter 3, results challenged previous observations in literature about the temperature sensitivity of aerobic and anaerobic soil respiration, instead finding that soil respiration and methanogenesis processes under anoxic conditions were more sensitive to temperature than under oxic conditions. However, the results from Chapter 3 aligned with existing work acknowledging the higher temperature sensitivity of methanogenesis compared to soil respiration. Overall, Chapter 3 findings indicate that an increasing CH_4:CO_2 ratio in soil carbon emissions may occur in a warming climate, with the effect especially pronounced in anoxic and/or cold region soils. Soil GHG emissions as well as contaminant biodegradation rates at PHC contaminated sites may potentially increase in warmer climates, which is important to acknowledge for an understanding of the changing soil carbon balance at the site-scale.

4.2 Recommendations for future research

In Chapter 2, the challenge of sampling porewater at low soil moistures prevented the desired collection of data across a more comprehensive range of conditions. Therefore, future similar research could benefit from using common naphthalene biodegradation proxies (such as CO_2/CH_4 and naphthalene carbon isotope signatures or total CO_2/CH_4 production) rather than directly measuring naphthalene concentrations in soil and porewater. The cost savings from omitting extraction and analysis of soil and porewater could be diverted to purchase carbon-isotope-tagged naphthalene to improve the accuracy of biodegradation proxies. This will be especially helpful for PHC biodegradation studies at low soil moistures.

The two-regime approach to simplifying aerobic and anaerobic naphthalene biodegradation presented in Chapter 2 holds promise as a potential simplified representation in PHC biodegradation models. However, more work is needed to accurately quantify the relative contributions of respiratory and fermentative regimes under different soil moistures and to validate this approach against experimental data and other modelling approaches.

The improvement in experimental data quality between Chapters 2 and 3 was a testimony to the improvements in experimental design made throughout the course of this work. The methodology described in Chapter 3 would be an excellent starting point for similar soil microcosm incubation experiments, including necessary further research to directly address the temperature sensitivity of the respiratory and fermentative naphthalene biodegradation kinetic regimes identified in Chapter 2. This further work would widen the potential applications of the simplified two-regime biodegradation approach.

Results from Chapter 3 regarding the relative temperature sensitivities of aerobic and anaerobic soil respiration seemed to disagree with most previous observations in the literature. Targeted work to contribute stronger evidence to anaerobic and aerobic soil respiration and methanogenesis temperature sensitivities in different environmental settings is yet to be conducted. A more definitive understanding on the topic would improve the generalization of expected effects of climate change on global soil GHG fluxes.

Overall, challenges were encountered during the experiments in Chapters 2 and 3 resulting from the evolution of soil microbial communities in storage. This occurred during long *ex situ* storage periods while preliminary work was conducted and experimental methodologies were designed,

tested, and refined. I acknowledge the heterogeneity of soil microbial communities over time, in storage, and in different locations in a soil profile or at different sampling sites. Minimizing soil storage time in future work is desirable but not always feasible and does not remove all sources of soil microbial community heterogeneity. Therefore, the characterization of a microbial community profile is recommended for future studies to allow assessment of the comparability between soil from different sites and experiments. This additional qualitative data point could help rule out community structure as a variable in otherwise-comparable experiments.

Data availability

The experimental data reported on in Chapters 2 and 3 are openly available in the Federated Research Data Repository (FRDR) at https://doi.org/10.20383/102.0699 (Chapter 2) and https://doi.org/10.20383/103.0783 (Chapter 3).

References

Agarry, S. E., Aremu, M. O., & Aworanti, O. A. (2013). Kinetic Modelling and Half-Life Study on Bioremediation of Soil Co-Contaminated with Lubricating Motor Oil and Lead Using Different Bioremediation Strategies. *Soil and Sediment Contamination*, *22*(7), 800–816. https://doi.org/10.1080/15320383.2013.768204

Agarry, S. E., & Oghenejoboh, K. M. (2015). Enhanced Aerobic Biodegradation of Naphthalene in Soil: Kinetic Modelling and Half-Life Study. *International Journal of Environmental Bioremediation & Biodegradation*, *3*(2), 48–53. https://doi.org/10.12691/ijebb-3-2-2

Aislabie, J., Saul, D. J., & Foght, J. M. (2006). Bioremediation of hydrocarbon-contaminated polar soils. *Extremophiles*, *10*(3), 171–179. https://doi.org/10.1007/s00792-005-0498-4

ASTM Standard D2488 − 09a. (2009). *Standard Practice for Description and Identification of Soils (Visual-Manual Procedure)*. ASTM International. https://doi.org/10.1520/D2488-09A

Atagana, H. I., Haynes, R. J., & Wallis, F. M. (2003). Optimization of soil physical and chemical conditions for the bioremediation of creosote-contaminated soil. *Biodegradation*, *14*(4), 297–307. https://doi.org/10.1023/A:1024730722751

Barcelo Culleres, D., Boesten, J., Bolognesi, C., Boobis, A., Buchert, A., Capri, E., Coggon, D., Hardy, A., Hart, A., Koepp, H., Liess, M., Luttik, R., Meyer, O., Michaelidou-Canna, S., Montforts, M., Moretto, A., Mueller, M. D., Ossendorp, B., Steurbaut, W., … Vleminckx, C. (2007). Scientific Opinion of the Panel on Plant Protection Products and their Residues on a request from EFSA related to the default Q10 value used to describe the temperature effect on transformation rates of pesticides in soil. *EFSA Journal*, *622*, 1–32. https://doi.org/10.2903/J.EFSA.2008.622

Bass, D. H., Hastings, N. A., & Brown, R. A. (2000). Performance of air sparging systems: a review of case studies. *Journal of Hazardous Materials*, *72*(2–3), 101–119. https://doi.org/10.1016/S0304-3894(99)00136-3

Beolchini, F., Rocchetti, L., Regoli, F., & Dell'Anno, A. (2010). Bioremediation of marine sediments contaminated by hydrocarbons: Experimental analysis and kinetic modeling. *Journal of Hazardous Materials*, *182*(1–3), 403–407. https://doi.org/10.1016/j.jhazmat.2010.06.047

Blagodatskaya, E., Zheng, X., Blagodatsky, S., Wiegl, R., Dannenmann, M., & Butterbach-Bahl, K. (2014). Oxygen and substrate availability interactively control the temperature sensitivity of CO2 and N2O emission from soil. *Biology and Fertility of Soils*, *50*(5), 775–783. https://doi.org/10.1007/s00374-014-0899-6

Bradford, J. B., Schlaepfer, D. R., Lauenroth, W. K., Palmquist, K. A., Chambers, J. C., Maestas, J. D., & Campbell, S. B. (2019). Climate-driven shifts in soil temperature and moisture regimes suggest opportunities to enhance assessments of dryland resilience and resistance. *Frontiers in Ecology and Evolution*, *7*(SEP), 444443. https://doi.org/10.3389/fevo.2019.00358

Brown, D. M., Okoro, S., van Gils, J., van Spanning, R., Bonte, M., Hutchings, T., Linden, O., Egbuche, U., Bruun, K. B., & Smith, J. W. N. (2017). Comparison of landfarming amendments to improve bioremediation of petroleum hydrocarbons in Niger Delta soils. *Science of The Total Environment*, *596–597*, 284–292. https://doi.org/10.1016/J.SCITOTENV.2017.04.072

Byun, E., Rezanezhad, F., Fairbairn, L., Slowinski, S., Basiliko, N., Price, J. S., Quinton, W. L., Roy-Léveillée, P., Webster, K., & Van Cappellen, P. (2021). Temperature, moisture and freeze–thaw controls on CO2 production in soil incubations from northern peatlands. *Scientific Reports*, *11*(1), 23219. https://doi.org/10.1038/s41598-021-02606-3

Calvo, C., Manzanera, M., Silva-Castro, G. A., Uad, I., & González-López, J. (2009). Application of bioemulsifiers in soil oil bioremediation processes. Future prospects. *Science of The Total Environment*, *407*(12), 3634–3640. https://doi.org/10.1016/J.SCITOTENV.2008.07.008

Canadian Council of Ministers of the Environment. (2001). Canada-wide Standards for Petroleum Hydrocarbons (PHC) in Soil. In *CCME Council of Ministers*. http://nwb-oen.ca/sites/default/files/cms_uploads/techguides/phc_standard_1.0_e.pdf

Canadian Council of Ministers of the Environment. (2016). *Guidance Manual for Environmental Site Characterization in Support of Environmental and Human Health Risk Assessment - Volume 4: Analytical Methods*. https://ccme.ca/en/res/guidancemanual-environmentalsitecharacterization_vol_4_epn1557.pdf

Carballeira, T., Ruiz, I., & Soto, M. (2017). Aerobic and anaerobic biodegradability of accumulated solids in horizontal subsurface flow constructed wetlands. *International*

Biodeterioration & Biodegradation, *119*, 396–404. https://doi.org/10.1016/J.IBIOD.2016.10.048

Carretero, S. C., & Kruse, E. E. (2012). Relationship between precipitation and water-table fluctuation in a coastal dune aquifer: Northeastern coast of the Buenos Aires province, Argentina. *Hydrogeology Journal*, *20*(8), 1613–1621. https://doi.org/10.1007/s10040-012-0890-y

Chang, W., Klemm, S., Beaulieu, C., Hawari, J., Whyte, L., & Ghoshal, S. (2011). Petroleum hydrocarbon biodegradation under seasonal freeze-thaw soil temperature regimes in contaminated soils from a sub-arctic site. *Environmental Science and Technology*, *45*(3), 1061–1066. https://doi.org/10.1021/es1022653

Chen, H., & Tian, H. Q. (2005). Does a General Temperature-Dependent Q10 Model of Soil Respiration Exist at Biome and Global Scale? *Journal of Integrative Plant Biology*, *47*(11), 1288–1302. https://doi.org/10.1111/J.1744-7909.2005.00211.X

Chen, H., Zou, J., Cui, J., Nie, M., & Fang, C. (2018). Wetland drying increases the temperature sensitivity of soil respiration. *Soil Biology and Biochemistry*, *120*, 24–27. https://doi.org/10.1016/J.SOILBIO.2018.01.035

Conrad, R. (2020). Importance of hydrogenotrophic, aceticlastic and methylotrophic methanogenesis for methane production in terrestrial, aquatic and other anoxic environments: A mini review. *Pedosphere*, *30*(1), 25–39. https://doi.org/10.1016/S1002-0160(18)60052-9

Davidson, E. A., & Janssens, I. A. (2006). Temperature sensitivity of soil carbon decomposition and feedbacks to climate change. *Nature*, *440*, 165–173. https://doi.org/10.1038/nature04514

Dibble, J. T., & Bartha, R. (1979). Effect of environmental parameters on the biodegradation of oil sludge. *Applied and Environmental Microbiology*, *37*(4), 729–739. https://doi.org/10.1128/AEM.37.4.729-739.1979

Dolfing, J., Xu, A., Gray, N. D., Larter, S. R., & Head, I. M. (2009). The thermodynamic landscape of methanogenic PAH degradation. *Microbial Biotechnology*, *2*(5), 566–574. https://doi.org/10.1111/j.1751-7915.2009.00096.x

Ehlers, G. A. C., & Loibner, A. P. (2006). Linking organic pollutant (bio)availability with geosorbent properties and biomimetic methodology: A review of geosorbent characterisation and (bio)availability prediction. *Environmental Pollution*, *141*(3), 494–512. https://doi.org/10.1016/J.ENVPOL.2005.08.063

Fairbairn, L., Rezanezhad, F., Gharasoo, M., Parsons, C. T., Macrae, M. L., Slowinski, S., & Van Cappellen, P. (2023). Relationship between soil CO2 fluxes and soil moisture: Anaerobic sources explain fluxes at high water content. *Geoderma*, *434*, 116493. https://doi.org/10.1016/j.geoderma.2023.116493

Fang, C., & Moncrieff, J. B. (2001). The dependence of soil CO2 efflux on temperature. *Soil Biology and Biochemistry*, *33*(2), 155–165. https://doi.org/10.1016/S0038-0717(00)00125-5

Fang, C., Smith, P., Moncrieff, J. B., & Smith, J. U. (2005). Similar response of labile and resistant soil organic matter pools to changes in temperature. *Nature*, *433*, 57–59. https://doi.org/10.1038/nature03138

Garg, S., Newell, C. J., Kulkarni, P. R., King, D. C., Adamson, D. T., Renno, M. I., & Sale, T. (2017). Overview of Natural Source Zone Depletion: Processes, Controlling Factors, and Composition Change. *Groundwater Monitoring and Remediation*, *37*(3), 62–81. https://doi.org/10.1111/gwmr.12219

Gieg, L. M., Fowler, S. J., & Berdugo-Clavijo, C. (2014). Syntrophic biodegradation of hydrocarbon contaminants. *Current Opinion in Biotechnology*, *27*, 21–29. https://doi.org/10.1016/J.COPBIO.2013.09.002

Gill, A. L., Giasson, M. A., Yu, R., & Finzi, A. C. (2017). Deep peat warming increases surface methane and carbon dioxide emissions in a black spruce-dominated ombrotrophic bog. *Global Change Biology*, *23*(12), 5398–5411. https://doi.org/10.1111/GCB.13806

Guarino, C., Spada, V., & Sciarrillo, R. (2017). Assessment of three approaches of bioremediation (Natural Attenuation, Landfarming and Bioagumentation – Assistited Landfarming) for a petroleum hydrocarbons contaminated soil. *Chemosphere*, *170*, 10–16. https://doi.org/10.1016/j.chemosphere.2016.11.165

Guerin, W. F., & Boyd, S. A. (1992). Differential bioavailability of soil-sorbed naphthalene to two bacterial species. *Applied and Environmental Microbiology*, *58*(4), 1142–1152. https://doi.org/10.1128/AEM.58.4.1142-1152.1992

Haider, F. U., Ejaz, M., Cheema, S. A., Khan, M. I., Zhao, B., Liqun, C., Salim, M. A., Naveed, M., Khan, N., Núñez-Delgado, A., & Mustafa, A. (2021). Phytotoxicity of petroleum hydrocarbons: Sources, impacts and remediation strategies. *Environmental Research*, *197*, 111031. https://doi.org/10.1016/J.ENVRES.2021.111031

Hao, X., Ball, B. C., Culley, J. L. B., Carter, M. R., & Parking, G. W. (2008). Chapter 57: Soil Density and Porosity. In M. R. Carter & E. G. Gregorich (Eds.), *Soil Sampling and Methods of Analysis* (2nd ed., pp. 743–759). CRC Press.

Henry, H. A. L. (2008). Climate change and soil freezing dynamics: Historical trends and projected changes. *Climatic Change*, *87*(3–4), 421–434. https://doi.org/10.1007/s10584-007-9322-8

Holman, H. Y., & Tsang, Y. W. (1995). Effects of soil moisture on biodegradation of petroleum hydrocarbons. In R. E. Hinchee, R. N. Miller, & P. C. Johnson (Eds.), *In situ aeration: air sparging, bioventing, and related remediation processes* (pp. 323–332). Colombus: Battelle.

Hur, J., Park, S. W., Kim, M. C., & Kim, H. S. (2013). Enhanced binding of hydrophobic organic contaminants by microwave-assisted humification of soil organic matter. *Chemosphere*, *93*(11), 2704–2710. https://doi.org/10.1016/J.CHEMOSPHERE.2013.08.073

Illman, W. A., & Alvarez, P. J. J. (2006). *Bioremediation and natural attenuation: process fundamentals and mathematical models*. John Wiley & Sons.

IPCC. (2023). Summary for Policymakers. In H. Lee & J. Romero (Eds.), *Climate Change 2023: Synthesis Report. A Report of the Intergovernmental Panel on Climate Change. Contribution of Working Groups I, II and III to the Sixth Assessment Report of the Intergovernmental Panel on Climate Change* (pp. 1–36). IPCC.

Janssens, I. A., & Pilegaard, K. (2003). Large seasonal changes in Q10 of soil respiration in a beech forest. *Global Change Biology*, *9*(6), 911–918. https://doi.org/10.1046/J.1365-2486.2003.00636.X

Kao, C. M., Chen, C. Y., Chen, S. C., Chien, H. Y., & Chen, Y. L. (2008). Application of in situ biosparging to remediate a petroleum-hydrocarbon spill site: Field and microbial evaluation. *Chemosphere*, *70*(8), 1492–1499. https://doi.org/10.1016/J.CHEMOSPHERE.2007.08.029

Kebede, G., Tafese, T., Abda, E. M., Kamaraj, M., & Assefa, F. (2021). Factors Influencing the Bacterial Bioremediation of Hydrocarbon Contaminants in the Soil: Mechanisms and Impacts. *Journal of Chemistry*, *2021*, 9823362. https://doi.org/10.1155/2021/9823362

Khan, F. I., Husain, T., & Hejazi, R. (2004). An overview and analysis of site remediation technologies. *Journal of Environmental Management*, *71*(2), 95–122. https://doi.org/10.1016/J.JENVMAN.2004.02.003

Kolhatkar, R., & Schnobrich, M. (2017). Land Application of Sulfate Salts for Enhanced Natural Attenuation of Benzene in Groundwater: A Case Study. *Groundwater Monitoring & Remediation*, *37*(2), 43–57. https://doi.org/10.1111/GWMR.12209

Kotsyurbenko, O. R. (2005). Trophic interactions in the methanogenic microbial community of low-temperature terrestrial ecosystems. *FEMS Microbiology Ecology*, *53*(1), 3–13. https://doi.org/10.1016/J.FEMSEC.2004.12.009

Kozerski, G. E., Xu, S., Miller, J., & Durham, J. (2014). Determination of soil-water sorption coefficients of volatile methylsiloxanes. *Environmental Toxicology and Chemistry*, *33*(9), 1937–1945. https://doi.org/10.1002/etc.2640

Krumina, L., Lyngsie, G., Tunlid, A., & Persson, P. (2017). Oxidation of a Dimethoxyhydroquinone by Ferrihydrite and Goethite Nanoparticles: Iron Reduction versus Surface Catalysis. *Environmental Science and Technology*, *51*(16), 9053–9061. https://doi.org/10.1155/2019/8124716

Lal, P., Shekhar, A., Gharun, M., & Das, N. N. (2023). Spatiotemporal evolution of global long-term patterns of soil moisture. *Science of The Total Environment*, *867*, 161470. https://doi.org/10.1016/J.SCITOTENV.2023.161470

Lautz, L. K. (2008). Estimating groundwater evapotranspiration rates using diurnal water-table fluctuations in a semi-arid riparian zone. *Hydrogeology Journal*, *16*(3), 483–497. https://doi.org/10.1007/s10040-007-0239-0

Lembrechts, J. J., van den Hoogen, J., Aalto, J., Ashcroft, M. B., De Frenne, P., Kemppinen, J., Kopecký, M., Luoto, M., Maclean, I. M. D., Crowther, T. W., Bailey, J. J., Haesen, S., Klinges, D. H., Niittynen, P., Scheffers, B. R., Van Meerbeek, K., Aartsma, P., Abdalaze, O., Abedi, M., … Lenoir, J. (2022). Global maps of soil temperature. *Global Change Biology*, *28*(9), 3110–3144. https://doi.org/10.1111/GCB.16060

Leroy, F., Gogo, S., Guimbaud, C., Bernard-Jannin, L., Hu, Z., & Laggoun-Défarge, F. (2017). Vegetation composition controls temperature sensitivity of CO2 and CH4 emissions and DOC concentration in peatlands. *Soil Biology and Biochemistry*, *107*, 164–167. https://doi.org/10.1016/J.SOILBIO.2017.01.005

Liang, B., Wang, L.-Y., Mbadinga, S. M., Liu, J.-F., Yang, S.-Z., Gu, J.-D., & Mu, B.-Z. (2015). Anaerolineaceae and Methanosaeta turned to be the dominant microorganisms in alkanes-

dependent methanogenic culture after long-term of incubation. *AMB Express*, *5*(1), 37. https://doi.org/10.1186/s13568-015-0117-4

Liu, Y. F., Liu, Z. L., Ye, Y. L., Zhou, L., Liu, J. F., Yang, S. Z., Gu, J. D., & Mu, B. Z. (2021). Aminirod propionatiphilus gen. nov., sp. nov., an isolated secondary fermenter in methanogenic hydrocarbon-degrading communities. *International Biodeterioration & Biodegradation*, *165*, 105323. https://doi.org/10.1016/J.IBIOD.2021.105323

Lupascu, M., Wadham, J., Hornibrook, E., & Pancost, R. (2018). Temperature Sensitivity of Methane Production in the Permafrost Active Layer at Stordalen, Sweden: A Comparison with Non-permafrost Northern Wetlands. *Arctic, Antarctic, and Alpine Research*, *44*(4), 469–482. https://doi.org/10.1657/1938-4246-44.4.469

Lv, H., Su, X., Wang, Y., Dai, Z., & Liu, M. (2018). Effectiveness and mechanism of natural attenuation at a petroleum-hydrocarbon contaminated site. *Chemosphere*, *206*, 293–301. https://doi.org/10.1016/J.CHEMOSPHERE.2018.04.171

Macintyre, W. G., Boggs, M., Antworth, C. P., & Stauffer, T. B. (1993). Degradation Kinetics of Aromatic Organic Solutes Introduced Into a Heterogeneous Aquifer. *Water Resources Research*, *29*(12), 4045–4051. https://doi.org/10.1029/93WR02276

Marr, L. C., Booth, E. C., Andersen, R. G., Widdowson, M. A., & Novak, J. T. (2006). Direct Volatilization of Naphthalene to the Atmosphere at a Phytoremediation Site. *Environmental Science and Technology*, *40*(17), 5560–5566. https://doi.org/10.1021/es060087+

Martin, B. C., George, S. J., Price, C. A., Shahsavari, E., Ball, A. S., Tibbett, M., & Ryan, M. H. (2016). Citrate and malonate increase microbial activity and alter microbial community composition in uncontaminated and diesel-contaminated soil microcosms. *SOIL*, *2*(3), 487–498. https://doi.org/10.5194/SOIL-2-487-2016

Martínez Álvarez, L. M., Ruberto, L. A. M., Gurevich, J. M., & Mac Cormack, W. P. (2020). Environmental factors affecting reproducibility of bioremediation field assays in Antarctica. *Cold Regions Science and Technology*, *169*, 102915. https://doi.org/10.1016/J.COLDREGIONS.2019.102915

Mayer, A. S., & Hassanizadeh, S. M. (2005). Soil and Groundwater Contamination: Nonaqueous Phase Liquids—Principles and Observations. In A. S. Mayer & S. M. Hassanizadeh (Eds.), *Water Resources Monograph Book Series: Soil and Groundwater Contamination:*

Nonaqueous Phase Liquids–Principles and Observations (Vol. 17). American Geophysical Union. https://doi.org/10.1029/WM017

Metje, M., & Frenzel, P. (2005). Effect of temperature on anaerobic ethanol oxidation and methanogenesis in acidic peat from a Northern Wetland. *Applied and Environmental Microbiology*, *71*(12), 8191–8200. https://doi.org/10.1128/AEM.71.12.8191-8200.2005

Meyer, N., Welp, G., & Amelung, W. (2018). The Temperature Sensitivity (Q10) of Soil Respiration: Controlling Factors and Spatial Prediction at Regional Scale Based on Environmental Soil Classes. *Global Biogeochemical Cycles*, *32*(2), 306–323. https://doi.org/10.1002/2017GB005644

Moscoso, F., Teijiz, I., Deive, F. J., & Sanromán, M. A. (2012). Efficient PAHs biodegradation by a bacterial consortium at flask and bioreactor scale. *Bioresource Technology*, *119*, 270–276. https://doi.org/10.1016/J.BIORTECH.2012.05.095

Moyano, F. E., Manzoni, S., & Chenu, C. (2013). Responses of soil heterotrophic respiration to moisture availability: An exploration of processes and models. *Soil Biology and Biochemistry*, *59*, 72–85. https://doi.org/10.1016/J.SOILBIO.2013.01.002

Moyano, F. E., Vasilyeva, N., Bouckaert, L., Cook, F., Craine, J., Curiel Yuste, J., Don, A., Epron, D., Formanek, P., Franzluebbers, A., Ilstedt, U., Kätterer, T., Orchard, V., Reichstein, M., Rey, A., Ruamps, L., Subke, J. A., Thomsen, I. K., & Chenu, C. (2012). The moisture response of soil heterotrophic respiration: interaction with soil properties. *Biogeosciences*, *9*(3), 1173–1182. https://doi.org/10.5194/BG-9-1173-2012

Mozo, I., Lesage, G., Yin, J., Bessiere, Y., Barna, L., & Sperandio, M. (2012). Dynamic modeling of biodegradation and volatilization of hazardous aromatic substances in aerobic bioreactor. *Water Research*, *46*(16), 5327–5342. https://doi.org/10.1016/j.watres.2012.07.014

Ngueleu, S. K., Al-Raoush, R. I., Shafieiyoun, S., Rezanezhad, F., & Van Cappellen, P. (2019). Biodegradation Kinetics of Benzene and Naphthalene in the Vadose and Saturated Zones of a (Semi)-Arid Saline Coastal Soil Environment. *Geofluids*, *2019*, 8124716. https://doi.org/10.1155/2019/8124716

Nozhevnikova, A. N., Nekrasova, V., Ammann, A., Zehnder, A. J. B., Wehrli, B., & Holliger, C. (2007). Influence of temperature and high acetate concentrations on methanogenensis in lake sediment slurries. *FEMS Microbiology Ecology*, *62*(3), 336–344. https://doi.org/10.1111/J.1574-6941.2007.00389.X

Oertel, C., Matschullat, J., Zurba, K., Zimmermann, F., & Erasmi, S. (2016). Greenhouse gas emissions from soils—A review. *Geochemistry*, *76*(3), 327–352. https://doi.org/10.1016/J.CHEMER.2016.04.002

Ossai, I. C., Ahmed, A., Hassan, A., & Hamid, F. S. (2020). Remediation of soil and water contaminated with petroleum hydrocarbon: A review. *Environmental Technology & Innovation*, *17*, 100526. https://doi.org/10.1016/J.ETI.2019.100526

Pathak, H., Kantharia, D., Malpani, A., & Madamwar, D. (2009). Naphthalene degradation by Pseudomonas sp. HOB1: In vitro studies and assessment of naphthalene degradation efficiency in simulated microcosms. *Journal of Hazardous Materials*, *166*(2–3), 1466–1473. https://doi.org/10.1016/J.JHAZMAT.2008.12.074

Peters, G. P., Marland, G., Le Quéré, C., Boden, T., Canadell, J. G., & Raupach, M. R. (2011). Rapid growth in CO2 emissions after the 2008–2009 global financial crisis. *Nature Climate Change*, *2*(1), 2–4. https://doi.org/10.1038/nclimate1332

Philp, J. C., & Atlas, R. M. (2014). Chapter 5: Bioremediation of Contaminated Soils and Aquifers. In *Bioremediation: Applied Microbial Solutions for Real-World Environmental Cleanup* (pp. 139–236). John Wiley & Sons, Ltd. https://doi.org/10.1128/9781555817596.CH5

Priemé, A., & Christensen, S. (2001). Natural perturbations, drying–wetting and freezing–thawing cycles, and the emission of nitrous oxide, carbon dioxide and methane from farmed organic soils. *Soil Biology and Biochemistry*, *33*(15), 2083–2091. https://doi.org/10.1016/S0038-0717(01)00140-7

Raich, J. W., & Potter, C. S. (1995). Global patterns of carbon dioxide emissions from soils. *Global Biogeochemical Cycles*, *9*(1), 23–36. https://doi.org/10.1029/94GB02723

Raich, J. W., & Schlesinger, W. H. (1992). The global carbon dioxide flux in soil respiration and its relationship to vegetation and climate. *Tellus, Series B*, *44 B*(2), 81–99. https://doi.org/10.3402/TELLUSB.V44I2.15428

Ramezanzadeh, M., Slowinski, S., Rezanezhad, F., Murr, K., Lam, C., Smeaton, C., Alibert, C., Vandergriendt, M., & Van Cappellen, P. (2023). Effects of freeze-thaw cycles on methanogenic hydrocarbon degradation: Experiment and modeling. *Chemosphere*, *325*, 138405. https://doi.org/10.1016/J.CHEMOSPHERE.2023.138405

Rockne, K. J., & Strand, S. E. (1998). Biodegradation of Bicyclic and Polycyclic Aromatic Hydrocarbons in Anaerobic Enrichments. *Environmental Science and Technology*, *32*(24), 3962–3967. https://doi.org/10.1021/ES980368K

Saha, S., Badhe, N., De Vrieze, J., Biswas, R., & Nandy, T. (2015). Methanol induces low temperature resilient methanogens and improves methane generation from domestic wastewater at low to moderate temperatures. *Bioresource Technology*, *189*, 370–378. https://doi.org/10.1016/J.BIORTECH.2015.04.056

Schjønning, P., Thomsen, I. K., Petersen, S. O., Kristensen, K., & Christensen, B. T. (2011). Relating soil microbial activity to water content and tillage-induced differences in soil structure. *Geoderma*, *163*(3–4), 256–264. https://doi.org/10.1016/J.GEODERMA.2011.04.022

Shi, B., Ngueleu, S. K., Rezanezhad, F., Slowinski, S., Pronk, G. J., Smeaton, C. M., Stevenson, K., Al-Raoush, R. I., & Van Cappellen, P. (2020). Sorption and desorption of the model aromatic hydrocarbons naphthalene and benzene: Effects of temperature and soil composition. *Frontiers in Environmental Chemistry*, *1*, 581103. https://doi.org/10.3389/FENVC.2020.581103

Shibata, A., Inoue, Y., & Katayama, A. (2006). Aerobic and anaerobic biodegradation of phenol derivatives in various paddy soils. *Science of The Total Environment*, *367*(2–3), 979–987. https://doi.org/10.1016/J.SCITOTENV.2006.01.031

Sierra, C. A., Malghani, S., & Loescher, H. W. (2017). Interactions among temperature, moisture, and oxygen concentrations in controlling decomposition rates in a boreal forest soil. *Biogeosciences*, *14*(3), 703–710. https://doi.org/10.5194/bg-14-703-2017

Sihota, N. J., & Mayer, K. U. (2012). Characterizing Vadose Zone Hydrocarbon Biodegradation Using Carbon Dioxide Effluxes, Isotopes, and Reactive Transport Modeling. *Vadose Zone Journal*, *11*(4), vzj2011.0204. https://doi.org/10.2136/VZJ2011.0204

Sihota, N. J., Singurindy, O., & Mayer, K. U. (2011). CO2-Efflux measurements for evaluating source zone natural attenuation rates in a petroleum hydrocarbon contaminated aquifer. *Environmental Science and Technology*, *45*(2), 482–488. https://doi.org/10.1021/es1032585

Silva-Castro, G. A., Rodriguez-Calvo, A., Laguna, J., González-López, J., & Calvo, C. (2016). Autochthonous microbial responses and hydrocarbons degradation in polluted soil during

biostimulating treatments under different soil moisture. Assay in pilot plant. *International Biodeterioration & Biodegradation*, *108*, 91–98. https://doi.org/10.1016/j.ibiod.2015.12.009

Singh, J. S., & Gupta, S. R. (1977). Plant decomposition and soil respiration in terrestrial ecosystems. *The Botanical Review 1977 43:4*, *43*(4), 449–528. https://doi.org/10.1007/BF02860844

Skopp, J., Jawson, M. D., & Doran, J. W. (1990). Steady-State Aerobic Microbial Activity as a Function of Soil Water Content. *Soil Science Society of America Journal*, *54*(6), 1619–1625. https://doi.org/10.2136/SSSAJ1990.03615995005400060018X

Szafranek-Nakonieczna, A., & Stêpniewska, Z. (2014). Aerobic and anaerobic respiration in profiles of Polesie Lubelskie peatlands. *International Agrophysics*, *28*(2), 219–229. https://doi.org/10.2478/intag-2014-0011

Tanco, R., & Kruse, E. (2001). Prediction of seasonal water-table fluctuations in La Pampa and Buenos Aires, Argentina. *Hydrogeology Journal*, *9*(4), 339–347. https://doi.org/10.1007/s100400100143

Thierrin, J., Davis, G. B., Barber, C., Patterson, B. M., Pribac, F., Power, T. R., & Lambert, M. (1993). Natural degradation rates of BTEX compounds and naphthalene in a sulphate reducing groundwater environment. *Hydrological Sciences Journal*, *38*(4), 309–322. https://doi.org/10.1080/02626669309492677

Tibbett, M., George, S. J., Davie, A., Barron, A., Milton, N., & Greenwood, P. F. (2011). Just add water and salt: The optimisation of petrogenic hydrocarbon biodegradation in soils from semi-arid Barrow Island, Western Australia. *Water, Air, and Soil Pollution*, *216*(1–4), 513–525. https://doi.org/10.1007/s11270-010-0549-z

Treasury Board of Canada Secretariat. (2022, May 1). *Contaminants and Media*. Federal Contaminants Site Inventory. https://www.tbs-sct.gc.ca/fcsi-rscf/cm-eng.aspx

Umar, Z. D., Aziz, N. A. A., Zulkifli, S. Z., & Mustafa, M. (2017). Rapid biodegradation of polycyclic aromatic hydrocarbons (PAHs) using effective Cronobacter sakazakii MM045 (KT933253). *MethodsX*, *4*, 104–117. https://doi.org/10.1016/J.MEX.2017.02.003

United States Environmental Protection Agency. (2023, May 22). *Importance of Methane*. Global Methane Initiative. https://www.epa.gov/gmi/importance-methane

Van Hulzen, J. B., Segers, R., Van Bodegom, P. M., & Leffelaar, P. A. (1999). Temperature effects on soil methane production: an explanation for observed variability. *Soil Biology and Biochemistry*, *31*(14), 1919–1929. https://doi.org/10.1016/S0038-0717(99)00109-1

Verginelli, I., & Baciocchi, R. (2011). Modeling of vapor intrusion from hydrocarbon-contaminated sources accounting for aerobic and anaerobic biodegradation. *Journal of Contaminant Hydrology*, *126*(3–4), 167–180. https://doi.org/10.1016/J.JCONHYD.2011.08.010

Vincent, G., Shahriari, A. R., Lucot, E., Badot, P. M., & Epron, D. (2006). Spatial and seasonal variations in soil respiration in a temperate deciduous forest with fluctuating water table. *Soil Biology and Biochemistry*, *38*(9), 2527–2535. https://doi.org/10.1016/J.SOILBIO.2006.03.009

Vincent, S. G. T., Jennerjahn, T., & Ramasamy, K. (2021). Environmental variables and factors regulating microbial structure and functions. *Microbial Communities in Coastal Sediments*, 79–117. https://doi.org/10.1016/B978-0-12-815165-5.00003-0

Wang, C., Lai, D. Y. F., Tong, C., Wang, W., Huang, J., & Zeng, C. (2015). Variations in Temperature Sensitivity (Q10) of CH4 Emission from a Subtropical Estuarine Marsh in Southeast China. *PLOS ONE*, *10*(5), 0125227. https://doi.org/10.1371/JOURNAL.PONE.0125227

Wegwu, M. O., Uwakwe, A. A., & Anabi, M. A. (2010). Efficacy of enhanced natural attenuation (land farming) technique in the remediation of crude oil-polluted agricultural land. *Archives of Applied Science Research*, *2*(2), 431–442. www.scholarsresearchlibrary.com

Wei, L., Zhu, Z., Liu, S., Xiao, M., Wang, J., Deng, Y., Kuzyakov, Y., Wu, J., & Ge, T. (2021). Temperature sensitivity (Q10) of stable, primed and easily available organic matter pools during decomposition in paddy soil. *Applied Soil Ecology*, *157*, 103752. https://doi.org/10.1016/J.APSOIL.2020.103752

Weiner, J. M., & Lovley, D. R. (1998). Rapid benzene degradation in methanogenic sediments from a petroleum- contaminated aquifer. *Applied and Environmental Microbiology*, *64*(5), 1937–1939. https://doi.org/10.1128/AEM.64.5.1937-1939.1998

Wentworth, C. K. (1922). A Scale of Grade and Class Terms for Clastic Sediments. *The Journal of Geology*, *30*(5), 337–392. https://doi.org/https://doi.org/10.1086/622910

Whiticar, M. J. (2020). The Biogeochemical Methane Cycle. In *Hydrocarbons, Oils and Lipids: Diversity, Origin, Chemistry and Fate* (pp. 1–78). Springer International Publishing. https://doi.org/10.1007/978-3-319-54529-5_5-1

Wozney, A., Clark, I. D., & Mayer, K. U. (2021). Quantifying natural source zone depletion at petroleum hydrocarbon contaminated sites: A comparison of 14C methods. *Journal of Contaminant Hydrology*, *240*, 103795. https://doi.org/10.1016/j.jconhyd.2021.103795

Wu, M., Ye, X., Chen, K., Li, W., Yuan, J., & Jiang, X. (2017). Bacterial community shift and hydrocarbon transformation during bioremediation of short-term petroleum-contaminated soil. *Environmental Pollution*, *223*, 657–664. https://doi.org/10.1016/J.ENVPOL.2017.01.079

Yadav, B. K., & Hassanizadeh, S. M. (2011). An overview of biodegradation of LNAPLs in coastal (Semi)-arid environment. *Water, Air, and Soil Pollution*, *220*(1–4), 225–239. https://doi.org/10.1007/s11270-011-0749-1

Yang, S., He, Z., & Chen, L. (2023). Different responses of CO2 and CH4 to freeze-thaw cycles in an alpine forest ecosystem in northwestern China. *Science of The Total Environment*, *863*, 160886. https://doi.org/10.1016/J.SCITOTENV.2022.160886

Zhang, X., Flato, G., Kirchmeier-Young, M., Vincent, L., Wan, H., Wang, X., Rong, R., Fyfe, J., Li, G., & Kharin, V. V. (2019). Changes in Temperature and Precipitation Across Canada; Chapter 4. In E. Bush & D. S. Lemmen (Eds.), *Canada's Changing Climate Report* (pp. 112–193). Government of Canada.

Zhang, Y., Chen, W., Smith, S. L., Riseborough, D. W., & Cihlar, J. (2005). Soil temperature in Canada during the twentieth century: Complex responses to atmospheric climate change. *Journal of Geophysical Research: Atmospheres*, *110*(D3), 1–15. https://doi.org/10.1029/2004JD004910

Zheng, D., Hunt, E. R., & Running, S. W. (1993). *A daily soil temperature model based on air temperature and precipitation for continental applications*. *2*, 183–191.

Zhou, T., Shi, P., Hui, D., & Luo, Y. (2009). Global pattern of temperature sensitivity of soil heterotrophic respiration (Q10) and its implications for carbon-climate feedback. *Journal of Geophysical Research: Biogeosciences*, *114*(G2). https://doi.org/10.1029/2008JG000850

Zhu, R., Liu, Y., Ma, E., Sun, J., Xu, H., & Sun, L. (2009). Greenhouse gas emissions from penguin guanos and ornithogenic soils in coastal Antarctica: Effects of freezing–thawing cycles.

Atmospheric Environment, *43*(14), 2336–2347. https://doi.org/10.1016/J.ATMOSENV.2009.01.027

I. Appendix I – Additional results from Chapter 2

Table AI-1. Net change in headspace methane (CH_4), headspace carbon dioxide (CO_2), headspace oxygen (O_2) and porewater dissolved inorganic carbon (DIC) after 44 days of incubation. Averages of triplicate jars and associated standard deviations (SD) are shown. Where no SD is given, triplicate jars did not yield enough sample volume for analysis, and a SD could not be calculated. Net change in CH_4, CO_2, and O_2 headspace concentrations are shown in units of µmoles of carbon or percent per litre of headspace volume. Net change in DIC porewater concentrations are shown in units of millimoles per litre of porewater volume.

Moisture and O_2 condition	Experimental treatment	**Headspace CH_4**		**Headspace CO_2**		**Headspace O_2**		**Porewater DIC**	
		Net change (µmol-C L^{-1})	SD	Net change (µmol-C L^{-1})	SD	Net change (%)	SD	Net change (mmol-C L^{-1})	SD
60% WFPS, oxic	Nap	9.59×10^{-3}	1.78×10^{-2}	3.08×10^{2}	1.85×10^{2}	-25.6	4.89	9.52×10^{-1}	--
	No Nap	1.39×10^{-2}	1.46×10^{-2}	3.39×10^{2}	6.52×10^{1}	-28.3	0.20	1.40×10^{0}	--
80% WFPS, oxic	Nap	2.60×10^{-3}	9.07×10^{-3}	4.34×10^{2}	7.88×10^{1}	-25.1	2.30	1.98×10^{0}	--
	No Nap	1.30×10^{-2}	1.88×10^{-2}	1.37×10^{2}	2.82×10^{1}	-28.2	0.08	9.11×10^{-1}	1.22×10^{-1}
	Abiotic	-1.07×10^{-2}	5.16×10^{-3}	6.55×10^{1}	1.36×10^{1}	-15.0	4.30	-5.42×10^{-1}	--
100% WFPS, oxic	Nap	1.37×10^{-2}	8.73×10^{-3}	7.05×10^{1}	2.52×10^{1}	-28.1	0.03	7.76×10^{-1}	1.31×10^{-1}
	No Nap	5.48×10^{-4}	5.48×10^{-3}	5.04×10^{1}	9.01×10^{0}	-28.1	0.02	7.05×10^{-1}	1.30×10^{-1}

100% WFPS, anoxic	Nap	1.90×10^{0}	1.61×10^{0}	4.74×10^{2}	2.82×10^{1}	9.49	2.24	2.36×10^{0}	6.67×10^{-1}
	No Nap	1.45×10^{0}	1.66×10^{0}	5.43×10^{2}	2.31×10^{2}	7.01	5.66	2.59×10^{0}	5.40×10^{-1}
	Abiotic	2.58×10^{-2}	3.15×10^{-2}	3.82×10^{1}	5.18×10^{0}	6.53	2.66	-8.07×10^{-1}	1.63×10^{-2}

Table AI-2. Initial total naphthalene mass, volatilized fraction of naphthalene, and effective initial naphthalene mass in each experimental soil moisture treatment. Initial total naphthalene mass is the known added naphthalene mass. The volatilized fraction was calculated (or extrapolated as indicated) from the differences between the initial aqueous naphthalene mass and aqueous naphthalene mass remaining after equilibration. Effective initial naphthalene mass was calculated as: initial total naphthalene mass × (1 – total volatilized fraction). Different initial total naphthalene masses are a result of different APW volumes in each soil moisture treatment.

Treatment	Initial total naphthalene mass (µmol-C)	Total volatilized fraction (%)	Effective initial naphthalene mass (µmol-C)
60% WFPS, oxic	5.17	13.5%*	4.47
80% WFPS, oxic	7.15	12.9%	6.23
100% WFPS, oxic	8.74	12.5%*	7.65
100% WFPS, anoxic	11.13	12.0%	9.79

*Extrapolated values.

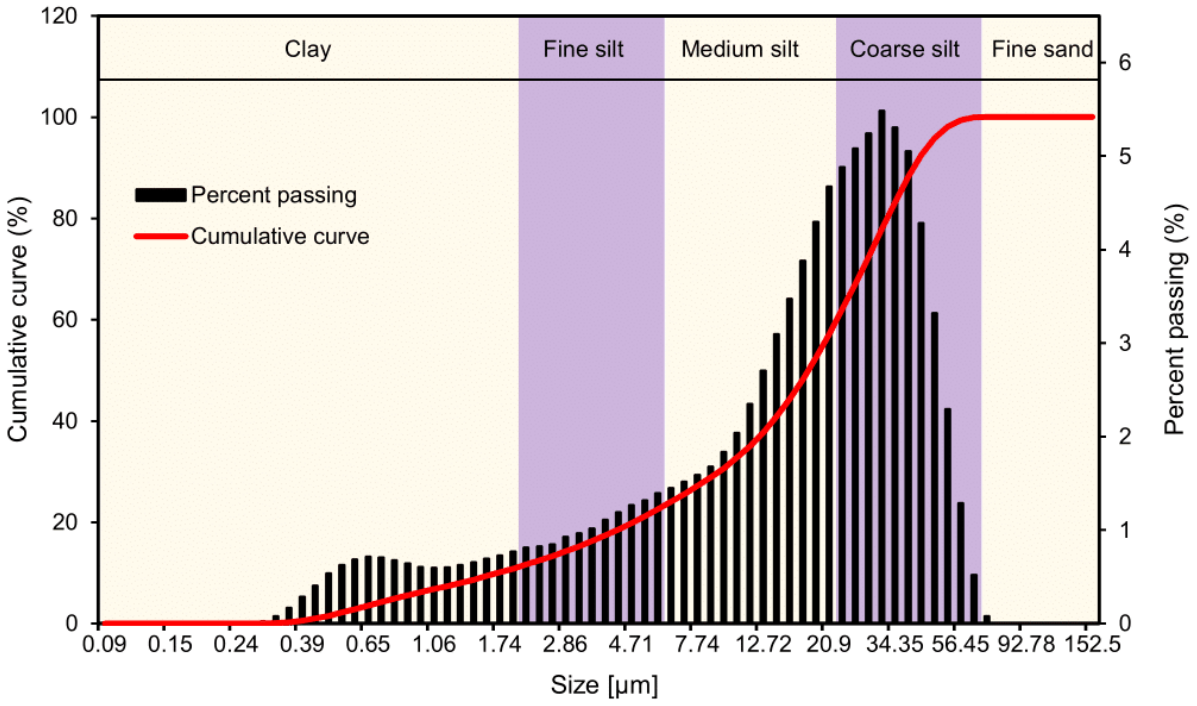

Figure AI-1. Particle size distribution and cumulative curve of soil used in the incubation experiment. Wentworth grain size classes (Wentworth, 1922) are indicated on the figure.

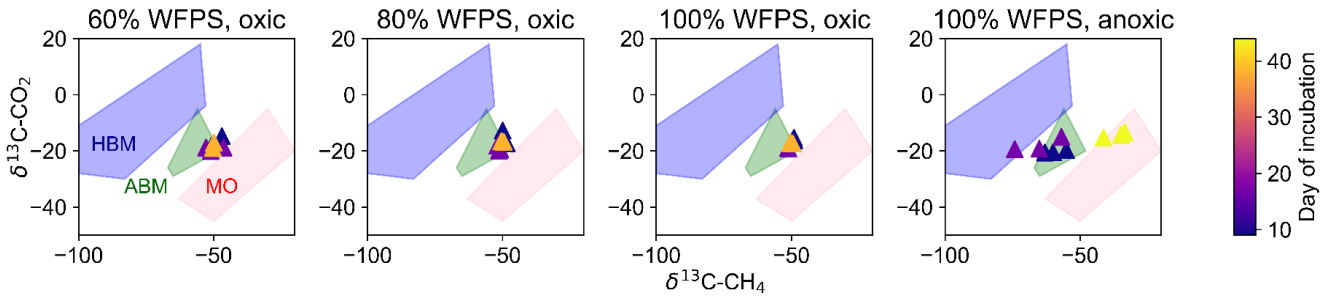

Figure AI-2. δ^{13}C-CH_4 versus δ^{13}C-CO_2 isotope compositions in the headspace of Nap-spiked jars. Points are coloured by the data of incubation. Data for 60% oxic, 80% oxic, and 100% oxic treatments were collected on Days 9, 17, and 38 of the incubation. Data for 100% anoxic treatments were collected on Days 9, 17, and 44. Blue, green, and pink coloured regions represent domains of δ^{13}C-CH_4 versus δ^{13}C-CO_2 isotope composition differentiation due to hydrogen-based methanogenesis (HBM), acetate-based methanogenesis (ABM), and methane oxidation (MO), as described in Whiticar (2020). The fourth panel indicates the presence of ABM, and possibly HBM, activity in the 100% WFPS anoxic incubation at Days 9 and 17.

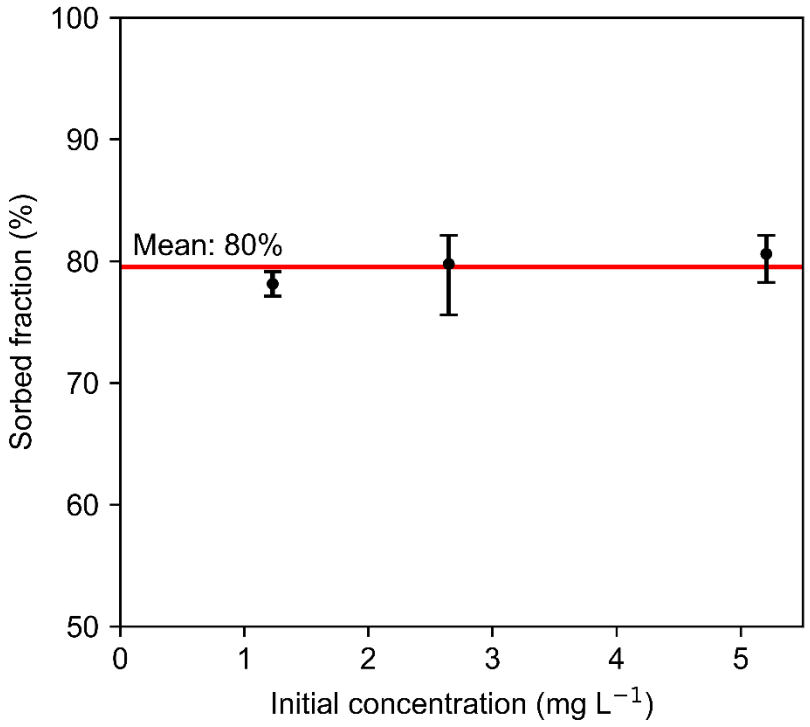

Figure AI-3. Percent of aqueous naphthalene that partitioned into the sorbed phase after 48 hours of equilibration at room temperature in the naphthalene sorption isotherm tests. Incubations at all three initial concentrations tested (1.25, 2.5, and 5 mg L^{-1} naphthalene) resulted in 80% partitioning into the sorbed phase (and 20% remained in the aqueous phase).

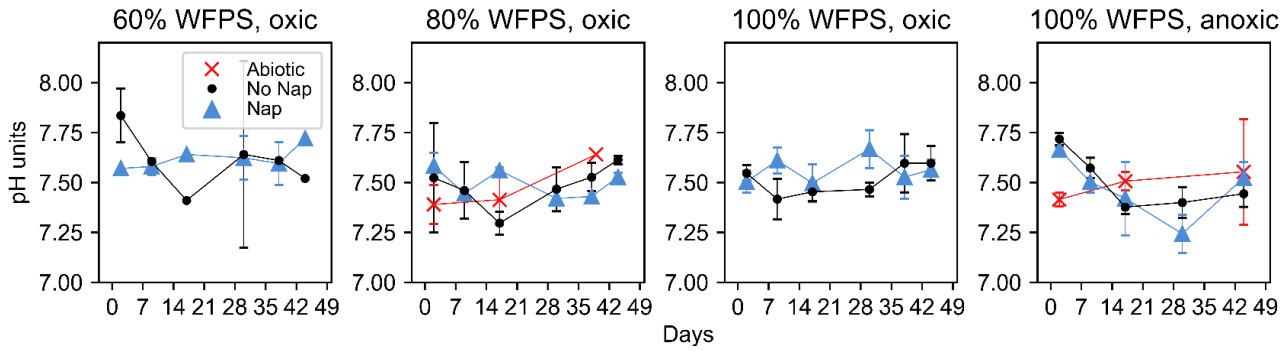

Figure AI-4. Time series of porewater pH. Data shown are the average of triplicate samples at each sampling time point, with error bars representing one standard deviation. Where no error bars are seen in the 60% oxic and 80% oxic treatments, triplicate jars did not yield enough sample volume for analysis, and a standard deviation could not be calculated.

II. Appendix II – Additional results from Chapter 3

Table AII-1. Summary of statistics from curve fitting used to obtain the 0^{th} order rate constant *k*, E_a and Q_{10} values for time series data sets of different processes under oxic and anoxic incubations. See Figure AII-6 for the associated curve fitting plots. Curve fitting for O_2 consumption data in anoxic incubations were omitted due to a lack of change over time in accumulated O_2. Curve fitting for acetate and propionate consumption data in anoxic incubations were also omitted due to the combination of production and consumption processes complicating the analysis (see discussion in section *3.4.2*).

	Oxic			Anoxic		
	10°C	**20°C**	**30°C**	**10°C**	**20°C**	**30°C**
CO_2 accumulation						
0^{th} order rate fit: *k*	1.37×10^{1}	4.63×10^{1}	7.28×10^{1}	1.44	6.07	1.08×10^{1}
0^{th} order rate fit: *n*	13	13	13	13	13	13
0^{th} order rate fit: R^2	0.96	0.96	0.94	0.69	0.94	0.90
E_a slope fit: R^2		0.9940			0.9506	
Q_{10} slope fit: R^2		0.9345			0.9419	
CH_4 accumulation						
0^{th} order rate fit: *k*	2.00×10^{-3}	6.00×10^{-3}	7.00×10^{-3}	6.00×10^{-3}	1.29×10^{-1}	4.83×10^{-1}
0^{th} order rate fit: *n*	13	13	13	13	13	13
0^{th} order rate fit: R^2	0.25	0.53	0.52	0.60	0.83	0.48
E_a slope fit: R^2		0.8160			0.9563	
Q_{10} slope fit: R^2		0.8005			0.9479	
DIC accumulation						
0^{th} order rate fit: *k*	1.61×10^{-1}	2.20×10^{-1}	2.47×10^{-1}	1.10×10^{-2}	4.10×10^{-2}	4.00×10^{-2}
0^{th} order rate fit: *n*	13	13	13	13	13	13
0^{th} order rate fit: R^2	0.77	0.91	0.92	0.80	0.83	0.72
E_a slope fit: R^2		0.9421			0.7410	
Q_{10} slope fit: R^2		0.9326			0.7235	
CO_2+CH_4+DIC accumulation						
0^{th} order rate fit: *k*	5.92×10^{1}	8.88×10^{1}	1.05×10^{2}	4.14	1.54×10^{1}	1.67×10^{1}

0^{th} order rate fit: n	13	13	13	13	13	13
0^{th} order rate fit: R^2	0.79	0.93	0.95	0.80	0.89	0.75
E_a slope fit: R^2		0.9553			0.8071	
Q_{10} slope fit: R^2		0.9469			0.7914	
O_2 consumption						
0^{th} order rate fit: k	5.85	1.65×10^{1}	2.15×10^{1}	--	--	--
0^{th} order rate fit: n	13	13	13	--	--	--
0^{th} order rate fit: R^2	0.73	0.95	0.95	--	--	--
E_a slope fit: R^2		0.9073			--	
Q_{10} slope fit: R^2		0.8955			--	
Acetate consumption						
0^{th} order rate fit: k	6.30×10^{-2}	9.50×10^{-2}	8.30×10^{-2}	--	--	--
0^{th} order rate fit: n	13	13	13	--	--	--
0^{th} order rate fit: R^2	0.31	0.79	0.49	--	--	--
E_a slope fit: R^2		0.4428			--	
Q_{10} slope fit: R^2		0.6869			--	
Propionate consumption						
0^{th} order rate fit: k	1.00×10^{-3}	2.00×10^{-3}	2.00×10^{-3}	--	--	--
0^{th} order rate fit: n	13	13	13	--	--	--
0^{th} order rate fit: R^2	0.19	0.65	0.36	--	--	--
E_a slope fit: R^2		0.6772			--	
Q_{10} slope fit: R^2		0.8014			--	

Table AII-2. Summary of E_a and Q_{10} values in this experiment, along with associated errors, measured for various processes under oxic and anoxic Nap incubations, excluding time series data from the initial lag period (as defined by the lag period in CO_2 accumulation time series, Figure AII-1B). Analyses for O_2, acetate, and propionate consumption were omitted due to a lack of lag period observed in these time series datasets (Figures 3-3 and AII-2).

	Oxic				**Anoxic**			
Net reaction	$\boldsymbol{E_a}$ (kJ mol^{-1})	$\boldsymbol{E_a}$ std. error (+/-)	$\boldsymbol{Q_{10}}$	$\boldsymbol{Q_{10}}$ std. error (+/-)	$\boldsymbol{E_a}$ (kJ mol^{-1})	$\boldsymbol{E_a}$ std. error (+/-)	$\boldsymbol{Q_{10}}$	$\boldsymbol{Q_{10}}$ std. error (+/-)
CO_2 accumulation	50	8.9	2.0	1.12	73	20.7	2.8	1.36
CH_4 accumulation	36	17.3	1.7	1.29	141	31.8	7.1	1.62
DIC accumulation	-55	72.3	0.5	2.80	56	36.7	2.2	1.70
CO_2+DIC+CH_4 accumulation	-28	54.0	0.7	2.15	57	37.1	2.2	1.71

Table AII-3. Summary of statistics from curve fitting used to obtain the 0th order rate constant *k*, E_a and Q_{10} values for time series data sets of different processes under oxic and anoxic incubations, excluding time series data from the initial lag period (as defined by the lag period in CO_2 accumulation time series, Figure AII-1B). See Figure AII-7 for the associated curve fitting plots. Analyses for O_2, acetate, and propionate consumption were omitted due to a lack of lag period observed in these time series datasets (Figures 3-3 and AII-2).

	Oxic			Anoxic		
	10°C	**20°C**	**30°C**	**10°C**	**20°C**	**30°C**
CO_2 accumulation						
0th order rate fit: *k*	2.14×10^{1}	3.55×10^{1}	8.65×10^{1}	1.09	5.14	8.31
0th order rate fit: *n*	6	6	6	12	12	12
0th order rate fit: R^2	0.98	0.74	0.86	0.86	0.91	0.90
E_a slope fit: R^2		0.9692			0.9254	
Q_{10} slope fit: R^2		0.9757			0.9149	
CH_4 accumulation						
0th order rate fit: *k*	2.00×10^{-3}	6.00×10^{-3}	7.00×10^{-3}	1.10×10^{-2}	1.84×10^{-1}	5.68×10^{-1}
0th order rate fit: *n*	13	13	13	6	9	9
0th order rate fit: R^2	0.25	0.53	0.52	0.52	0.92	0.34
E_a slope fit: R^2		0.8160			0.9514	
Q_{10} slope fit: R^2		0.8005			0.9426	
DIC accumulation						
0th order rate fit: *k*	2.60×10^{-1}	2.10×10^{-2}	5.80×10^{-2}	6.00×10^{-3}	3.10×10^{-2}	2.70×10^{-2}
0th order rate fit: *n*	6	6	6	6	9	12
0th order rate fit: R^2	1.00	0.14	0.50	0.47	0.59	0.65
E_a slope fit: R^2		0.3642			0.7024	
Q_{10} slope fit: R^2		0.3453			0.6843	
CO_2+CH_4+DIC accumulation						
0th order rate fit: *k*	9.51×10^{1}	1.75×10^{1}	4.52×10^{1}	2.24	1.23×10^{1}	1.07×10^{1}
0th order rate fit: *n*	6	6	6	12	9	6
0th order rate fit: R^2	1.00	0.41	0.76	0.52	0.75	0.69
E_a slope fit: R^2		0.2075			0.6996	
Q_{10} slope fit: R^2		0.1918			0.6813	

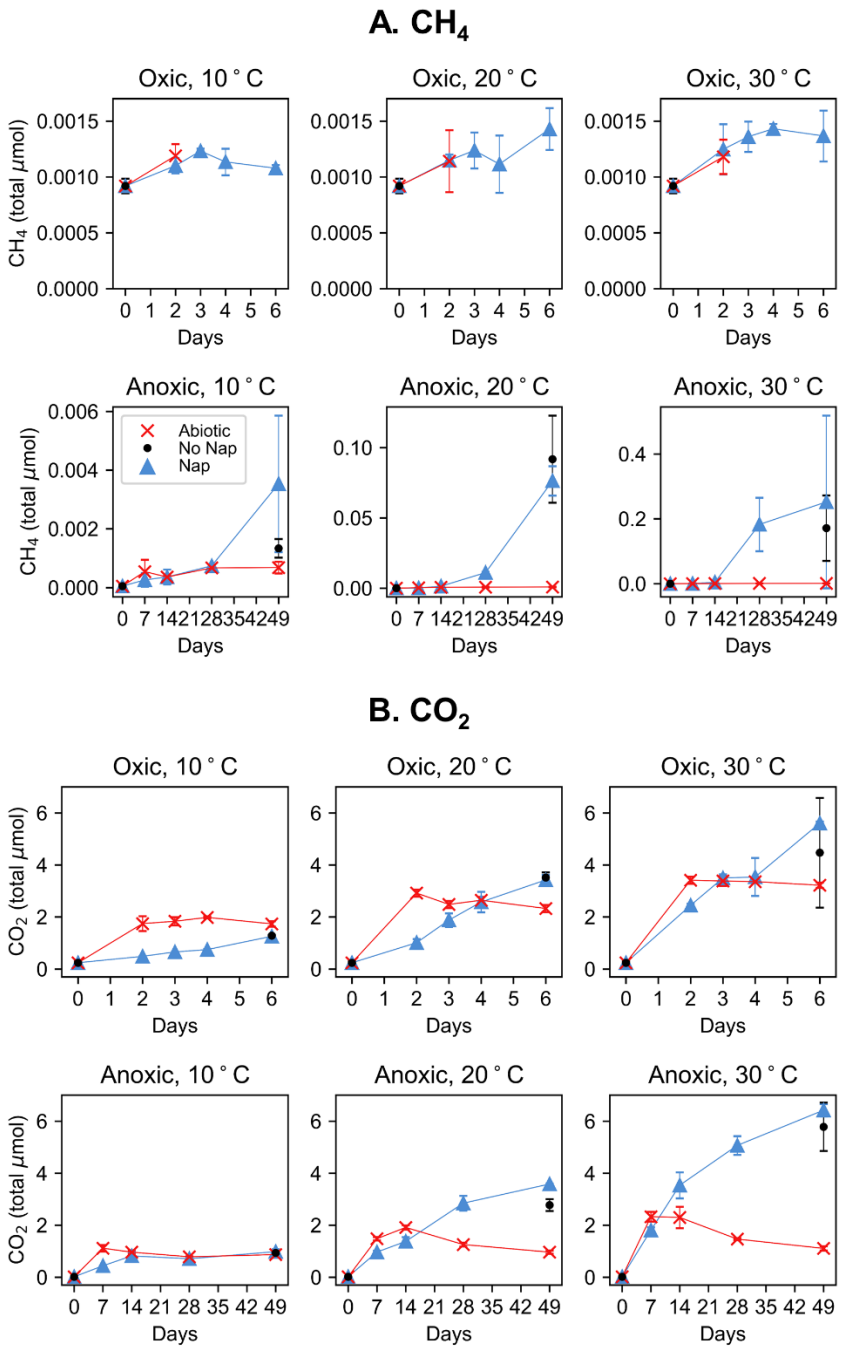

Figure AII-1. Time series of (A) CH_4 and (B) CO_2 in headspace. Data shown are the average of triplicate samples at each sampling time point, with error bars representing one SD. Appropriate CH_4 data for abiotic controls is not available past Day 2 of oxic incubations.

Supplementary discussion accompanying Figure AII-1

I observed an apparent initial lag period for CH_4 accumulation in anoxic Nap incubations where CH_4 accumulation was similar to that in abiotic controls. After the lag period, the rate of CH_4 accumulation increased in Nap treatments, with total accumulation greatly exceeding that of abiotic controls. I also observed lag periods for CO_2 accumulation in anoxic incubations, where CO_2 accumulation was similar or lower to that in abiotic controls before exceeding that in abiotic controls. Shorter lag periods were observed in oxic incubations. The initial lag periods observed in the time series of CH_4 and CO_2 accumulation were likely attributable to a period of biological population growth, during which micro-organisms multiplied until they reached a sustained community population level at which their activity was observable.

The length of the lag period may be temperature- as well as oxygen- dependant. This can be observed in the anoxic data in Panel A: the first measurement points when accumulated CH_4 in Nap incubations exceeded that in abiotic controls occurred on Days 49, 28, and 28 at 10, 20, and 30°C respectively in anoxic incubations. The same for accumulated CO_2 occurs on Day >6, 6, and 4 in oxic incubations and on Day 49, 28, and 14 in anoxic incubations.

During the initial lag period, accumulated CO_2 in abiotic controls actually exceeded that in Nap treatments for all temperature-oxygen conditions. After the initial lag period, accumulated CO_2 in abiotic controls plateaued or decreased while continuing to increase in Nap treatments. This could be the result of abiotic degassing (dissolution of inorganic carbon in soil and subsequent conversion to gaseous CO_2) occurring in all jars upon rehydration of the soil, coupled to CO_2 oxidation occurring in the Nap incubations but not abiotic controls.

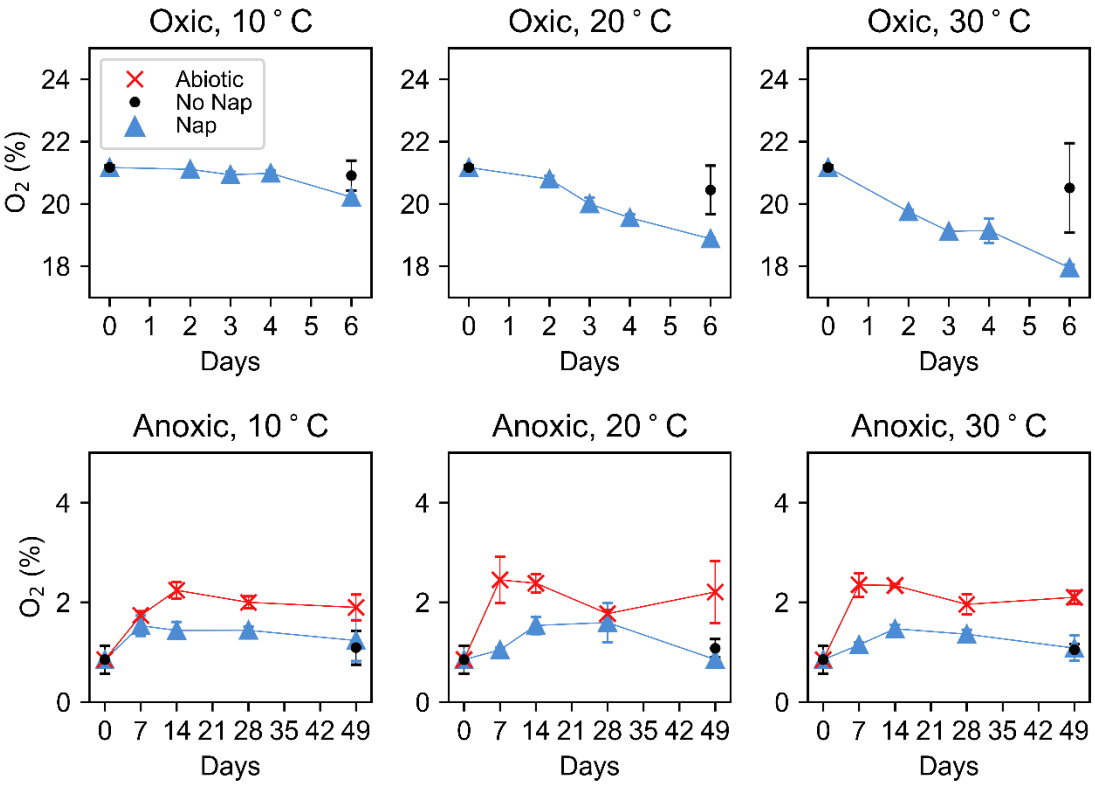

Figure AII-2. Time series of O_2 in headspace. Data shown are the average of triplicate samples at each sampling time point, with error bars representing one SD. Appropriate data for Abiotic controls was not collected during the oxic incubation.

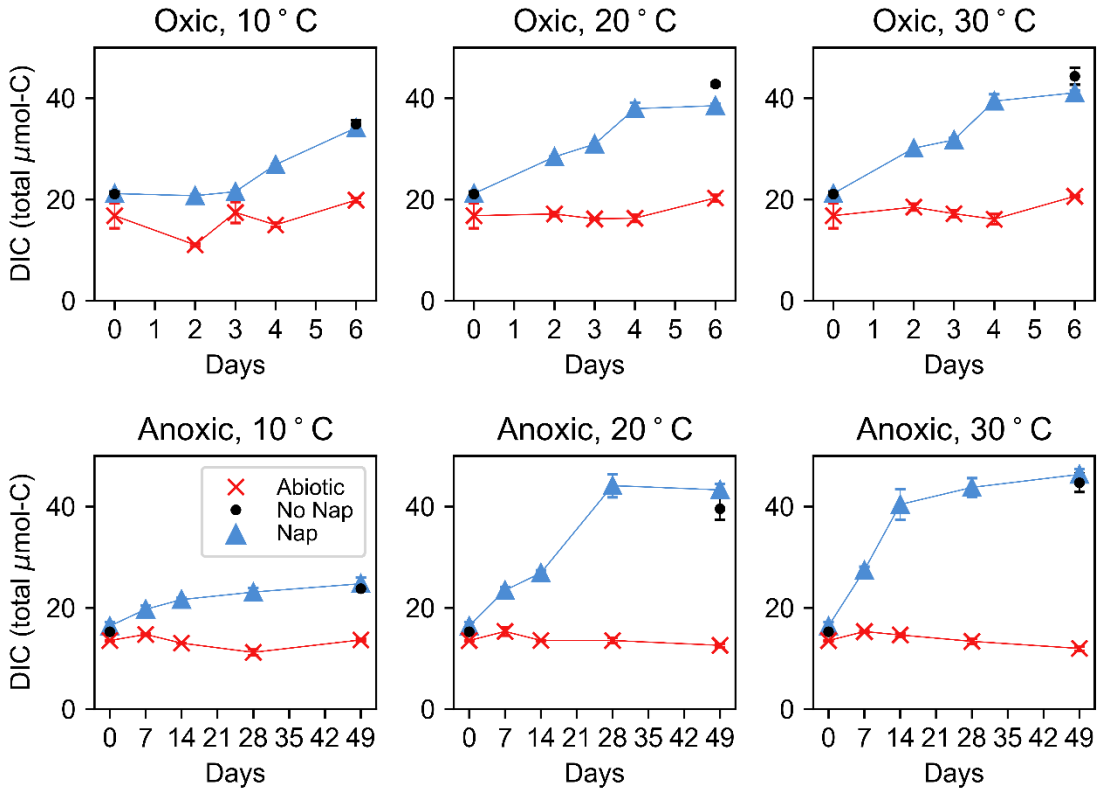

Figure AII-3. Time series of DIC in porewater. Data shown are the average of triplicate samples at each sampling time point, with error bars representing one SD.

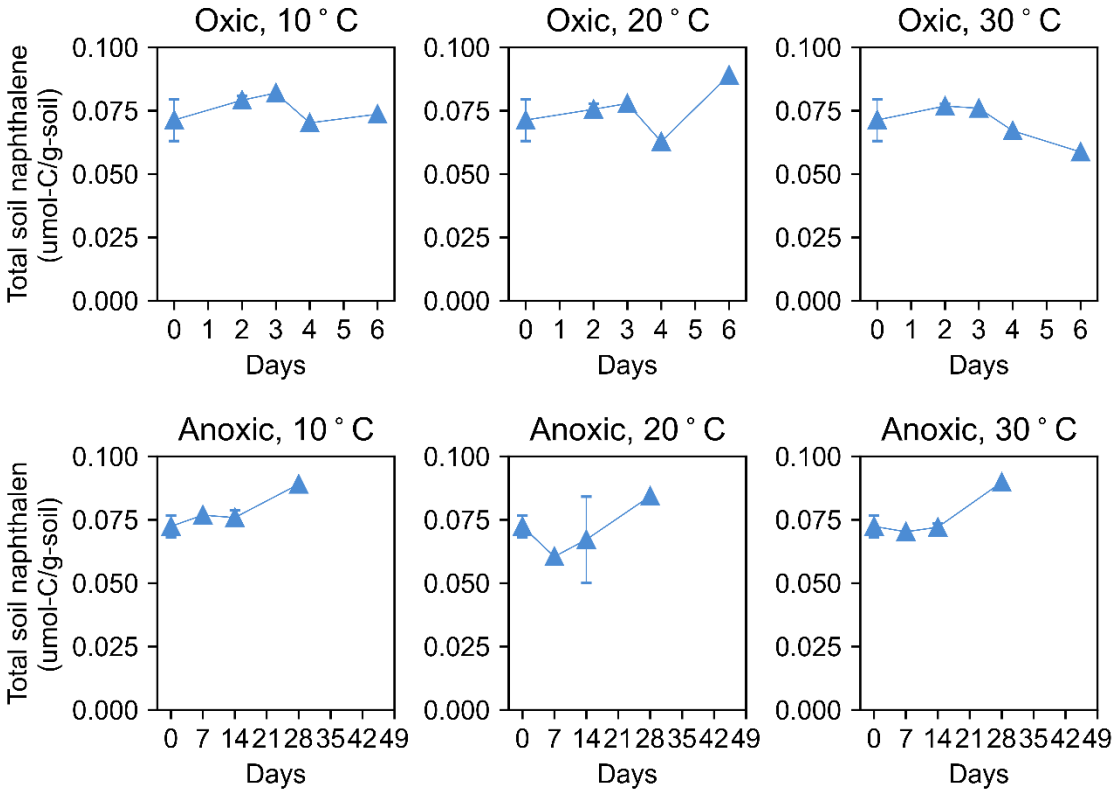

Figure AII-4. Time series of total soil naphthalene (representing sum of aqueous and sorbed naphthalene phases) in Nap incubations. Data points represent single composite samples of all triplicates at that time point, except for Day 0 and 2 data from oxic incubations and Day 0 and 14 data from anoxic incubations which were used to assess triplicate variability. For these data points, data shown are the average of triplicate samples at each sampling time point, with error bars representing one SD. Data are only available for Nap incubations. Data on Day 49 of the anoxic Nap incubation was not collected.

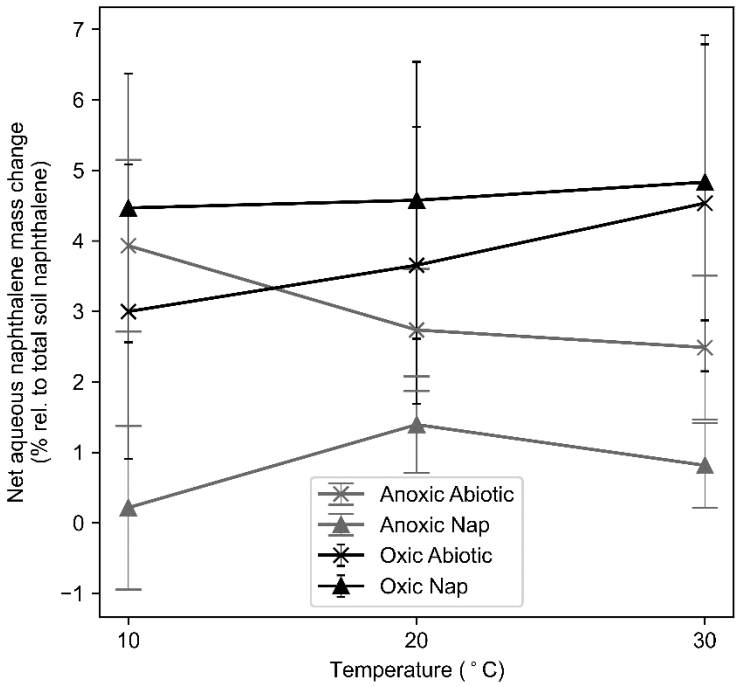

Figure AII-5. The percent of initial total soil naphthalene (calculated based on naphthalene mass added via APW spike) that was lost from the aqueous phase (Figure 3-6) in anoxic abiotic, anoxic Nap, oxic abiotic, and oxic Nap incubations at different temperatures. Data shown are the average of triplicate samples at each sampling time point, with error bars representing one SD.

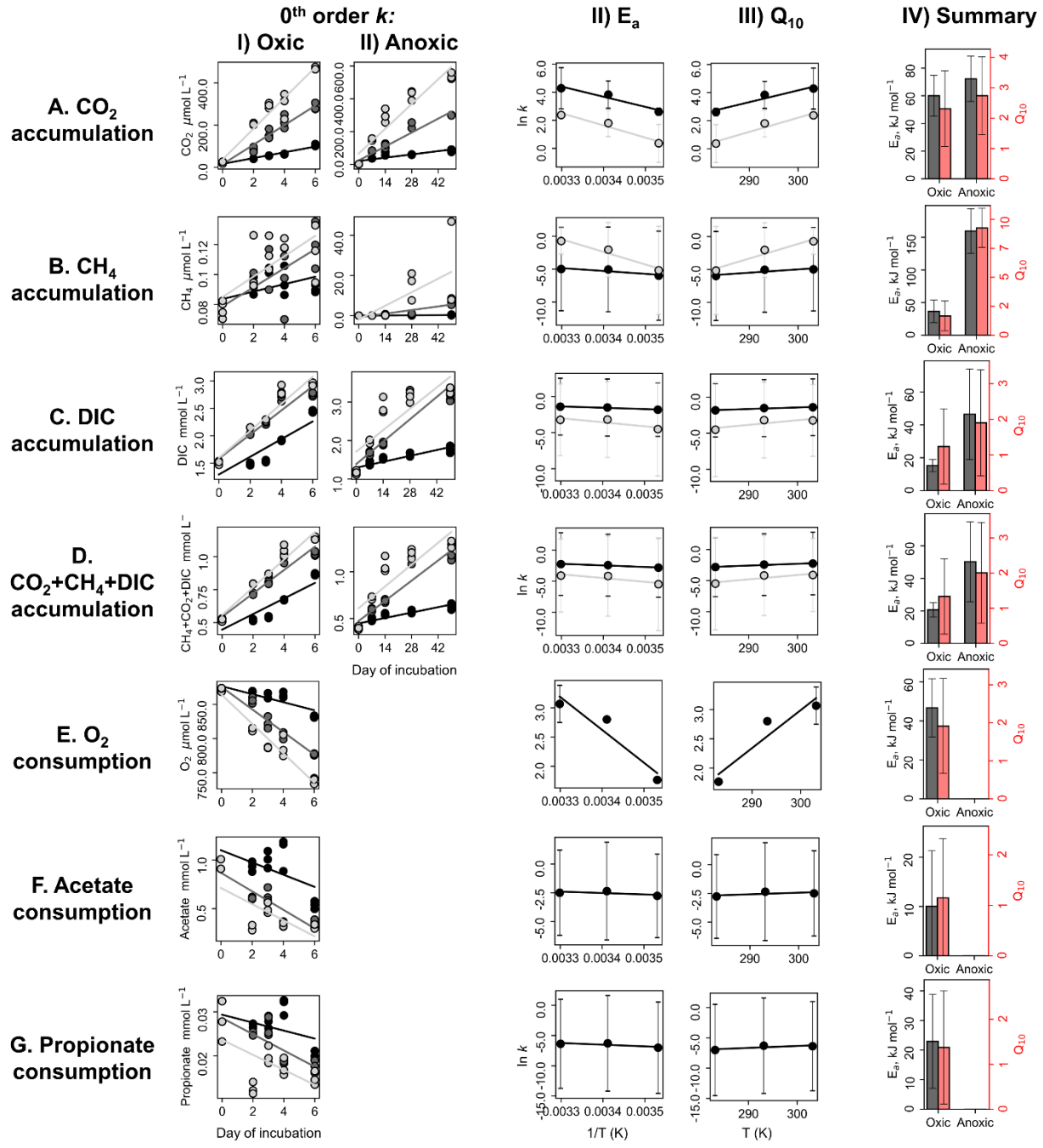

Figure AII-6. Curve fitting plots from which parameters Table 3-2 were obtained. Column I shows linear time series fitting for oxic datasets at three temperatures to obtain the slope *k* in units of concentration day^{-1}. Column II shows linear time series fitting for anoxic datasets at three temperatures to obtain the slope *k* in units of concentration day^{-1}. Column III shows linear curve

fitting of inverse temperature (1/T) in units of K against ln *k* such that the slope is equal to $-E_a/R$ (Equation 3.1). Column IV shows linear curve fitting of temperature (T) in units of K against ln *k* such that the slope is equal to ln $Q_{10}/10$ (Equation 3.2). For columns I and II: black symbols = 10°C, dark grey symbols = 20°C, light grey symbols = 10 °C. For columns III and IV: black symbols = oxic, light grey symbols = anoxic. Column V compares E_a and Q_{10} for oxic and anoxic incubations (bar plots shown in more detail in Figure 3-7).

Rows A through G represent results for the dataset indicated on the figure (CH_4 accumulation, O_2 consumption, etc.). Curve fitting statistics are summarized in Table AII-1. Curve fitting for O_2 consumption data in anoxic incubations were omitted due to a lack of change over time in accumulated O_2. Curve fitting for acetate and propionate consumption data in anoxic incubations were also omitted due to the combination of production and consumption processes complicating the analysis (see discussion in section *3.4.2*).

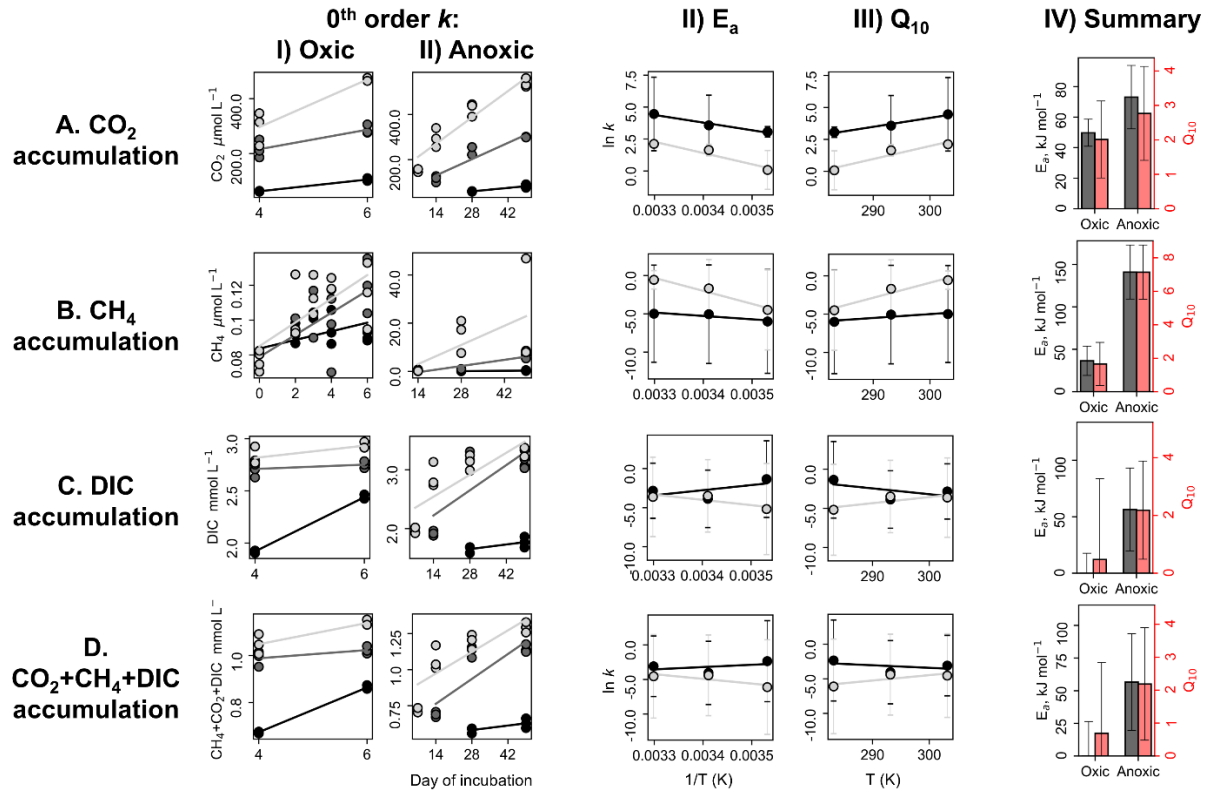

Figure AII-7. Curve fitting plots from which parameters Table AII-2 were obtained, excluding time series data from the initial lag period (as defined by the lag period in CO_2 accumulation time series, Figure AII-1B). Column I shows linear time series fitting for oxic datasets at three temperatures to obtain the slope *k* in units of concentration day^{-1}. Column II shows linear time series fitting for anoxic datasets at three temperatures to obtain the slope *k* in units of concentration day^{-1}. Column III shows linear curve fitting of inverse temperature (1/T) in units of K against ln *k* such that the slope is equal to $-E_a/R$ (Equation 3.1). Column IV shows linear curve fitting of temperature (T) in units of K against ln *k* such that the slope is equal to ln $Q_{10}/10$ (Equation 3.2). For columns I and II: black symbols = 10°C, dark grey symbols = 20°C, light grey symbols = 10 °C. For columns III and IV: black symbols = oxic, light grey symbols = anoxic. Column V compares E_a and Q_{10} for oxic and anoxic incubations (bar plots shown in more detail in Figure 3-7).

Rows A through D represent results for the dataset indicated on the figure (CH_4 accumulation, CO_2 accumulation, etc.). Curve fitting statistics are summarized in Table AII-3. Analyses for O_2,

acetate, and propionate consumption were omitted due to a lack of lag period observed in these time series datasets (Figures 3-3 and AII-2).